UNIVERSITÀ DEGLI STUDI DI MILANO

Scuola di Dottorato in Fisica, Astrofisica e Fisica Applicata

Dipartimento di Fisica

Corso di Dottorato in Fisica, Astrofisica e Fisica Applicata

Ciclo XXV

Synthesis and electrochemical investigation of cluster assembled carbon thin films

Settore Scientifico Disciplinare FIS/03

Supervisore: Professor Paolo Piseri

Coordinatore: Professor Marco Bersanelli

Tesi di Dottorato di:

Luca Giacomo Bettini

Anno Accademico 2011/2012

Commission of the final examination:

External Referee:
Professor Andrea Li Bassi, Politecnico di Milano, Energy Department, Milano, Italy

External Member:
Professor Ladislav Kavan, J. Heyrovský Institute of Physical Chemistry of the Academy of Sciences of the Czech Republic, Department of Electrochemical Materials, Prague, Czech Republic

Internal Member:
Professor Elena Selli, Univesità degli Studi di Milano, Department of Physical Chemistry and Electrochemistry, Milano, Italy

Final examination:

11 February 2013

Università degli Studi di Milano, Dipartimento di Fisica, Milano

MIUR subjects:

FIS/03 - Condensed Matter Physics

PACS:

36.40.-c
81.05.U-
82.45.-h

Preface

This thesis represents the result of my PhD research project carried out under the supervision of Professor Paolo Piseri and Professor Paolo Milani in the Molecular Beam Laboratory (LGM) of the Physics Department at the Università degli Studi di Milano. The experimental work has been mainly devoted to the synthesis and characterization of porous carbon and nickel:carbon nanocomposite thin films, inspired by the potential relevance of these materials to the energy storage issue. Thin films were synthesized by the Supersonic Cluster Beam Deposition, SCBD, of clusters produced in a Pulsed Microplasma Cluster Source, PMCS, a proprietary technique developed during the last ten years at LGM, and then characterized by means of several techniques with the aim of assessing their electrochemical interfacial properties. Although the thorough expertise in cluster assembled materials held by the LGM group, the electrochemical characterization of cluster assembled electrodes as well as the codeposition of clusters of different materials produced separately in different PMCSs are for the first time reported in this work and are indeed to be seen as the main original contribution of this thesis.

In order to present and discuss the experimental work in an effective way, I organized this thesis as follow. The first part is addressed to briefly introduce the reader to the field of carbon based materials (chapter 1), focusing in particular on cluster assembled carbon grown by SCBD, and of the electrochemistry of porous interfaces (chapter 2). The second part reports the discussion of the experimental results, established within the PhD project, on carbon (chapter 3) and nickel:carbon nanocomposite (chapter 4) cluster assembled thin films.

Abstract

The assembly of small atomic aggregates, i.e. clusters, into nanostructured materials that preserve the original size dependent features of their building blocks is a pursuit of vast fundamental scientific interest. Furthermore, being able to build up materials with tailored structural and functional properties starting from preformed elements with selected properties holds tremendous technological potential and is pivotal toward the development of green, cheap and efficient energy storage and harvesting systems, including photovoltaics, catalysis and batteries. The deposition of clusters with low kinetic energy appears as promising method to prepare original nanostructured materials from cluster preformed in the gas phase. The low kinetic energy of the clusters substantially avoids their fragmentation and coalescence upon landing on the substrate and originates nanostructured materials characterized by high surface area and porosity.
Among nanostructured materials, porous carbon exhibits exciting physico-chemical features that encourage its use in practical technological applications. Porous forms of carbon with high specific surface area are widely used as electrode material in electric double layer (EDL) capacitors to store energy through the reversible electrostatic adsorption of ions. Thanks to this charge storage mechanism, EDL capacitors, also known as supercapacitors, are unique devices that not only fill the gap between capacitors and batteries, but can also replace or complement the latter, playing an important role for the breakthrough of renewable energy sources. Although the outstanding advances in safety and reliability boost the large scale implementation of supercapacitors, the growing demand for higher energy and power densities pushes the interest toward the development of advanced nanostructured carbon with tailored properties. Fabricating thin film

based supercapacitors suitable for portable devices or integrable in micro electromechanical systems is another challenge that drives the development of new routes for the synthesis of nanostructured carbon.

This dissertation deals with the growth of porous nanostructured carbon (ns-C) thin films by the Supersonic Cluster Beam Deposition (SCBD) of clusters formed in a Pulsed Microplasma Cluster Source (PMCS). The energy storage behavior of ns-C thin films has been assessed by the characterization of the electrochemical interfacial properties of ns-C based electrodes soaked in liquid electrolytes, specifically focusing on how electrochemical properties change with the ns-C structure and composition. These studies are carried out by means of atomic force microscopy (AFM), Raman spectroscopy, x-ray photoelectron spectroscopy (XPS), transmission electron microscopy (TEM) and electrochemical techniques, such as cyclic voltammetry (CV) and electrochemical impedance spectroscopy (EIS).

First, the issue of the optimization of ns-C based electrode fabrication protocol is handled. The impact of a mild thermal treatment and of the current collector morphology on the EDL formed at the interface between a ns-C thin film 200 nm thick and a standard aqueous electrolyte (KOH) is addressed. Increasing in the ns-C mechanical adhesion to the current collector and enhancements of the specific gravimetric energy density of the carbon are measured as consequences of the heating and of the matching of the surface roughness of the current collector and the ns-C. The ns-C based electrode with nanostructured Ni current collector deposited by SCBD showed a specific EDL capacity of 120 F/g.

Then, the electrochemical energy storage properties of ns-C thin films soaked in room temperature ionic liquids (RTILs) featuring the same anion and different cations have been studied as function of cation dimension and ns-C thickness. The use of RTILs in supercapacitors is appealing due to their wide electrochemical stability window that easily excesses 4V. EIS of the ns-C/RTIL interface showed that ns-C is characterized by an open porosity, easily wettable and accessible by RTILs and specific capacity up to 75 F/g was measured over a wide range of thicknesses. An influence of the size of the ions over the amount of charge stored in the EDL is observed. The proof-of-principle of the fabrication of a planar thin film supercapacitor based on ns-C with promising volumetric energy and power densities is reported.

Finally, the inclusion of nickel clusters in the porous ns-C matrix has been studied as route toward the synthesis of carbon based electrodes with optimized properties. The electrochemical properties of Ni:C nanocomposite electrodes with

constant thickness and different volumetric nickel concentration exhibited an almost constant volumetric energy density, meaning that the porous nanostructure is not affected by the Ni inclusion, and a volumetric power density linearly related to the Ni loading, proving the enhancement in the nanocomposite electric conductivity due to the inclusion of Ni clusters. Embedded nickel nanoparticles have been shown to catalyze the formation of tubular onion-like carbon structures upon mild thermal treatment in inert atmosphere. Electrochemical characterization of heated nanocomposite electrodes evidenced that the germination of ordered sp2 structures preserves the high surface area available for EDL formation and further improves the energy storage properties in terms of power delivery and uptake.

The findings of this thesis contribute to the general understanding of the interfacial properties of nanostructured porous carbon grown by SCBD and assess the viability of the electrochemical techniques toward the characterization of cluster assembled materials. Furthermore, the results obtained by the codeposition of clusters of different materials disclose new stimulating perspectives toward the use of SCBD in the synthesis of nanocomposite nanostructured thin films with tailored properties. From a more applicative point of view, this study demonstrates the suitability of ns-C as electrode material in electrochemical energy storage devices and promotes its use in planar thin film supercapacitors where the accurate control, ensured by SCBD, over the thickness, the structure and the shape of the deposited material is needed. The compatibility of the SCBD technique with planar microtechnology and temperature sensitive substrates are other attractive features toward the employment of ns-C thin films in portable and flexible micro-sized supercapacitors.

Contents

Introduction

Nanoscale systems have been attracting more and more the interests and the efforts of the scientific community over the last twenty years thanks to the extraordinary richness of physical and chemical information which is integral to their intrinsic reduced size. Among various type of nanoscale systems, clusters are an original class of structures with size in the nanometer range. As atomic aggregates containing typically from few tens to few thousands of atoms, they are deeply studied due to their unique size dependent properties which differ from both the constituting atoms and the bulk material. Physical techniques to produce size selected clusters with relative high efficiency underwent pivotal advances over the last decades opening the way to the thorough study of clusters both in the gas phase and upon deposition on a substrate. Even more intriguing is the possibility to use clusters as building blocks to grow cluster assembled thin films. As long as the cluster structure is not lost upon deposition, cluster assembled materials retain the characteristics of the preformed clusters (e.g. the high surface to volume ratio) and their properties can therefore be tailored controlling the structure of the building blocks. For these reasons cluster assembled materials are one of the more promising examples of the bottom-up approach to nanotechnology and can represent the breakthrough for the transfer of the fundamental scientific results obtained by the study of clusters to real high technology applications.

Materials with high surface to volume ratio hold enhanced interfacial properties and are therefore the key of several emerging energy storage and energy conversion devices such as solar harvesting systems, lithium batteries, fuel cells and supercapacitors in which the nanostructure of the electrode boosts the overall

performances [1–4].

In this context a very high relevance is addressed to the nanoforms of carbon since the first observations of fullerene clusters by Kroto in 1985 [5] and carbon nanotubes by Iijima in 1991 [6], until the more recent renewed interest on graphene thanks to the work of Novoselov and Geim [7]. Besides these nanostructures, carbon presents further stable allotropic forms, ranging from diamond-like structures to linear chain of atoms, which mainly differ for the degree of hybridization and structural order. According to the specific structure, carbon spans over a virtually infinite range of physico-chemical properties inspiring the development of a carbon based technology where the key role is played by the controlled synthesis of nanostructured carbon assembled material and by the understanding of how these nanostructures behave as macroscopic material.
Nanostructured carbons with high specific surface area are widely used as electrode material in electric double layer (EDL) capacitors to store energy through the reversible electrostatic adsorption of ions [8, 9]. Thanks to this charge storage mechanism, EDL capacitors, also known as supercapacitors, are unique devices that not only fill the gap between capacitors and batteries, but can also replace or complement the latter, playing an important role for the breakthrough of renewable energy sources. Although the outstanding advances in safety and reliability boost the large scale implementation of supercapacitors, the growing demand for higher energy and power densities pushes the interest toward the development of advanced nanostructured carbon with tailored properties. Furthermore, the recent boom in microelectronic devices and nomad electronics, such as sensors, implantable medical systems and micro-electromechanical-systems (MEMS), triggers the need for small sized power and energy sources. Designing efficient, miniaturized energy-storage systems with high energy and power per unit mass and/or volume integrable on-chip remains a challenge to be met. The development of EDL capacitors miniaturized to micron scale could provide a solution [10–14]. However, porous carbon fabrication protocols commonly employed in the manufacturing of supercapacitor are not easily integrable with thin film deposition processes and/or micro-patterning techniques, being, therefore, one of the main bottlenecks toward the development of high-performance small sized supercapacitors.

The PhD work reported in this thesis is devoted to the synthesis and characterization of cluster assembled carbon thin films by the Supersonic Cluster Beam Deposition (SCBD) of carbon clusters formed in the gas phase by a Pulsed

Microplasma Cluster Source (PMCS), aiming to assess their electrochemical capacitive properties. Compared to other approaches to the synthesis of porous carbon, cluster beam technique has the great advantage of decoupling the particle formation process, which occurs inside a cluster source, from the deposition stage, leading to a good control of the structure of the deposited materials. The compatibility with standard planar microtechnology fabrication processes and temperature sensitive substrates are other relevant features of SCBD that motivated the work presented in this dissertation.
The firs part of this thesis provides a description of the cluster deposition technique employed in this work for the growth of porous carbon thin films and a brief review of the recent progresses and present challenges in supercapacitor technology. Moreover, it presents the essential background necessary for understanding the electrochemistry of the solid/liquid interface. In the second part of the thesis the structural and electrochemical properties of the cluster assembled carbon thin films produced by SCBD are characterized and discussed by means of atomic force microscopy (AFM), electron transmission microscopy (TEM), Raman spectroscopy, x-ray photoelectron spectroscopy (XPS) and electrochemical techniques such as cyclic voltammetry (CV) and impedance spectroscopy (EIS). This thesis reports also about the synthesis and characterization of cluster assembled carbon thin films seeded with nickel nanoparticles produced in a separated PMCS and mixed with the carbon clusters in the supersonic beam. Toward the development of new advanced electrode materials for electrochemical energy storage applications, metal nanoparticles embedded in carbon matrix are well known to originate nanocomposites with interesting and technologically promising properties [15] that can be potentially well controlled and tuned by the synthetic approach, based on cluster mixing, proposed in this thesis.

Part I

Background

Chapter 1

Cluster assembled carbon

Carbon-based materials play a fundamental role in nanoscience and nanotechnology. Carbon is an abundant and environmentally friendly element and in the structural form of porous carbon has received great deal of attention due to its many applications. Porous carbon is extensively applied in various technological areas, including gas sensors, water purification systems, catalyst supports and as host for the immobilization of biomolecules for biosensors. Although it is widely used as the active material in some key electrochemical systems, both conventional and emerging, such as metal-air primary and rechargeable batteries, fuel cells, supercapacitors, lithium-ion and lithium polymer rechargeable batteries, many challenges and the understanding of the role of carbon and its synthesis, characterization, stability and efficiency in charge storage applications still exist [16]. By this chapter the advantages arising from the use of carbon clusters as building blocks to grow porous carbon materials, the foremost features of the SCDB process and the main properties of cluster assembled carbon and metal/carbon nanocomposites, which are the object of the experimental work presented in the second part of this dissertation, will be introduced.

1.1 Cluster assembled materials

Clusters are finite aggregates of atoms, from few to few thousands, with size up to few tens of nanometers which can be also referred to as nanoparticles. The main interest in this original class of structures arise from the size and structure dependent properties that confer to clusters the peculiarity of being the link between isolated atoms and bulk materials exhibiting a wide and virtually tunable range of interesting electric, magnetic and chemical properties [17–21]. As nanometric aggregates they are furthermore characterized by a high surface to volume ratio

resulting of particular interest when surface mediated physico-chemical processes are considered.
Clusters can be produced in several ways which can be roughly grouped in two main methodologies: the chemical synthesis and the gas-phase vapor condensation. While the former generally suffers the lack of easily implementable cluster manipulation techniques, the latter, despite being typically more complicated and expensive, presents the fundamental advantage of enabling the formation of a molecular beam of clusters which consequently can be manipulated (e.g. ionized, mass selected, chemically modified), characterized in the gas phase as isolated objects or deposited on a substrate to serve as building blocks for the bottom up approach to the growth of nanostructured materials.

The synthesis of nanostructured cluster assembled materials in the form of thin films appears as the opportunity to build a novel class of materials which can not only be object of fundamental studies devoted to the understanding of the collective behavior of supported clusters but represent also the chance of transferring cluster unique properties to technological applications [22–25]. By depositing preformed clusters on a substrate, one can build cluster assembled materials in which cluster physico-chemical properties, as long as inter-clusters aggregation is suppressed, are preserved. In this way the size dependent characteristics as well as the large surface to volume ratio of the pre formed clusters are in principle transfered to the thin film and is possible to speak about a *memory effect*. The result is a nanostructured material whose properties rely on the characteristics of the building blocks and can be properly tailored, accordingly to the control over the cluster aggregation process. In order to avoid clusters fragmentation and coalescence, the key role is played by the impact phenomena that govern the interaction between the clusters and the surface of the substrate [26]. Clusters deposited by molecular beams must have a kinetic energy sufficiently low to prevent cluster diffusion and reorganization on the substrate with the consequent formation of compact thin films [26, 27]. Under this constraint the deposition process is named low-energy cluster beam deposition (LECBD) and the growth of films can be viewed as a random stacking of particles, as for ballistic deposition, that leads to materials showing a granular and porous nanostructure and a lower density compared to that of films assembled by depositing particles at high energies [23].

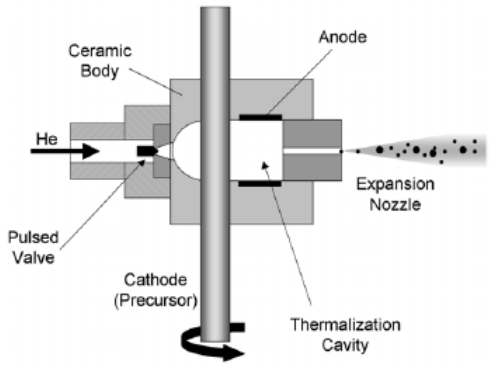

Figure 1.1: PMCS: schematic view [25].

1.1.1 Cluster mixing: route to porous nanocomposites

Cluster deposition technique is a very versatile synthetic approach and has been extensively employed for the growth of nanocomposites, a particular class of cluster assembled materials with great potential in a wide range of technological applications. Nanocomposite materials have been obtained by the embedding of clusters on pre-existing or co-deposited matrix (e.g [28, 29]), by the deposition of clusters produced starting from a composite precursor (e.g [30–32]) and by the codeposition of clusters produced in different sources (e.g [33, 34]). Providing that the cluster deposition regime belongs to LECBD, this latter method is a viable route to the production of porous nanocomposites systems with a precise control of the nanoscale structure. Materials made of distinctly different components mixed at the nanometer scale can be obtained by the mixing of clusters of at least two different phases, preformed in separate cluster sources and characterized by a kinetic energy sufficiently low to avoid fragmentation and coalescence upon landing on the substrate. The mixing of clusters of different materials leads to the growth of systems with properties that depend not only on the properties of the single components but also on the specific way in which the different components are mixed, opening the way to the synthesis of nano engineered systems with tailored properties.

1.1.2 Supersonic Cluster Beam Deposition

Manipulation of clusters and nanoparticles in the gas phase is pivotal to obtain the high intensity beam of clusters with low kinetic energy and controlled mass

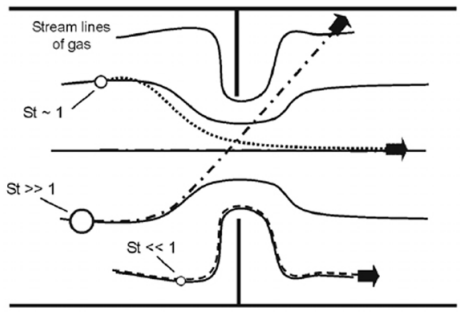

Figure 1.2: Schematic illustration of the basic principles of an inertial focusing lens [25].

and spatial distribution which is requested for the synthesis of cluster assembled materials that mirror the properties of isolated clusters. This thesis deals with the growth of nanostructured porous materials and composites by the Supersonic Cluster Beam Deposition (SCBD) of clusters formed in the gas phase by a Pulsed Microplasma Cluster Source (PMCS). This approach, developed in the last decade at the Molecular Beam Laboratory of the Università degli Studi di Milano, combines the advantages of the gas-phase synthesis of nanoparticles with the benefits arising from supersonic molecular beams and aerodynamic focusing methods which are crucial for the control of the particle beam shape and the particle velocities. The implications and the applications of this technique for the synthesis of nanostructured materials with tailored structural and functional properties are described in details in several papers, e.g [25, 35–40], and therefore in this section only the basic operating principles of both the cluster source, i.e. the PMCS, and the deposition method, i.e. the SCBD apparatus, are reported.

The PMCS, schematically represented in figure 1.1, is a pulsed vaporization source with a typical repetition frequency of 1÷10 Hz based on the ablation of a target by a pulsed confined plasma ignited by an electrical discharge. Briefly, an inert gas (e.g. argon or helium) at high pressure (30÷50 bar) is injected into the source cavity by a pulsed solenoid valve (valve opening time is 150÷250 μs). The strong density gradient, generated by the gas jet which impacts on the side of the cathode rod, together with a high potential difference (500÷1000 V), applied after the valve closed (delay time ca. 600 μs) between the cathode and the anode, causes the firing of the discharge (duration ca. 80 μs) and the formation of a strong-localized plasma (micro-plasma). The rod, which can be of any conductive solid material, is thus locally vaporized by the plasma and the vapor is quenched

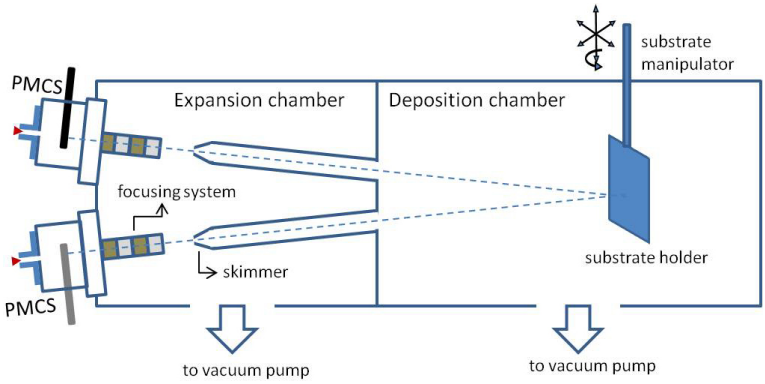

Figure 1.3: SCBD apparatus at LGM: schematic view

by inert gas forming small aggregates. During the time the clusters spend in the cavity they undergo further cluster-cluster interactions, aggregations and rearrangements leading to a cluster size and structure which evolve with increasing residence time in the source [41]. The gas-clusters mixture then expands from the condensation chamber of the PMCS, into a vacuum chamber, i.e. the expansion chamber, passing through a focusing system, which consists of multiple aerodynamic lenses (figure 1.2), and producing a collimated supersonic molecular beam of clusters. The supersonic expansion of the cluster seeded gas cools the translational temperatures of the clusters quenching their evolution and forming a collision-free environment of gas phase isolated particles, i.e. the free molecular flow. Furthermore the supersonic expansion produces a high outward radial velocity which varies with the radial position in the jet dragging at the periphery of the beam the nanoparticles that are not located in central region of the jet. The cluster response to this radial drag is not simply function of their position in the beam but it also depend on their size. As shown in figure 1.2, after passing an aerodynamic lens, only particles with a critical size (Stokes number, St, $\sim$1) move closer to the centerline, while bigger clusters (St$>>$1) and smaller clusters (St$<<$1) do not merge the lens axis. This effect is exploited by the aerodynamic focusing systems of the SCBD to inertially size select and reduce the angular distribution of the clusters produced by the PMCS [25, 40]. After the focusing system, the central part of the beam is selected by a skimmer, which preserves a differential vacuum between the expansion chamber and the deposition chamber, and an intense and collimated beam of neutral size selected nanoparticles with

kinetic energy lower than 0.5 eV/atom, well below the cluster binding energy, reaches the substrate in the deposition chamber. No substantial fragmentation of the aggregates is then expected upon landing on the substrate and a film keeping memory of the structure the clusters had in the gas phase can be deposited at room temperature on every kind of substrate with very high lateral resolution [36, 39]. The SCBD apparatus employed in this work and schematically reported in figure 1.3 is equipped with two PMCSs which can operate simultaneously in order to produce at the same time clusters of different elements. The system is specially designed to extract the clusters formed in each PMCS forming two separate supersonic cluster beams that intersect on the substrate leading to the co-deposition.

1.2 Carbon-based nanomaterials

Carbon is one of the most versatile elements. As shown in figure 1.4, it can aggregate in many different allotropic forms and form an infinite number of compounds [42]. This is basically due to carbon ability to hybridize its atomic orbitals in to a new set of hybrid orbitals, commonly known as sp1, sp2 and sp3. Depending on the type of hybrid bonding, carbon materials exhibit a wide variety of physico-chemical properties that not only formed the backbone of biology for life on Earth (carbon-based life) but appear also very suitable for technological applications (carbon-based technology) as testified by the recent Nobel prize in Chemistry shared by Curl, Kroto and Smalley [43–45] in 1996 for the discovery of fullerens and the even more recent Nobel prize in Physics shared by Geim and Novoselov [46, 47] in 2010 for groundbreaking experiments regarding the two-dimensional material graphene. Stable and ordered allotropes of carbon other than graphite and diamond, which are respectively the bulk forms of sp2- and sp3-bonded systems, comprehend a vast group of the so called carbon transitional forms that include intermediate forms of carbon in which the hybridization number n of carbon atoms is not integral but fractional, and mixed forms of carbon where carbon atoms hybridized sp1, sp2 and sp3 coexist. This class of carbonaceous systems do not include only fullerenes and graphenes but a wide variety of carbon nanostructures ranging from the multi-walled and single-walled nanotubes, first reported by Iijima in the early '90s [6], to so far less studied systems such as carbon nano-onions, carbon nano-horns, carbon nano-torus, carbon nano-buds, carbon nano-cups and carbon peapods [48]. Surprisingly carbon, due to the spectacular properties of these nanoforms, is currently considered on of the elements

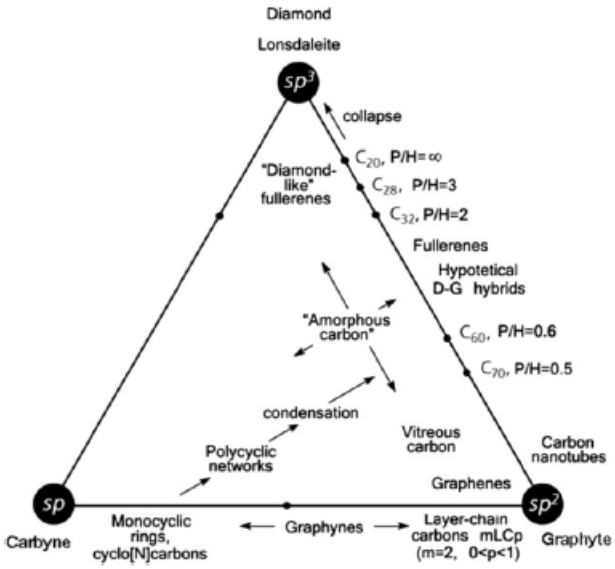

Figure 1.4: Ternary *phase* diagram of carbon allotropes [42].

which can most help mankind to find a solution to the energy problem originated as if on purpose by the same carbon in the form of carbon-based fossil fuels which combustion is the origin of the huge amounts of carbon dioxide production and emission. Fullerenes, graphenes and carbon nanotubes are today at the forefront among carbon nanostructure as the most studied and therefore the closest to find practical applications in different sustainable energy related fields like solar energy harvesting and conversion, energy storage and hydrogen uptake and storage (for a recent review about carbon nanostructures for energy see reference [49]). As interesting as these nanostructures are carbon based nanomaterials, a variety of carbon based macroscopic systems that can be synthesized using carbon nanostructures (e.g. clusters, fullerenes, nanotubes, chain of carbon atoms) as building blocks. Carbon based nanomaterials are typically short range-order carbon systems and comprise carbon materials defined as amorphous carbon, diamond-like carbon and glassy carbon, as well as carbon blacks, soot, cokes, etc. Besides the relative low costs of production, the increasing applicative importance of carbon nanomaterials is mainly due to their high surface area, porosity and chemical inertness which are by far their most important characteristics.

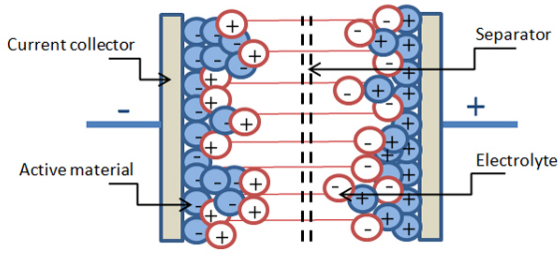

Figure 1.5: Schematic view of a supercapacitor.

1.2.1 Porous carbon: electrochemical energy storage

Porous carbon in different forms (e.g powders, fibres, foams, felts, tissues, composites) has a great role in changing the energy sources and consumption patterns and has therefore become a primary focus of the major world energy harvesting and scientific community. Highly porous carbon has the potential to facilitate major advances in the energy storage field and is widely used as electrode material in fuel cells, lithium-ions batteries and electrochemical energy storage devices, also known as electric double layer capacitors, supercapacitors or ultracapacitors. Supercapacitors are extensively studied energy storage devices due to the increasing demand for a new kind of electrical energy accumulators of long durability (over 10^6 cycles) and high specific power (more than 10 kW/kg). The main advantage of this storage system is a high dynamic of charge propagation which generate short-term power pulses that can be very useful in hybrid electrical vehicles, digital telecommunications systems, UPS (uninterruptible power supply) for computers and pulsed laser technique [50, 51].

A typical supercapacitor consists of two polarizable electrodes composed of a metallic current collector in contact with the active material, which usually is a porous form of carbon (see figure 1.5). The electrodes are immersed in an electrolyte which can be both aqueous (e.g. KOH and H_2SO_4) and organic (e.g. tetraethylammonium tetrafluoroborate salt dissolved in acetonitrile or propylene carbonate). A dielectric separator permeable to the electrolyte prevents the electric contact between the electrodes. The charge is stored by the reversible adsorption of ions at the active material/electrolyte interface, in the so called Helmholtz double layer (see section 2.1.1). This mechanism is based on the electrostatic separation of charges, as in conventional capacitors, and does not involve any

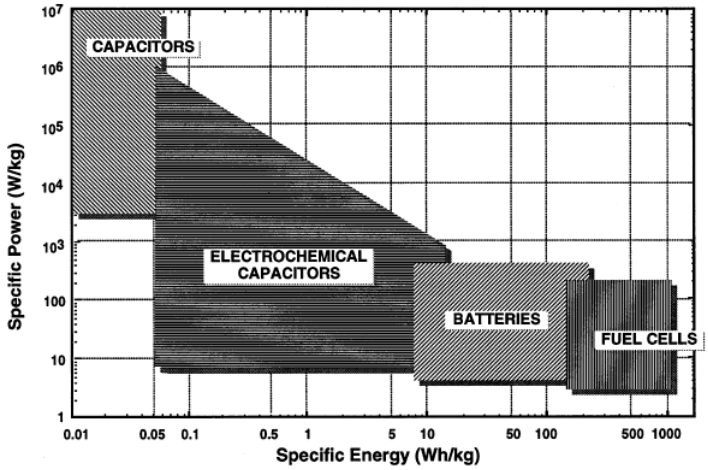

Figure 1.6: Ragone plot for various energy storage and conversion devices [52].

Faradaic processes (i.e. oxidation-reduction reactions) leading to much longer cycle life than typical accumulators based on charge transfer phenomena. In terms of specific energy and specific power, supercapacitors are intermediate systems between conventional capacitors and batteries with higher specific energy than conventional capacitors and higher specific power than batteries. As shown in the Ragone plot reported in figure 1.6, both the specific energy and specific power ranges for supercapacitors can cover several orders of magnitude and this makes them extremely versatile as a stand-alone energy supply or in combination with batteries as a hybrid system [52]. The maximum electric energy stored (U) and power delivered (P) of a supercapacitor can be calculated according to the equations

$$U = \frac{1}{2} C E^2 \tag{1.1}$$

$$P = \frac{1}{4} \frac{E^2}{R} \tag{1.2}$$

where C, E and R are the capacity, the maximum voltage and the overall series resistance of the supercapacitor, respectively. Since the capacitance C rely on the extension of the electrode surface area where the Helmholtz double layer is formed, highly porous electrode materials with high surface area are needed in order to store high energy densities.

The ideal electrode for electrochemical capacitors should have (i) high specific real areas, on the order of 1000 m^2/g, (ii) good intra- and inter-particles conductivity in porous matrices and (iii) good electrolyte accessibility to intra-pore surface area [53]. Porous carbon, in a variety of forms, is the most frequently used active material in supercapacitors [8, 9, 54]. Considerable research is presently being directed towards the enhancing of the specific energy of supercapacitors by the development of high surface carbon materials with a tailored pore-size distribution as well as to the incorporation of redox materials (e.g., metal oxides or conducting polymers) into carbon electrodes [55]. The use of electrolytes capable of operating at higher voltages (>3 V) compared to aqueous (1V) and organic (2.5V) electrolytes is also receiving increased attention as a means of enhancing both the energy (U) and the power (P) [56]. Among different carbon materials, activated carbons (ACs) are especially attractive as electrodes for supercapacitors due to their relatively low cost and non-toxicity [57, 58]. Activated carbons are a porous form of carbon produced from a wide variety of carbonaceous source materials (e.g. coal, coconut shells, wood and peat) which are converted to high surface area carbon by thermal decomposition (the activation process) in a furnace (typical temperatures are as high as 1000°C) using a controlled atmosphere (e.g. CO_2) and/or chemicals (e.g. KOH, H_3PO_4, $ZnCl_2$). ACs have a broad pore size distribution consisting of micropores (< 2 nm), mesopores ($2 \div 50$ nm) and macropores (>50 nm) which leads to a very developed surface area of the order of 2000 m^2/g. This results in an ideal attainable capacitance of 500 F/g (considering an average capacity value of 25 $\mu F/cm^2$) [59]. Typical gravimetric capacitance values of ACs are in the range from 100 to 300 F/g in aqueous electrolyte and less than 150 F/g in organic electrolyte [9]. Despite being the dominant active material in commercially available supercapacitors [60], ACs usually suffer of poor electrical and mechanical properties and thus are often blended with conductive agents (e.g. carbon black) and binders (e.g. PTFE) which increase the overall weight of the supercapacitor, decrease the energy and power density and lead to higher series resistance. Advanced carbon materials, such as carbon nanotubes and graphenes are as well being considered as outstanding active materials for supercapacitor electrodes [9, 55, 61–63]. Although their smaller specific surface area as compared to ACs, these materials possess superior electrical properties, and good mechanical and thermal stability which can be beneficial toward the development of supercapacitors with higher power density. A thorough review of the recent research progresses on carbon-based electrode materials for supercapacitors and of the current research and development on supercapacitor technology

can be found in [8, 9, 15, 54, 58] and [60], respectively.

Besides the potential for high power industrial and electric vehicle applications [60], supercapacitors hold great promise in the rapidly expanding field of miniaturized and portable electronic (e.g. sensors, implantable medical systems, micro-electromechanical-systems MEMS) where the increased functionality risks to be limited by the existing technologies for energy management [64]. However, synthesizing thin film electrodes with precise control of thickness, integrating supercapacitors into portable systems and designing low weight, miniaturized, planar and flexible devices are still challenges to be met and few works in the literature report on the fabrication of thin film and/or micro-supercapacitors. Recently, the integration of carbon based micro-supercapacitors onto silicon substrate has been reported by Durou and coworkers [65] and Huang and coworkers [66] using as active material activated carbon blended with binders and carbide derived carbon, respectively. Onion-like carbon [11], graphene [13], reduced graphite oxide [12] and carbon nanotubes [14] are among the other materials that have been tested as active material in micro-supercapacitors. Despite the high specific energy (e.g. [65]) and power (e.g. [11]) density exhibited by these prototype devices, the main difficulty lies in the integration of the active material within a microfabrication process. The various technologies considered for miniaturization and integration of supercapacitors, e.g printing [14, 67], doctor blading [65] and magnetron sputtering followed by chlorination at high temperature [66] are not inherently compatible with standard microtechnology fabrication techniques or involve high-temperature and/or corrosive treatments which might limit the selection of substrates and manufacturing routes.

1.2.2 Nanostructured porous carbon made by SCBD

The standard methods for preparation of porous carbon can basically be grouped in two types: activation processes and template methods [54, 68]. Synthetic methods involving activation processes, which can be both physical and chemical, are relatively cheap and have a high yield of porous carbon but suffer of efficiency in producing porous carbon with well defined porous structure (e.g [69]). On the other hand template methods, despite being more complicate and less scalable, lead to the synthesis of porous carbon with tailored and uniform pores size that can be controlled by the use of preformed templates which act as scaffolds for the carbonization and have to be removed after the synthesis (e.g [70, 71]). Although many porous carbon materials are developed using the above-mentioned

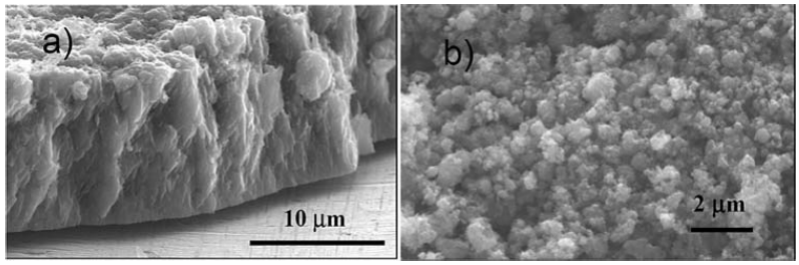

Figure 1.7: SEM images of cluster-assembled carbon films: a) section showing features characteristic of columnar growth mechanism; b) granular porous structure of the surface. Reproduced by [72].

methods, both activation and template methods rely on procedures that require chemically aggressive environments and high temperature thermal treatments. These drawbacks harshly limit the synthesis of porous carbon directly on the substrate required, which can be chemically and thermally damaged.

The wide scope for development of porous carbon in various forms with optimized characteristics for desired specific applications pushes a lot of research efforts towards the development of novel techniques addressed to the synthesis of nanostructured carbon with tailored nanostructure and surface functionality. Among different techniques, the growth of nanostructured carbon by SCBD is, as highlighted in section 1.1, one of the potentially most versatile bottom-up approach to the synthesis of porous materials in terms of both material properties control and compatibility with standard planar microtechnology fabrication processes and temperature sensitive substrates. In the particular field of thin film carbon based electrodes for electrochemical energy storage, the synthesis of porous carbon by SCBD can overcome some of the manufacturing problems caused by the use of activated carbon and templated porous carbon, as the need of binders and post deposition aggressive treatments. Furthermore, SCBD ensures the precise control of the carbon thickness on the nanometer scale, the uniform coating and the adaptability on various substrates including glass and flexible polymers which are all mandatory requirements toward the development of efficient and reliable thin film micro-supercapacitors.

The work presented in this thesis deals with the characterization of the electrochemical properties of porous carbon grown by SCBD (see section 1.1.2). As cluster assembled material, porous carbon grown by SCBD is intrinsically nanostructured and in the course of this work will be referred to as ns-C. The carbon

clusters and nanoparticles are formed in a PMCS by the plasma sputtering of a carbon rod and the subsequent condensation of the sputtered species in an inert gas atmosphere [35]. The mass distribution of the produced nanoparticles ranges between 100 and 1000 atoms and both even- and odd-numbered large particles are produced with sp chains coexisting with sp2 networks [73–76]. The kinetic energy of the nanoparticles is about 0.2 eV/atom [39], well below the cluster binding energy, and fragmentation of the aggregates upon landing on the substrate is substantially avoided. The films keeps the memory of the structure the clusters had in the gas phase and the result is a carbon film with a porous structure consisting of closed graphitic particles and curved graphene foils embedded in an amorphous matrix [77]. Figure 1.7 shows SEM images of the cross section and of the surface of a typical ns-C film assembled by SCBD. The structure is characteristic of a columnar growth mechanism arising from the ballistic sticking and the reduced surface mobility of the clusters [72]. The material is very porous and exhibit a density lower than that of films assembled atom by atom, with typical values between 0.5 and 1 g/cm3. The porosity has been measured from adsorption/desorption isotherms, obtaining a pore size distribution ranging between 20 and 500 Å(mesopore region), with a maximum at around 34 Å. The specific surface area, evaluated by means the full BET law, is equal to 700 m^2/g [78].

In the last decade, ns-C films have been tested in view of many applications. Ns-C was proposed as promising material for electron field emission and the production of cold flat cathodes with the advantages, compared to conventional materials, of a lower threshold field and saturation current densities as well as in higher site emission densities [79, 80]. Capacitive-type humidity sensors made with ns-C films as active material showed a fast dynamic response and a good sensitivity compared to capacitive commercial systems [81, 82]. Finally the highly accessible surface area of ns-C was used for electrochemical energy storage applications such as supercapacitors. Films with a density of 1 g/cm3 showed, in the dc regime, a specific capacitance per electrode of 75 F/g on a single-cell device with polycarbonate as the organic electrolyte [83]. The performance of these ns-C based prototypes suggests interesting perspective for further development of ns-C based devices and, moreover, the possibility of patterning cluster-assembled carbon films produced by SCBD by shadow masking [36] or by ultraviolet photon irradiation [84] may open the way to the integration of nanostructured carbon films on the quickly growing field of microfabricated devices.

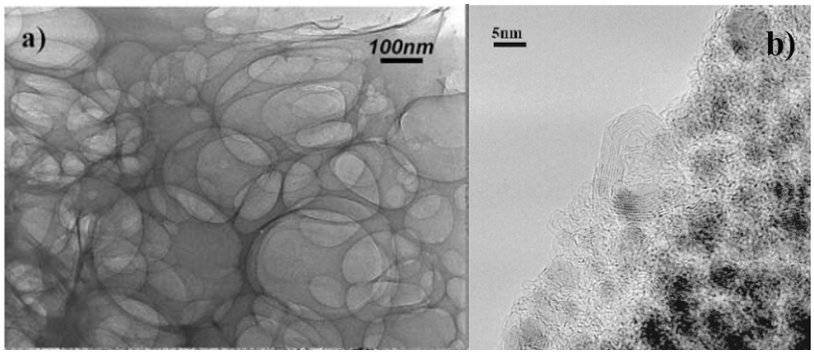

Figure 1.8: a) TEM micrograph of a spongy form of carbon with a negative curved structure catalyzed by traces of Mo-based metallorganic precursor in the inert carrier gas. b) TEM image of a ns-C film containing Ni nanoparticles obtained operating a PMCS with a graphite-nickel composite cathode. Adapted from [72, 85].

Metal seeded ns-C

The interest on porous carbons is not only triggered by its properties as stand alone material but also as matrix for the dispersion of metal nanoparticles. Metal/carbon nanocomposites are complex systems with both fundamental interest and applicative promise in a variety of technological fields (e.g fuel cells, catalysis and energy storage). Supersonic Cluster Beam Deposition has been proposed as a promising technique for the synthesis of metal-carbon nanocomposite materials and ns-C has been shown to represents an ideal matrix for supporting metallic nanoparticles [86]. Even more intriguing, is the possibility of tailoring the structure of ns-C at the nano- and mesoscales by introducing metallic catalysts during the cluster formation process in the PMCS [31, 87, 88]. Nanoparticles of transition metals (Ti and Ni), included in the cluster assembled ns-C matrix by using a graphite-metal composite cathode, are known to promote the formation of ordered carbon structures consisting of open and defective graphitic cages as well as of graphitic ribbon-like structures (see figure 1.8b) [31, 85]. Moreover it has been shown that is possible to control the porosity of the ns-C by poisoning the inert carrier gas with Mo- or Co-based metallorganic precursors [87, 88]. In the presence of traces of metallorganic species, ns-C grows with a negative curved spongy structure (see figure 1.8a), typical of schwarzites, originated by three dimensional fully connected sp2 networks and characterized by a meso- and macroporosity which could be very interesting for catalysis and electrochemical applications.

Chapter 2

Electrochemistry: why? and how?

Electrochemistry is attracting great attention in the fields of nanoscience an nanotechnology given that many nano-scale phenomena encountered in biological, chemical and physical processes rely on the interchange of chemical and electrical energy at the solid/liquid interface. Furthermore, the recent advances in material sciences are prompting an unprecedented revolution in the synthesis of material with tailored properties (e.g. nanostructure, porosity) unraveling the relation between the electrochemical and the structural properties of the interfaces, and boosting, for instance, the development of affordable, reliable and clean energy conversion and storage electrochemical systems. In this context, porous materials are the class of materials that seems to have the greatest breakthrough potential.

As one of the pivotal activity of my PhD work deals with the characterization of the interfacial properties of carbon and nickel/carbon porous thin films grown using cluster as building blocks, this chapter provides material that covers the fundamental concepts needed to understand both the basis of the solid/liquid interfacial electrochemistry, with particular emphasis on the Helmholtz double layer (also known as electric double layer), and the features of the techniques employed in the experimental work. The coverage of these topics is limited to what is needed to understand the core of the second part of this thesis and for a more thorough overview one can lean on the references indicated in the text.

2.1 The solid/liquid interface

The solid/liquid interface is a complex system that in general deals with electrochemical phenomena associated with charge separation and charge transfer between the surface of a solid metal or semiconductor (i.e the electrode) and a

liquid environment (i.e. the electrolyte). The most important solid/liquid interface is, probably, the cell-membrane/water interface in living organisms. The chemical and physical processes at this interface control many physiological processes (e.g. the docking of proteins, the transmission of signals and the transport of molecules in and out of the cell) resulting crucial to the functioning of cells, tissues and organs. Apart from life sciences, the electrochemical principles of the solid/liquid interface played a fundamental role in the energy conversion, production and storage field and they were at the basis of the first battery invented in 1800 by Alessandro Volta [89] alternating stacks of copper and zinc disks separated by paper soaked in acid solution. Nowadays, the solid/liquid interface is strictly connected with material sciences and is the core of the development of new environmentally benign solar energy harvesting systems such as water splitting photoelectrochemical cells for the production of hydrogen [90] or cheap yet efficient solar cells (dye sensitized solar cell [91]), which basic components are nanostructured semiconductor oxide materials in contact with an electrolytic solution. Solid/liquid interfacial processes are also pivotal to store chemical energy and convert it into electric energy, or vice versa, in several emerging devices, such as fuel cells and lithium ion batteries. Although these electrochemical systems are conceptually quite simple, a relative slow progress due to the lack of suitable electrode materials, optimized electrode synthesis techniques and appropriate electrolytes is observed. Thus, mastering the solid/liquid interfaces appears today as one of the nanotechnology challenges that most can impact on the transition to a green and sustainable energy system.

The solid/liquid interface is, basically, a junction between an electronic conductor, i.e the electrode, and a ionic conductor, i.e the electrolyte. This particular form of junction is called galvanic circuit and its realization is also called galvanic cell or electrochemical cell. As in electric circuits, current can flow in a galvanic cell crossing the solid/liquid interface and passing from the electrode to the electrolyte and vice versa. Depending on the direction of current flow in the galvanic cell the electrode is named anode (if the current enters in the electrolyte) or cathode (if current exits from the electrolyte). As the current is carried by different species in the two adjacent phases (the electrons and the ions), a continuous flow of carriers cannot cross the solid/liquid interface and, in order to sustain a steady current flow, chemical reactions, also known as electrochemical reactions, occurring at the the electrode surface and involving carriers from both phases are needed. Anodic electrochemical reactions (also known as oxidative processes) involve electrons withdrawal from the ions of the electrolyte while cathodic elec-

trochemical reactions (also known as reductive processes) involve electrons supply to the ions of the electrolyte (a thorough discussion of charge transfer interfacial processes is far beyond the scope of this chapter and can be found in several dedicated volumes, eg. [92, 93]). When the interfacial charge transfer is not electrochemically favored and/or promoted, the electrode/electrolyte interaction is purely electrostatic. As no electrochemical reactions are involved, in this case no current flows across the interface and the charges which, both spontaneously and under the action of an electric potential, approach the interface are electrostatically stored in the so called electric double layer (EDL). EDL presents several features that promoted this particular interfacial process to be the basis of energy storage devices known as supercapacitors (see section 1.2.1). Its relevance to technological applications is even potentially boosted whenever nanoporous electrodes are involved and is therefore the main object of the electrochemical characterization carried out during this PhD project.

2.1.1 Electric double layer

A metal/electrolyte interface in which any accumulation of charge both on the electrode and on the electrolyte cannot be removed by charge transfer (or leakage of charges) represents the simplest solid/liquid electrochemical system. In such a system the excess of charges sufficiently near the interface in one of the two phases attracts electrostatically the accumulation of charge of opposite sign at the other phase boundary to ensure the electrical neutrality of the interface. As result, two parallel layers of charges with opposite signs are formed, i.e. the so called electric double layer (EDL), each on the surface of one of the contacting phases. Once the EDL is formed, this interfacial region constitutes a well defined capacitive region where charge separation occurs. The two layers forming the double layer are a very small distance apart (typically few angstrom) and EDL capacitances can consequently reach very high values (e.g. tenths of μF/cm2).

The earliest studies on the EDL date back to more than 100 years ago and were conducted by Helmholtz [94]. Since then several models, such as the ones introduced by Gouy [95], Chapman [96], Stern [97] and Grahame [98], have been proposed to improve the oversimplified EDL description given by Helmholtz. The model of Helmholtz [94], whose view is reported in the panel A of figure 2.1, treats the EDL as a capacitor, in which a single layer of ions electrostatically attracted on the electrode surface represents one plate (the Helmholtz plane), and the second plate is constituted by the charge of opposite sign accumulated on the electrode surface. The potential drop is assumed to be linear across the

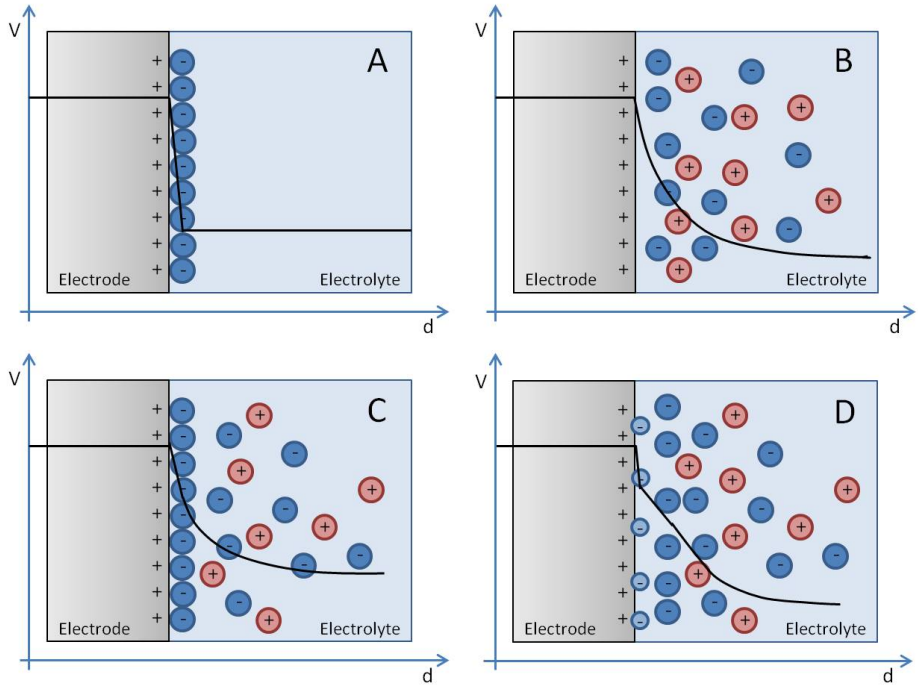

Figure 2.1: Sketch of the electric double layer (EDL) models of Helmholtz (A), Gouy-Chapman (B), Stern (C) and Grahame (D).

distance between the electrode surface and the plane going through the center of the ions forming the Helmholtz plane (i.e. the half of the size of the solvated ions) which therefore represents the distance between the two plates of the capacitor. This model, despite being rather intuitive, is not complete and does not account for many factors such as ions mobility and diffusion in solution and the interaction between solvent dipole moments and the electrode. The contribution of thermal motion of ions near the surface was introduced independently by Gouy and Chapman considering a mathematical model based on combined application of the Boltzmann's energy distribution equation and Poisson's equation [95, 96]. Instead of the rigid compact Helmholtz layer Gouy and Chapman consider a so called diffuse double layer described by a charged electrode surface in contact with a cloud of oppositely charged ions in the solution, the concentration of the oppositely charged ions decreasing with distance from the electrode (figure 2.1B). Ions are assumed to be able to move in solution and their electrostatic interaction

with charges on the electrode is in competition with their Brownian motion in the solvent. The result is still a region close to the electrode surface containing an excess of one type of ions but as consequence of the diffuse layer the electric potential drops exponentially across the interface, which by the way extends deeper in the electrolyte than in the Helmholtz model. Within the Gouy-Chapman model the finite dimensions of the ions are neglected leading to unrealistically high concentrations of counterions near the surface (and an overestimation of the EDL capacity) when high concentrated electrolyte solutions are considered. Gouy-Chapman description was improved by the EDL model proposed in 1924 by Stern [97] who unified the Helmholtz and Gouy-Chapman theories considering a inner compact layer of ions residing close to the charged electrode surface (the Stern layer or Helmholtz layer) and an outer ionic atmosphere extending in the solution similar to the diffuse layer of the Gouy-Chapman model (figure 2.1C). Within Stern's view the double layer capacity is the result of the series combination of the capacity contribution arising from the different layers:

$$\frac{1}{C_{Stern}} = \frac{1}{C_H} + \frac{1}{C_{G-C}} \tag{2.1}$$

However, in case of high concentrated electrolyte the capacity of the rigid layer remains constant while the one of the diffuse layer increases. At very high concentrations (typically above 10^{-3}M solution) the contribution of the Gouy-Chapman diffuse layer to the total capacity is almost negligible and the Stern and Helmholtz models coincide ($C_{Stern} = C_H$). Finally, a further refinement was brought by Grahame in 1947 [98]. This latter model distinguishes three different EDL regions adding to the Stern (now named OHP, i.e. Outer Helmholtz Plane) and diffuse layers an even inner layer (named IHP, i.e. Inner Helmholtz Plane) of ions which are specifically adsorbed on the electrode surface. These ions lose their solvation shell reducing their size and therefore can approach the electrode closer.

Within the limit of very high concentrated electrolyte, the commonly accepted expression for the EDL capacity goes back to Helmholtz and is possible to simply assume that the charge of the metal surface is compensated by a thin layer of counterions residing on the surface of electrode. The resulting capacity is given by

$$C_H = \epsilon \frac{S}{r} \tag{2.2}$$

where S is the area of the electrode surface in contact with the electrolyte, r is the

radius of the solvated counterions, which in practical situation is in the order of few angstroms, and ϵ is the dielectric constant of the electrolyte. From equation 2.2 it appears clear that EDL capacity is directly proportional to the extension, i.e. the geometry, of the electrode surface and that increased capacity values can be reached employing large specific-area electrodes such as electrodes with pronounced surface roughness or porous electrodes. Among the latter, nanoporous electrodes are particularly interesting systems characterized by dramatic enlargements of the specific surface areas and with electrochemical properties strictly bonded to their porous structure. However, nanoscale porosity can lead to extremely complex interface morphologies in which the specific surface area is larger than the electrochemical active area due to limited electrolyte accessibility in to pores. In order to form the EDL on the overall geometric interface both proper pore architectures (e.g. size and shape of the pores) and proper electrolyte features are needed. Liquid confinement inside nano pores provides unique conditions that strongly complicate the solid/liquid interfacial electrochemistry and, despite the physico-chemical mechanisms governing the behavior of liquids inside complex nanostructure are still not quite clear, the major advances in the field are reported and discussed in a couple of recent reviews by Chung and coworkers [99, 100]. Along with the anomalous EDL capacity enhancement observed in carbide derived carbons with unimodal micropores smaller than 1 nm that challenged the long-held axiom that pores smaller than the size of solvated electrolyte ions are incapable of contributing to charge storage [101, 102], one of the most interesting features of the EDL at nanoporous electrodes is known as EDL overlapping. As shown in figure 2.2, in nanoporous systems the shape of the interface between the electrical double layer and the bulk solution phase shifts from the flat to the porous and vice versa as the concentration of electrolyte varies over a certain characteristic value, which is closely related to the pores diameter [103]. Lower electrolyte concentration as well as smaller pores lead to EDL overlapping and result in loss of EDL capacity indicating that the use of nanoporous electrode does not automatically boost the charge stored in EDL and that further phenomena arising from the nanostructure need to be considered.

2.2 Probing the nanostructure

It is now clear that the physical properties of the electrode, such as porosity, specific surface area and surface roughness and morphology, are strictly related to its electrochemical properties and strongly affect its interfacial behavior. Thus, the

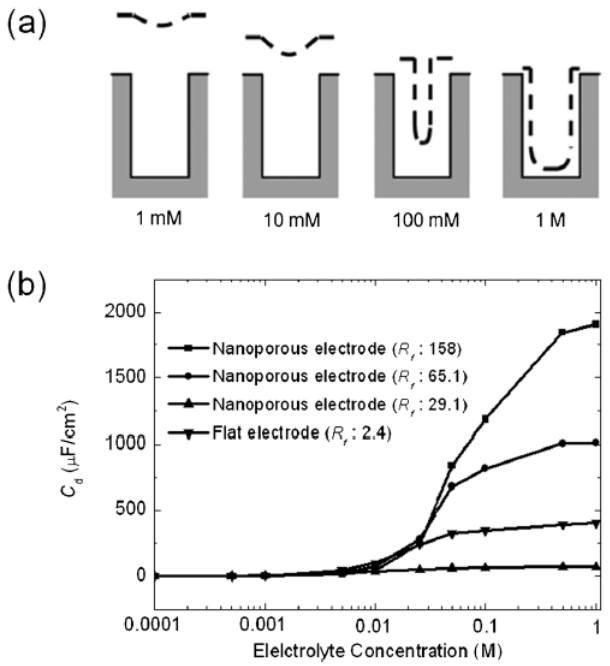

Figure 2.2: (a) Schematic diagram displaying the shape of the electrical double layer (dotted line) as function of the electrolyte concentration. (b) Differential capacitances of flat and nanoporous Pt electrodes in various electrolyte concentrations at -0.5 V versus Hg/Hg2SO4. Capacitances were calculated with respect to geometric area (flat electrode, 3.14 10^{-2} cm^2; porous electrode, 7.85 10^{-3} cm^2) [103].

electrochemical characterization of the solid/liquid interface can provide relevant insights about the electrode material structural properties with a sensibility that, if the ions of the electrolyte are considered as the experimental probes, can be in the nanometer range. Electrochemical methods attracted great attention over the last decade due to the explosion of the research on several energy conversion systems based on electroactive porous materials, and electrochemical experimental techniques as cyclic voltammetry (CV) and impedance spectroscopy (EIS) have been shown to give powerful information on the electrode material physicochemical properties [104, 105].

In the next sections the main features of the electrochemical experimental techniques employed in this work will be briefly presented and discussed. References to topical papers will be provided in order to furnish the interested reader

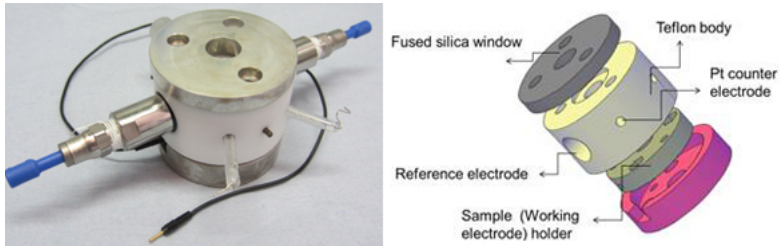

Figure 2.3: The home built electrochemical cell used in this work for the characterization of the interfacial properties of the electrodes synthesized by SCBD.

with the literature materials to deepen the understanding of these topics.

2.2.1 Electrochemical cell

The core of every electrochemical experiment is the electrochemical cell, i.e. the cell were the junction between the electronic and the ionic conductors is realized. Basically, an electrochemical cell is a closed environment filled with a liquid electrolyte where the electrode to be analyzed (i.e. the working electrode, WE) is immersed. Electrochemical cell can be realized in several configurations which mainly differ from each other according to the number of electrodes that are present in addition to the WE. The most common configuration is the three-electrodes one which is also the configuration adopted in this work. This configuration require two further electrodes immersed in the electrolyte, named counter electrode (CE) and reference electrode (RE). The CE is the electrode in the cell that completes the current path (current flows in the electrolyte between the WE and CE). Usually the CE is simply the current source or sink and typically no processes of interest (under study) occur at its surface. It is composed by relatively inert materials like graphite or platinum. RE is the electrode that serves as experimental reference point for the potential measurement. It should, therefore, hold a constant (and well known on an absolute scale) potential during testing. This is accomplished by employing a reversible redox system (a further solid/liquid interface) and having, ideally, no current flow through it. Several RE are commonly used and commercially available: Silver/Silver Chloride, Saturated Calomel, Mercury/Mercury Oxide, Mercury/Mercury Sulfate, Copper/Copper Sulfate, etc.
Figure 2.3 shows a picture of the home built electrochemical cell employed in this work for the electrochemical characterization of the cluster assembled electrodes grown by SCBD. The cell is equipped with a platinum coil as CE and a platinum

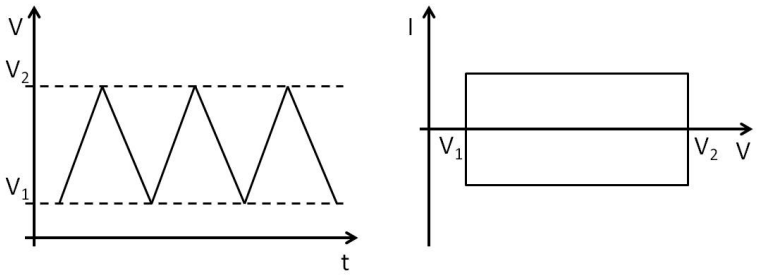

Figure 2.4: Triangular potential waveform applied to the WE during a CV measurement (left panel) and CV plot of an ideal capacitor (right panel).

wire or a SCE (Saturated Calomel) as pseudo reference and reference electrode, respectively. The area of the WE in contact with electrolyte inside the cell is ca. 0.8 cm^2.

2.2.2 Cyclic voltammetry

Cyclic voltammetry (CV) is an electrochemical technique by which the potential of the WE is linearly swept at a fixed scan rate (V/s) back and forth between two fixed switching potentials measured versus RE. This ramp can be applied over several number of cycles resulting in a triangular potential waveform (see the left panel in figure 2.4). The current developed in the cell by the potential scan is the monitored variable. It is measured between the WE and the CE and than plotted as function of the potential (i Vs. V). CV is a powerful diagnostic tool and is often the first experiment performed in an electrochemical study as it rapidly enables to detect the presence of Faradaic interfacial processes (which are identified by current peaks), to distinguish between reversible and irreversible ones and provide precise information about the charge transfer kinetics. Since the focus of the electrochemical characterization of this work deals in EDL charge storage, the treatise on cyclic voltammetry analysis in redox systems will be skipped (one can find thorough treatment in dedicated textbooks, eg. [92, 93]) and only the case of non-Faradaic electrodes will be considered.

A polarized electrode/electrolyte interface in absence of Faradaic reactions is characterized by the presence of an EDL: no current flows through the interface that ideally behaves as a parallel plate capacitor. In such a system, assuming that the capacitance C is constant, the charge or discharge current i is proportional to the derivative of the applied potential V according to equation 2.3 and is

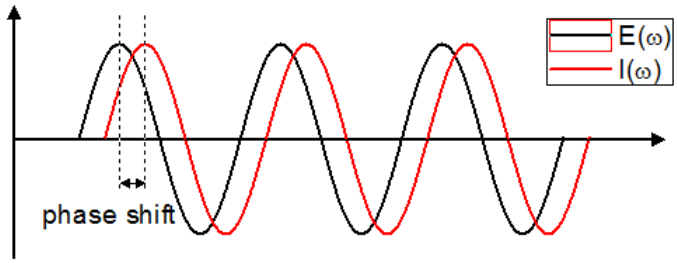

Figure 2.5: Sinusoidal current response in a linear system.

constant when the potential V is swept at a fixed scan rate s as in the case of cyclic voltammetry.

$$i = C\frac{dV}{dt} = Cs \tag{2.3}$$

Therefore the CV plot of an ideal polarizable electrode presents a rectangular shape without current peaks (see the right panel in figure 2.4). The current switches instantaneously from positive to negative as the voltage scan rate is changed from increasing to decreasing. The capacitance can be easily calculated by equation 2.3 and, by integration of a segment of the CV curve, the stored charge can be estimated. If a resistance is present in series with the capacitor, it causes slow rise in the current and rounds two corners of the rectangle at the beginning of the charge and discharge process. Real situations significantly differ from the ideal one and, in particular in case of porous electrode, usually the accessible capacitance is dependent both on the scan rate and on the bias potential of the WE, due to fundamental reasons connected with the structure of the double layer and the adsorption of ions on electrode surface [98]. Porous interface generally leads to the capacitance becoming diminished with increasing s meaning that, over a given voltage range in CV, the extents of charge acceptance or delivery become diminished with increasing sweep rate. These effects depend directly on the conductivity of the electrolyte in the pores of the electrode and, to some extent, on the conductivity of the electrode matrix material [106].

2.2.3 Electrochemical impedance spectroscopy

Electrochemical impedance spectroscopy (EIS) is a very sensitive electrochemical technique that, in recent years, has found widespread applications in the field of characterization of materials and devices. EIS is essentially a steady-state

technique that with a single experimental procedure is capable of accessing relaxation phenomena whose relaxation times vary over many orders of magnitude. It is well described and discussed in several books (e.g. [107]) and review papers (e.g. [108–110]). Briefly, in EIS experiments a small amplitude sinusoidal voltage perturbation (typically in the order of few mV rms) is applied to the WE over a wide range of frequencies (typically from 10^6 to 10^{-3} Hz) and the current between the WE and CE is monitored. If the amplitude of the input sine wave perturbation signal is small enough to keep the selected state of the system unchanged, than the linear response approximation is satisfied and is possible to calculate the complex impedance of the system. Considering an excitation signal E of the form

$$E(\omega) = E_0 exp(j\omega t) \tag{2.4}$$

where E_0 is the amplitude of the signal and ω the radial frequency, within the linear approximation, the response signal I will have the form

$$I(\omega) = I_0 exp(j\omega t + \phi) \tag{2.5}$$

with a different amplitude I_0 compared to the excitation signal and a shift ϕ in the phase (see figure 2.5). The AC analog of the Ohm's law allows to calculate the complex impedance of the system $Z(\omega)$ as

$$Z(\omega) = \frac{E(\omega)}{I(\omega)} = Z_0 exp(j\phi) = Z_0(cos\phi + jsin\phi) = Z_{real} + jZ_{im} \tag{2.6}$$

which is commonly presented as plots of $-Z_{im}$ vs. Z_{real} (i.e Nyquist plot) or as $log|Z|$ and ϕ vs. $log\omega$ (Bode plot).

Experimental EIS data are typically interpreted in term of equivalent electric circuit models (electric circuits with the same impedance spectrum of the analyzed system) constructed from passive circuital elements such as resistors, capacitors and inductors (which complex impedance are R, $\frac{1}{j\omega C}$ and $j\omega L$, respectively). The values and arrangement of the circuit elements ideally represent physical properties or interfacial phenomena and, therefore, circuit analysis must consider the nature of the overall current flowing through the interface meaning that the circuital elements in the model must have a basis in the physical electrochemistry of the system. Different electric circuits can yield a mathematically equivalent frequency response and a good fit does not, in itself, validate the model used. In general, for electrochemical systems the overall impedance is the sum

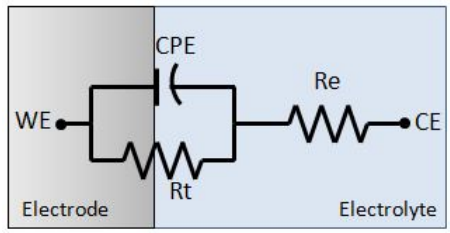

Figure 2.6: Equivalent electric circuit corresponding to an electrode/electrolyte interface. CPE, R_f and R_e model the EDL capacity, the charge transfer resistance and the electrolyte resistance, respectively.

of an interfacial impedance plus the electrolyte resistance. In the most general case (reported in figure 2.6) the overall current at the interface is the result of both a Faradaic current related to redox species and charging current related to the EDL. Thus, the interface impedance can be ideally modeled with an electric circuit composed by a solution resistance R_e in series with a parallel combination of a double layer capacitor C_{dl}, which is modeled by the CPE element (see section 2.2.3), and a charge transfer resistance R_f which is infinite if no Faradaic reactions are involved and the EDL is the only electrochemical features of the interface.

In order to briefly introduce some basic concepts of EIS data representation, the Nyquist plot of the complex impedance spectrum in the frequency range between 10^5 and 10^{-2}Hz of the circuit of figure 2.6 in the case that $R_e = 100\Omega$, $R_p = 1000\Omega$ and $CPE = C = 100\mu F$ is shown in figure 2.7. Even if the frequency at which the complex impedance is recorded is not shown explicitly, each point in a Nyquist plot represents the complex impedance of the circuit at one frequency. As the complex impedance of an electrochemical system generally increases with decreasing frequency, low frequency data are on the right side of the plot and high frequency portion of the impedance spectrum is near the origin, with the frequency that gradually decreases moving from the left to the right side of the Nyquist diagram. The qualitative shape of the complex impedance in a Nyquist plot gives important information about the electrochemical processes occurring at the electrode/electrolyte interface and is thus the starting point for the equivalent circuit analysis of the system. For instance, a semicircle, as the one shown in the Nyquist plot of figure 2.7, is characteristic of a charge transfer process between the two phases of the interface, which can be therefore modeled by a single parallel RC network (see figure 2.6). To obtain the circuit parameters, the

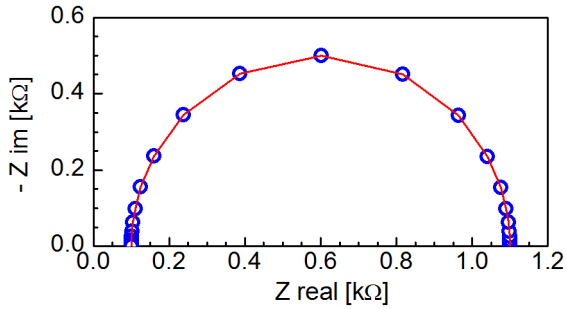

Figure 2.7: Nyquist plot of the complex impedance of the electric circuit of figure 2.6 where $R_e = 100\Omega$, $R_p = 1000\Omega$ and $CPE = C = 100\mu F$.

fitting of the equivalent impedance of the model to the experimental data should be performed. Nevertheless, some of the equivalent circuit parameters can be inferred directly by the plot. In particular, real axis intercepts are ascribable to the ohmic resistances of the equivalent circuit. In the case of the impedance spectrum of figure 2.7 referred to the circuit of figure 2.6, the high and low frequency real axis intercepts give the value of the resistance in series with the electrochemical interface ($Re = 100\Omega$) and of the charge transfer resistance ($Rp = 1000\Omega$, i.e. the diameter of the semicircle), respectively.
Common interfacial responses are often more complicated and very complex equivalent circuits are needed to interpret the experimental data. Furthermore, not all the measured impedances can be described in terms of traditional passive elements and it is necessary to introduce in the circuit new elements (the so called distributed elements) such as the Warburg impedance Z_W, which basically is an infinite series of RC parallels that accounts for mass transfer from the solution bulk to the electrode surface, and the Constant Phase Element, Z_{CPE}, an ad hoc element used to model the complex impedance of the EDL formed at rough and/or porous electrode surfaces.

CPE

The impedance response of electrochemical interfaces rarely shows the ideal behavior and typically reflects a distribution of reactivity, resulting from distributions of physical properties including structure, dielectric constants and resistivity, that is represented in the equivalent circuit analysis as a constant phase element (CPE). It is an empirical model often used to fit impedance data aris-

ing from a broad range of experimental systems. The impedance of the CPE is described mathematically as

$$Z_{CPE} = \frac{A}{j\omega^{\alpha}} \tag{2.7}$$

where A and α are empirical constants. When α is 1, 0, -1, and 0.5, the CPE reduces to a capacitor, a resistor, an inductor and a Warburg element, respectively. However, in most practical situations, CPE is thought of as the capacitive response of real world electrochemical interfaces and α is in the range between 0.5 and 1. Despite being empirically justified, CPE lacks any physical basis and the controversial hypothesis on its physical origins are thorough treated in a couple of recent papers [111, 112]. It is generally accepted that constant phase element behavior may be attributed to the distribution of physical properties in films and, as reported in many theoretical (e.g [113]) and experimental (e.g. [114]) published works, that the CPE impedance response can be related both to the EDL formed at interfaces which are not perfectly smooth but has some roughness and/or porosity, and to capacitance dispersion of interfacial origin, connected with slow adsorption of ions and chemical inhomogeneities of the surface. Furthermore CPE behavior is often associated to electrode fractal geometries and a number of researches tried to unravel the relation between the fractal dimension of the electrode surface and the CPE α exponent (e.g. [115, 116]). Methods for determination of effective capacity from CPE parameters have been extensively explored. The most employed relationships are derived by Brug [117] and Hsu and Mansfeld [118] and are reported, according to [119], in equations 2.8 and 2.9, respectively.

$$C = A^{1/\alpha} R_e^{(1-\alpha)/\alpha} \tag{2.8}$$

$$C = A^{1/\alpha} R_f^{(1-\alpha)/\alpha} \tag{2.9}$$

where R_e is the Ohmic resistance in series to the CPE and R_f represent the resistive contribution in parallel to the CPE. Even in this case there is no general consent on the choice of the proper formula and, only recently, Hirschorn and coworkers [119] tried to unambiguously illustrate the importance of using the correct equation that corresponds to a given type of electrochemical system suggesting to use the Brug equation only for a surface distribution of physico-chemical properties and the Hsu and Mansfeld equation only for electrode characterized by a distribution of physico-chemical properties in the direction normal

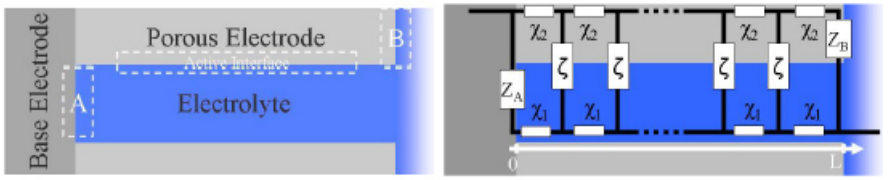

Figure 2.8: Porous electrode: the three interfacial regions that are of electrochemical interest (left panel) and a transmission line (right panel). χ_1 , χ_2 and ζ are the repeating circuit blocks on the rails and the steps. Z_A and Z_B correspond to impedances across the interfaces A and B defined in the left panel. Readapted from [120].

to the electrode surface (e.g. changes in the electrode resistivity across the film thickness).

Porous electrode: transmission line model

The great interest in increasing the real interface area of electrochemical systems triggered off the use of porous electrodes. The analysis of porous electrode impedance is extremely difficult and distributed circuit elements, explained by the mathematics of transmission lines (TLs), are often employed for proper modeling. A transmission line that models in generic form the impedance of a cylindrical pore of length L is shown in the right panel of figure 2.8. χ_1, χ_2, ζ, Z_A and Z_B are defined as subcomponents that can take various forms. These may be as basic as single resistors and as complicated as necessary. χ_1, χ_2 and ζ represent the solution impedance, the bulk impedance of the porous electrode material, and the impedance of the active interface, respectively. Z_A and Z_B are the impedances of the two interfaces A and B shown in the left panel of figure 2.8 [120]. In the general case, χ_1 and ζ are function of the distance from the base of the electrode due to the potential distribution in the porous electrode and/or the electrolyte concentration distribution in the pore. The first theory of porous electrode dates backs to 1960s and was introduced by deLevie who calculated analytically the complex impedance of a general porous electrode using a transmission line [121, 122]. Briefly, if a simplified single-pore model, as the one reported in figure 2.8, in which pores are assumed to have a cylindrical shape with length l and radius r is considered and if the electrolyte concentration distribution and the potential distribution in the pore are neglected, deLevie derived

the impedance of one pore to be

$$Z_{deLevie} = (R_0 Z_0)^{(1/2)} coth(l\sqrt{\frac{R_0}{Z_0}}) \tag{2.10}$$

where R_0 is the electrolyte resistance per unit pore length, Z_0 is the interfacial impedance per unit pore length and l is the pore length. Considering n pores and the electrolyte resistance outside the pore R_e, the impedance of the overall electrode results to be

$$Z = R_e + \frac{Z_{deLevie}}{n} = R_e + \frac{(\rho Z_{eq})^{1/2}}{\sqrt{2}\pi n r^{(3/2)}} coth(l\sqrt{\frac{2\rho}{r Z_{eq}}}) \tag{2.11}$$

where ρ is the electrolyte resistance and Z_{eq} is the interfacial impedance per surface unit. This model has been subsequently generalized by several authors who took in to account the presence of concentration gradient and a potential drop in the pores [123, 124], the influence of various pore shape and geometries [125, 126], the effect of pore size distribution [127], inhomogeneities of the electrode surface [128]. Recently transmission lines have been applied to the interpretation of EIS data of dye-sensitized solar cells, quantum dot-sensitized solar cells and organic bulk heterojunction solar in several papers published by Bisquert and coworkers who demonstrated the great potential of TLs in determining the internal features of the devices [105].

Part II

Results and discussion

Chapter 3

Porous carbon grown by SCBD

The second part of this thesis is devoted to the presentation and the discussion of the experimental results related to the synthesis of carbon based cluster assembled thin films and the characterization of their electrochemical capacitive behavior. By this chapter the morphological, structural and electrochemical properties of porous carbon grown by SCBD will be exposed as function of deposition time (i.e. ns-C thickness), post deposition thermal treatment and current collector morphology. Two different electrolyte media are employed in the study of the electric double layer formed at ns-C interface: an aqueous solution of potassium hydroxide (KOH) and room temperature ionic liquids (RTILs). The most of the established work is reported in the form of two manuscripts submitted to journals for publication. These manuscripts provide also the review of the background to which the single sections of this chapter belong as well as the description of the experimental apparatus and methods.

3.1 Ns-C: overview

The general features of the cluster assembled carbon (ns-C) grown by the supersonic cluster beam deposition (SCBD) of clusters produced in a pulsed micro plasma cluster source (PMCS) have been already introduced in section 1.2.2. Hereafter, an overview of the typical morphological and structural properties of the ns-C, as obtained by means of atomic force microscopy (AFM), Raman spectroscopy and x-ray photoelectron spectroscopy (XPS), is presented. The aim of this section is to give a general understanding of the cluster assembled carbon properties arising from the particular deposition regime employed in this thesis. A thorough discussion about the specific structural and morphological properties of the ns-C thin films used in my PhD work as electrode material can be found

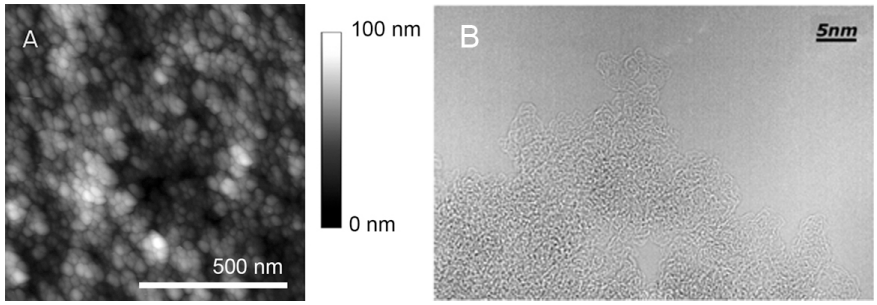

Figure 3.1: AFM surface topography (panel A) and TEM micrograph (panel B, reproduced from [129]) of an as deposited ns-C film grown by SCBD.

in the manuscripts reported in sections 3.2.1 and 3.2.2.

Ns-C exhibits a surface morphology characterized by nanograins as shown by the typical surface topography map of a ns-C film reported in figure 3.1A. The granular nature of the film is characteristic of cluster assembled materials [38, 39] and is the consequence of the low kinetic energy of the clusters deposited by SCBD and of the ballistic deposition regime, where dispersed clusters impact on the surface avoiding substantially fragmentation and with marginal diffusion and relaxation processes occurring after landing [25, 40].
The TEM micrograph of ns-C reported in figure 3.1B highlights a random assembly of highly curved graphene sheets interlinked and aggregated to form a disordered and irregular nanostructure [129]. This structure suggests poor mechanical properties since clusters do not coalesce during the deposition because of their low kinetic energy. However, for the same reason, these materials are extremely porous and have very high effective surfaces, suggesting promising properties toward their use in electrochemical energy storage applications.
The highly disordered graphitic structure is evidenced also by the ns-C typical Raman spectrum (figure 3.2A). Two main features are observable: (i) a broad peak at approximately 1350 cm^{-1} and (ii) a peak at about 1550 cm^{-1} related to the D band and the G band of graphite, respectively. The overall shape of the spectrum is consistent with a highly disordered structure characterized by substantial dominance of sp2 hybridization [130–133]. It has been shown [131, 132] that Raman spectroscopy performed in situ on nanostructured carbon films produced by SCBD in UHV conditions, highlights the presence of a large quantity of sp linear carbon structures in the films (giving origin to peaks at 2100 and 1980

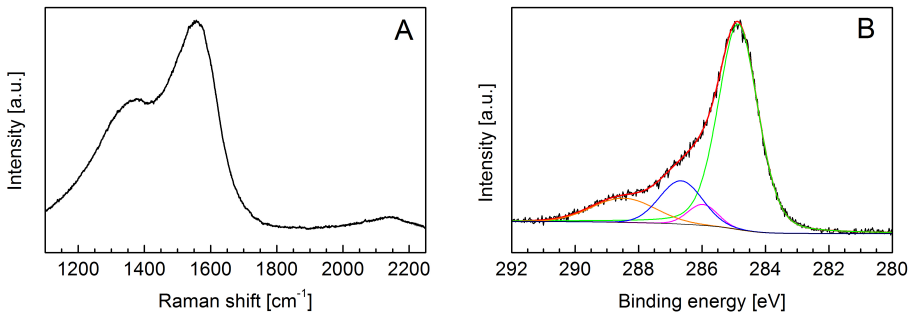

Figure 3.2: Raman spectrum (A) and C1s x-ray photoemission line (B) of an as deposited ns-C film.

cm^{-1}). However sp carbon clusters are quite reactive and are almost completely destroyed after ns-C film exposure to air.
The C1s core-level photoemission line of ns-C is reported in figure 3.2B. C1s peak is broad and asymmetric with a main component occurring at a binding energy of ca. 284.8 eV, ascribable to the C-C bonds in graphite [134]. Other components placed at higher binding energies (286, 286.6 and 288.5 eV) are needed to mathematically reconstruct the whole C1s XPS spectrum. These components are ascribable to the presence, on the surface of ns-C, of carbon directly bound to oxygen (C-O, C=O and O-C=O, respectively).
Ns-C density has been calculated by the correlation between the nominal thickness (i.e. the amount of deposited material) measured in-situ by a quartz crystal microbalance (operated with $1 g/cm^3$ as material density) placed closed to the sample and the thickness of ns-C measured ex-situ by AFM in correspondence of the film step as the average distance between the film surface and the substrate. A linear relationship has been found between the thickness measured by the two different techniques, meaning that the amount of deposited carbon is finely controllable during the synthesis process (see figure 3.3A). A ns-C density of about $0.5 g/cm^3$ has been estimated by the best fit parameters, about a quarter of the density of the bulk materials (ca. $2.2 g/cm^3$ for graphite). This finding confirms the porous nature of the carbon deposited by SCBD which drives the interest in the study of its electrochemical properties.
Surface root mean square roughness (i.e. the standard deviation of surface heights) linearly increases as function of the film thickness (figure 3.3B). It is known that the surface roughness of cluster assembled materials strongly influ-

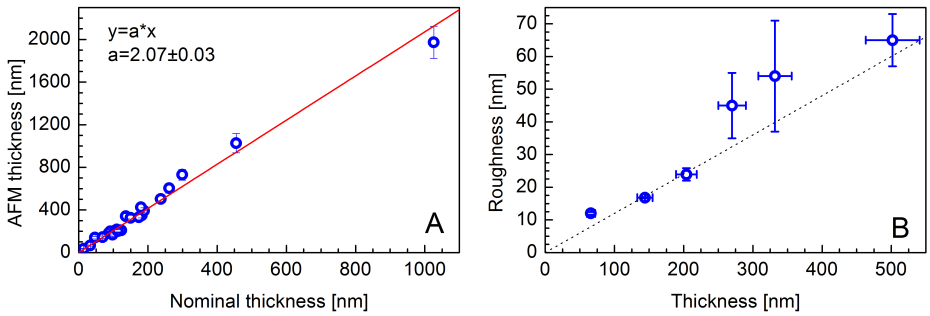

Figure 3.3: (A) Linear correlation between the ns-C step measured ex-situ by the AFM and the nominal ns-C thickness measured in-situ by the quartz crystal microbalance. (B) Ns-C surface roughness evolution at increasing thickness.

ences their wettability [135, 136]. Its control and its tuning at the deposition stage can thus result crucial for the soaking of ns-C based electrodes in the electrolyte. Even if the ns-C thin films deposited in this work have not been characterized by sessile drop method, previous measurements [135] showed that, although the overall hydrophilic character of ns-C is preserved, the contact angle of water on the ns-C surface varies with ns-C surface roughness.

3.2 Ns-C: electrochemical energy storage

The characterization of the electric double layer (EDL) formed at the interface between ns-C and an electrolyte has been selected as route to assess the electrochemical energy storage properties of the cluster assembled carbon grown by SCBD. To this end, an home built electrochemical cell dedicated to the electrochemical characterization of cluster assembled carbon has been designed (see section 2.2.1) and working electrodes featuring ns-C thin films as active material have been fabricated employing nickel as metal current collector. The choice of the nickel is determined by its electrochemical stability, i.e. the absence of Faradaic processes, in the potential window in which the electrodes are characterized. A sketch of the working electrodes can be seen in figure 3.4. Electrochemical characterizations have been carried out by means of cyclic voltammetry (see section 2.2.2) and electrochemical impedance spectroscopy (see section 2.2.3).

First of all, to optimize the electrode fabrication process and compare the ns-C

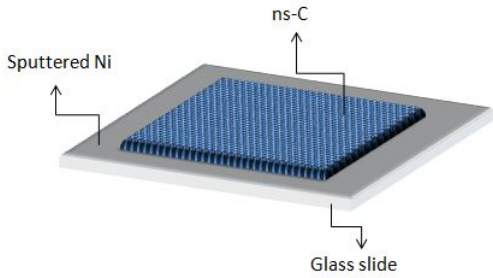

Figure 3.4: Sketch of the ns-C electrode design (electrode dimensions are 15x15 mm^2).

performances with the ones of the porous carbons commonly used as active material in supercapacitors (see section 1.2.1), a standard aqueous ionic conductor widely utilized in supercapacitors has been employed as electrolyte. Afterwards, room temperature ionic liquids (RTILs) have been tested as electrolyte due to their promising properties, such as high thermal stability and wide electrochemical window. The obtained results encouraged toward the use of ns-C grown by SCBD as active material for energy storage electrodes hosted in planar micro electromechanical devices and inspired the design of a ns-C based planar supercapacitor employing RTIL as electrolyte.

3.2.1 Ns-C/aqueous electrolyte

EDL capacity of the interface between a ns-C film 200 nm thick and a KOH 1M aqueous solution has been investigated by means of EIS and CV measurements. The experimental data showed specific gravimetric capacity in agreement with other forms of porous carbon materials even if a poor electric contact at the interface between ns-C and nickel current collector was reported. To improve the electrode performance, two different strategies have been employed without affecting ns-C porosity: a short thermal treatment at 300°C, and the deposition of a thin inter layer of nanostructured ns-Ni between the current collector and the active material.

The results of this study are the subject of the following manuscript that has been accepted for publication in Journal of Nanoparticle Research (Springer).

Electrochemical Impedance Spectroscopy on nanostructured carbon electrodes grown by Supersonic Cluster Beam Deposition

Luca Giacomo Bettini, Giorgio Bardizza, Alessandro Podestà, Paolo Milani and Paolo Piseri

Dipartimento di Fisica and CIMaINa, Università degli Studi di Milano, via Celoria 16, 20133 - Milano, Italy

Abstract

Nanostructured porous films of carbon with density of about 0.5 g/cm^3 and 200 nm thickness were deposited at room temperature by supersonic cluster beam deposition (SCBD) from carbon clusters formed in the gas phase. Carbon film surface topography, determined by atomic force microscopy (AFM), reveals a surface roughness of 16 nm and a granular morphology arising from the low kinetic energy ballistic deposition regime. The material is characterized by a highly disordered carbon structure with predominant sp2 hybridization as evidenced by Raman spectroscopy. The interface properties of nanostructured carbon electrodes were investigated by cyclic voltammetry (CV) and electrochemical impedance spectroscopy (EIS) employing KOH 1M solution as aqueous electrolyte. An increase of the double layer capacitance is observed when the electrodes are heat treated in air or when a nanostructured nickel layer deposited by SCBD on top of a sputter deposited film of the same metal is employed as a current collector instead of a plain metallic film. This enhancement is consistent with an improved charge injection in the active material and is ascribed to the modification of the electrical contact at the interface between the carbon and the metal current collector. Specific capacitance values up to 120 F/g have been measured for the electrodes with nanostructured metal-carbon interface.

Nanostructured carbon, nanostructured current collector, supercapacitor, clusters, interface contact, electrochemical impedance spectroscopy

1 Introduction

Nanostructured carbons play a fundamental role in nanotechnology as unique systems in terms of their unprecedented physical properties such as high specific surface area, high porosity and low density. For these reasons they are of great interest for emerging energy storage and energy conversion devices such as lithium batteries, fuel cells and supercapacitors (Aricò et al. 2005; Guo et al. 2008; Simon and Gogotsi 2008). Nanostructured carbons are produced by cathodic arc processes or d.c. magnetron sputtering in the presence of a relatively high pressure of gas, usually nitrogen, to favor the aggregation of sp2 clusters to be incorporated in the films. The embedding of three-dimensional networks, consisting of buckled planes with fullerene-like features, induces the formation of systems with very high values of hardness and elasticity. Their structure consists of a dense and compact array of curved graphene sheets resembling turbostratic carbon but with a nanometer-scale curvature.

A different strategy to grow nanostructured carbonaceous materials is based on the deposition of carbon clusters with low kinetic energy. The growth of films via low-energy cluster beam deposition (LECBD) can be viewed as a random stacking of particles as for ballistic deposition. The resulting material is characterized by a low density compared to that of films assembled by depositing particles at high energies and it shows different degrees of order, depending on the scale of observation. The characteristic length scales are determined by cluster dimensions and by their degree of fragmentation and coalescence after deposition. The low degree of coalescence of clusters does not favor the formation of a hard material, however, it causes a large porosity and surface corrugation which can be beneficial for electrochemical applications.

Electrochemical capacitors, also known as supercapacitors, are devices that store energy thanks to the electrostatic separation of charged species at the interface between a conductive electrode and an electrolyte (forming the so called Helmholtz double layer) (Grahame 1947; Conway 1999; Kötza 2000). Among nanostructured carbons, porous, high surface, low density and chemically inert carbon is of crucial interest in the electrochemical energy storage field (Simon and Gogotsi 2008; Zhai et al. 2011; Frackowiak 2007; Pandolfo and

Hollenkamp 2006; Frackowiak and Béguin 2001). Along with the recent advances suggesting a forthcoming breakthrough of this technology (Simon and Gogotsi 2010; Zhang and Zhao 2009; Chmiola et al. 2010), the study of the Helmholtz double layer formed at the solid/liquid interface is a powerful tool for the characterization of nanostructured interfaces and for the understanding of ion adsorption mechanism in nanoporous materials.

Here we present the electrochemical impedance spectroscopy (EIS) characterization of electrodes formed by cluster assembled nanostructured carbon (ns-C) films deposited by supersonic cluster beam deposition (SCBD) (Milani et al. 2001; Barborini et al. 1999; Piseri et al. 2001; Piseri et al. 2004; Wegner et al. 18; Bongiorno et al. 2006; Bottani et al. 1998; Lenardi et al. 2001). This technique allows the deposition of porous carbon electrodes without employing binders and post deposition activation processes. Porosity of SCBD ns-C grown by PMCS has been measured by Lenardi et al. (Lenardi et al. 2001) from adsorption/desorption isotherms, obtaining a pores size distribution ranging between 20 and 500 Å with maximum at around 34 Å. The specific surface area, measured by means the full BET law, is about 700 m^2/g (Lenardi et al. 2001). Previous studies also investigated the energy storage performance of ns-C and have shown it to be potentially promising in electrochemical applications (Diederich et al. 1999) although a thorough characterization of double layer capacitance performance of this material is still lacking. Two different strategies have been applied here to highlight the interface properties of ns-C electrodes in aqueous electrolyte: a post deposition thermal treatment in air, and the deposition of a nanostructured cluster assembled current collector. We discuss hereafter by electrochemical impedance spectroscopy measurements and equivalent circuit modeling the effect of such treatments on electrode response and their performance for supercapacitor applications.

2 Experimental part

2.1 Electrode preparation

Ns-C films were deposited on 15 x 15 mm^2, 1 mm thick glass substrates previously coated with nickel (thickness ca. 200 nm) which serves as current collector. Nickel deposition is carried out by Ar ion sputtering of a nickel target under vacuum (with an RF magnetron ion

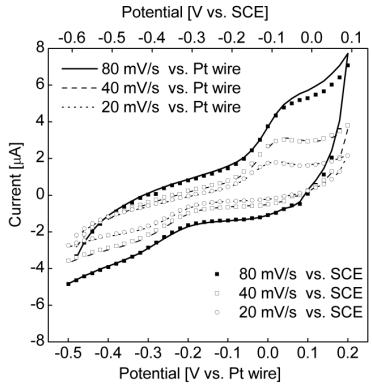

Fig. 1 Cyclic voltammetry of a bare sputtered nickel electrode immersed in KOH 1M aqueous electrolyte performed at three different scan rates (20, 40 and 80 mV/s). Both the CV curves measured employing a Pt wire as pseudo reference electrode (lines) and CV curves measured employing a SCE reference electrode (symbols) are reported. A rigid shift of about 110 mV vs. SCE is found for the Pt wire pseudo reference electrode.

beam source; working pressure ~10^{-4} mbar). Ns-C is deposited on the top of the nickel-coated substrate by SCBD implemented with a Pulsed Microplasma Cluster Source (PMCS), that is described in detail elsewhere (Barborini et al. 1999). We describe here in brief only the main points of its operating principle. A graphite target, inserted in the PMCS, is sputtered by an inert gas plasma from an intense electric discharge confined by exploiting the pressure gradient produced by a He jet impinging on a graphite target (the cathode in the discharge). Sputtered C atoms thermalize within the inert gas and condense to form clusters. The mixture of clusters and inert gas is then extracted from the PMCS through a nozzle to form a seeded supersonic beam of aerodynamically accelerated nanoparticles that are collected on a substrate which is located on the beam trajectory. The cluster kinetic energy is low enough to avoid fragmentation upon landing, and hence a nanostructured film of relatively soft-landing particles is grown with typical density of 0.5 g/cm^3. In the present work ca. 200 nm thick ns-C films have been deposited.

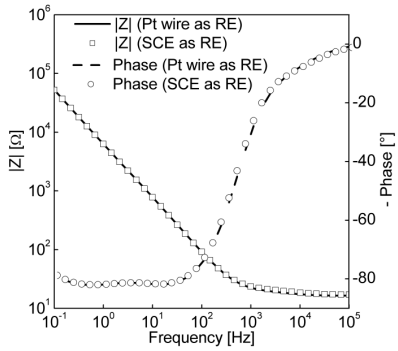

Fig. 2 Bode plot of the complex impedance of a bare sputtered nickel electrode immersed in KOH 1M solution as aqueous electrolyte. Both the spectrum collected employing a Pt wire as pseudo reference electrode (solid and dashed lines) and the spectrum collected employing a SCE reference electrode (open symbols) are reported.

In the case of electrodes with a nanostructured current collector, a film, ca. 20 nm thick, grown by the deposition of Ni clusters generated in the PMCS was deposited by the SCBD apparatus on the sputtered nickel before ns-C deposition.

In this study, post-deposition thermal treatment was performed in air atmosphere in an open joule-heated furnace for 15 minutes at constant temperature (300°C, measured with a K-type thermocouple). When not otherwise specified, the electrodes have been characterized without performing any previous thermal treatment.

2.2 Morphological and structural characterization

Cluster-assembled films were characterized by atomic force microscopy (AFM) using a Multimode Nanoscope IV microscope (Bruker) operated in tapping mode in air (standard single-crystal silicon tips have been used, with radius of curvature 5-10 nm). From AFM topographies, root mean square roughness (i.e. the standard deviation of sampled surface heights) has been calculated. Film thickness has been measured from AFM topography data captured in correspondence of film steps. The measurement is obtained from height histograms as the average distance of topographic height measured at sample positions

covered by the film from the one sampled at positions where the bare substrate was observed. Raman spectra of the films deposited on silicon substrate were recorded by a home-made setup consisting in an Ar ion laser emitting at 514 nm (Spectra Physics, beamlok series 2065-7) as the excitation source, a single monochromator (ActonSP-2558-9N) equipped with a 1200 blaze mm^{-1} grating, a notch filter (RazorEdge® long wave pass filter LP02-514RE-25), and a liquid nitrogen-cooled CCD camera (Roper-Princeton Instruments SPEC10:400B/LN).

2.3 Electrochemical characterization

Electrochemical measurements have been carried out in a three electrodes home-built electrochemical cell equipped with a platinum coil as counter electrode and a platinum wire as pseudo reference electrode. The cell was filled with a KOH 1M aqueous electrolyte solution, and the area of the working electrode in contact with electrolyte inside the cell was ca. 0.8 cm^2. Cyclic voltammetry has been performed in the potential range between -0.5 and 0.2 V vs. the Pt wire reference. Impedance spectra have been acquired with a potentiostat/galvanostat (Gamry Ref 600), in the frequency range from 10^{-1} to 10^5 Hz, under open circuit potential condition (ca. -90 mV vs. Pt wire) at an AC perturbation amplitude of 5mV rms. The equivalent circuit fitting has been performed using Gamry Echem Analyst software. In order to determine the accuracy of the Pt wire as reference electrode, the stability of the Pt pseudo reference in the KOH environment was previously checked by CV and EIS measurements performed on the bare sputtered Nickel electrode in an electrochemical cell equipped both with a standard SCE reference electrode and a Pt wire as pseudo reference. As shown in Fig.1 and Fig. 2, the cyclic voltammetries acquired at three different scan rates, and the complex impedance spectrum collected employing the Pt wire as pseudo reference electrode, are consistent with the measurements acquired employing the SCE as the reference electrode, thus supporting the stability and the suitability, within the bias level of our measurements, of the Pt wire as a reference electrode.

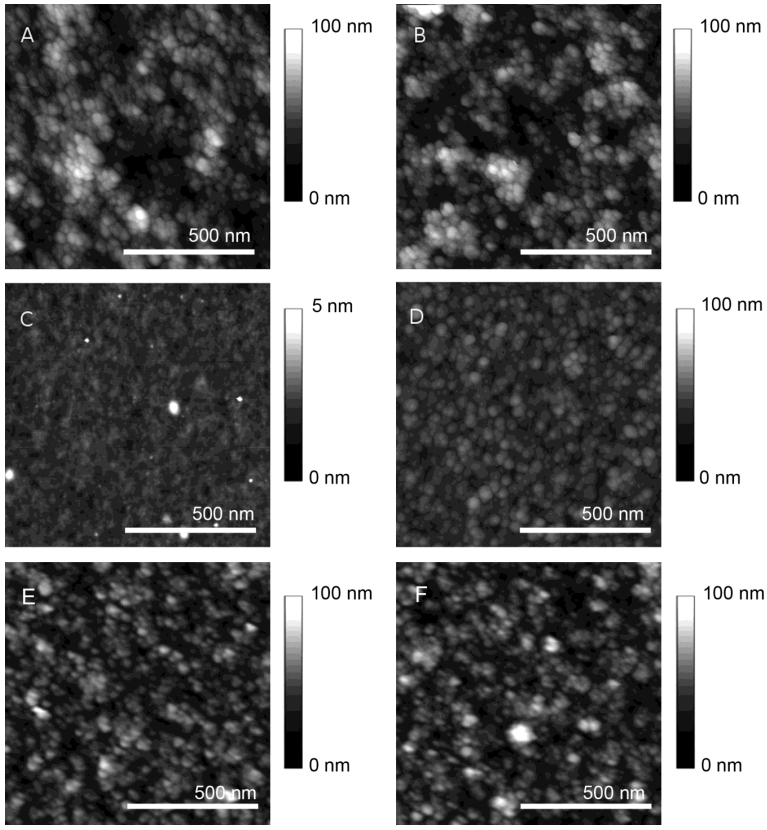

Fig. 3 AFM images of ns-C film as deposited (a), ns-C film post thermal treatment (b), sputtered nickel (c) and ns-Ni (d). All films are deposited on Si/SiO2 substrates. Images e and f reports the AFM surface topography of two ns-C films from the same batch of samples (i.e. deposited simultaneously in a single deposition process), on the top of the flat sputtered Ni of panel c) and of the ns-Ni of panel d, respectively. All image sizes are 1 μm x 1 μm and the height scale is 100 nm except for image c where is 5 nm. Thickness and roughness data of the films obtained by AFM analysis are reported in Table 1.

3 Results and discussion

3.1 Morphology and structure of the electrodes

Fig. 3 shows AFM images acquired on different samples, that are representative of the topographies of the ns-C films and of the Ni substrates prior to film deposition. The vertical scale in panels a, b,d, e and f is the same (100 nm) in order to allow direct comparison of surface morphologies; in panel c, where the surface topography of the sputtered Ni is reported, the vertical scale is 5 nm. Scan size is 1μm x 1μm for all images. The morphology of an as deposited cluster assembled ns-C film can be inferred from the AFM image displayed in Fig. 3a. The AFM data show a surface topography characterized by a disordered stack of nano-scale grains, as typically observed on cluster assembled films (Milani et al. 2001; Piseri et al. 2001). The granular nature of the film is the consequence of the low-energy deposition regime typical of supersonic cluster beam deposition, and of the ballistic deposition regime, where dispersed clusters impact on the surface substantially without fragmentation and with marginal diffusion and relaxation processes occurring after landing (Piseri et al. 2001; Piseri et al. 2004; Wegner et al. 2006). Nanostructured carbon porosity extends over different scales, from the clusters morphology as determined by gas-phase aggregation (beyond the lateral resolution of AFM observation), to the stochastic distribution of nanoparticles throughout the film, as determined by the deposition process. The results of the characterization of the surface morphology of the films performed by AFM are reported in Table 1. Morphological features of ns-C films do not undergo significant modification after the thermal treatment as can be deducted by comparison of Fig. 3a and 3b and from Table 1.

The surface morphologies of the current collector metallic substrates used to prepare the electrodes (respectively for flat sputtered nickel and cluster assembled ns-Ni) are shown in Figs. 3c, d. The nanostructured Ni film deposited by SCBD shows a surface roughness enhancement by a factor ca. 20 compared to the Ni film deposited by sputtering (Table 1). Fig. 3e and 3f show the AFM images of the surface of two ns-C films from the same batch of samples (i.e. deposited simultaneously in a single deposition process), on the top of the

Table 1 Structure parameters of films shown in Fig. 1 as determined by analysis of AFM topography data.

Sample	Thickness (nm)	Roughness (nm)
A	209 ± 17	16.8 ± 2.8
B	205 ± 19	16.1 ± 1.3
C	202 ± 7	0.30 ± 0.05
D	22.7 ± 1.7	6.1 ± 0.2
E	167 ± 15	16.8 ± 2.0
F	167 ± 15	16.8 ± 0.4

two different Ni substrate morphologies shown in Fig. 3c (flat nickel surface produced by sputtering) and 3d (nanostructured nickel film grown by SCBD), respectively. As the images illustrate and the quantitative parameters determined by the analysis of AFM topological data (see Table 1) confirm, the surface roughness of the Ni substrate does not affect the morphological properties of the deposited ns-C.

In Fig. 4, a typical Raman spectrum of ns-C film deposited by SCBD from the PMCS is reported. The top spectrum shows Raman spectrometry performed on an as deposited ns-C film. Two main features are present: a broad peak at approximately 1350 cm^{-1} and a second one at about 1550 cm^{-1}. These structures are respectively related to the D band and the G band of graphite. Spectrum shape is consistent with a highly disordered structure characterized by substantial dominance of sp_2 hybridization (Milani et al. 2001; Robertson 1991; Ravagnan et al. 2007). The bottom spectrum is acquired on a ns-C film heat treated at 300°C for 15 minutes in air. After the thermal treatment, the overall Raman response of the film does not considerably change and the film maintains its highly disordered structure. However, as evidenced by the difference spectrum shown in the inset (Fig. 4), after the heat treatment, the G peak is slightly narrower (FWHM is 111 cm^{-1} after thermal treatment, compared to 129 cm^{-1} before it) and exhibits an upshift (peak position moves from ca. 1577 cm^{-1} to ca. 1580 cm^{-1} by thermal treatment). This evolution is in agreement with a gradual graphitization of the sample. AFM and Raman analysis provide sample parameters in accord with the typical results obtained for SCBD ns-C, thus justifying the assumption of similar values to those obtained from previous studies for the low density and high surface area of ns-C electrode samples (Bongiorno et al. 2006; Lenardi et al. 2001).

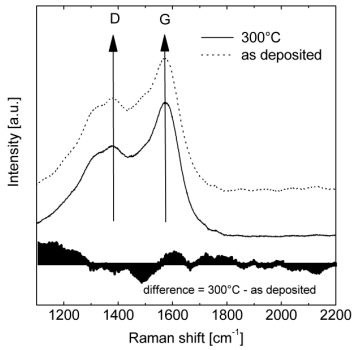

Fig. 4 Raman spectra of ns-C films (ca. 200 nm thick) as deposited (top spectrum) and after thermal treatment at 300°C for 15 minutes in air (bottom spectrum). Spectra show the presence of D peak at approximately 1350 cm^{-1} and G peak at about 1550 cm^{-1}. In the figure, the difference spectrum between the heated ns-C film and the as deposited one is also reported.

3.2 Cyclic voltammetry and electrochemical impedance spectroscopy

Fig. 5 shows the cyclic voltammetry curves acquired at different scan rates (20, 40 and 80 mV/s) at the interface between the as deposited ns-C electrode 200 nm thick and the KOH 1M aqueous electrolyte. CV curves basically have a rectangular shape, i.e. a capacitive response, in the potential region between -0.2 and -0.04 V and they present a slightly distorted shape over the entire potential window with an increase of both the anodic and cathode currents at the extremes of the scanned potential window which can be associated to the presence of slow electron transfer processes probably due to functional groups on the carbon surface or faradic reactions at the nickel substrate surface (Fig.1). These features are especially pronounced in the CV curve acquired at 20 mV/s due to the reduced scan rate. The gravimetric capacity can be derived from equation 1

$$C = \frac{I}{s}\frac{1}{m}, \quad (1)$$

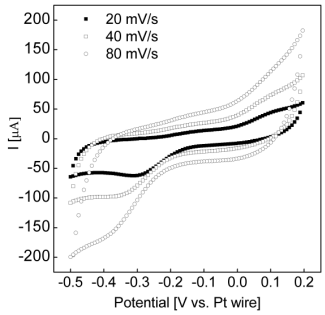

Fig. 5 Cyclic voltammetry of as deposited ns-C electrode immersed in KOH 1M solution as aqueous electrolyte performed at three different scan rates (20, 40 and 80 mV/s) in the potential range between -0.5 and 0.2 V.

where *I* is the average anodic current in the potential range between -0.2 and 0.04 V where no faradic current is present, *s* is the potential scan rate, and *m* is the weight of the carbon material. The calculated gravimetric capacities for the as deposited ns-C electrode are 76, 76, 67 F/g respectively for 80, 40, 20 mV/s scan rate. Electrochemical impedance spectrum of the as deposited ns-C electrode in the KOH 1M aqueous electrolyte solution acquired at the open circuit potential in the frequency range from 10^{-1} to 10^{5} Hz is reported in Fig. 6. The Nyquist plot of the complex impedance shows two different features: a high frequency arc in the frequency range from 0.1 MHz to 10 Hz, and a straight line at frequencies lower than 10 Hz. The high frequency semi-circle is attributed to a mixed response of the contact interface between the sputtered flat Ni current collector and the ns-C and of the Ni/KOH double layer formed after electrolyte infiltration in the porous carbon (Portet et al. 2004; Nian and Teng 2003). The behavior of this contact interface can be simply modeled by an equivalent circuit composed by a parallel combination of a resistance, which accounts for the charge flow through the interface, and a constant phase element, which accounts for the capacitive-like behavior of the interface. The high frequency feature of the complex impedance plot has been fitted by the response curve of an equivalent circuit composed by a resistance, R_u, in series with a parallel combination of a resistance, R_1, and a constant phase element, CPE_1

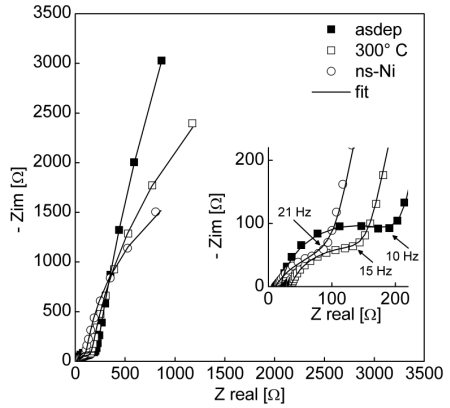

Fig. 6 Nyquist plot of the complex impedance of ns-C electrodes immersed in KOH 1M aqueous electrolyte as deposited (solid squares), after thermal treatment at 300° C for 15 minutes in air (open squares) and with nanostructured nickel (ns-Ni) current collector (open circles). The spectra are fitted (solid lines) with the equivalent circuit of Fig. 7. Fit parameters are reported in Table 2.

(Portet et al. 2004). R_u accounts for the cell overall response at 0.1 MHz (where impedance imaginary part is zero) and is the sum of the ionic conductivity of the electrolyte and the electric conductivity of the electrode. R_1 and CPE_1 are related to the mixed response at Ni/ns-C interface. The low frequency (<10Hz) part of the Nyquist plot is ascribable to the capacitive response of the ns-C/KOH interface. It deviates from the ideal behavior (a straight line with infinite slope) basically due to the porous nature of the electrode, but it confirms the capacitive behavior of the interface and the absence of faradic processes at the open circuit potential (ca. -90 mV vs. Pt wire), in agreement with CV curves. Due to its essentially capacitive character, the complex impedance in this range of frequencies has been fitted by a constant phase element, CPE_2, describing the interfacial double layer, in parallel with a resistance, R_2, that in principle could be associated to the leakage currents. The overall complex impedance behavior is therefore described as the complex impedance of the equivalent circuit shown in Fig. 7 which has been used as a model for data fitting. The high values of CPE_1 and R_1 resulting from the fitting and reported in Table 2 indicate a poor electric contact between carbon and nickel which affects the biasing of the carbon and is

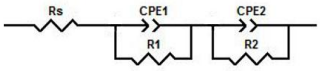

Figure 7 Equivalent circuit used to fit impedance data. Rs includes the resistance of the electrolyte and the bulk resistance of the electrode, the CPE1-R1 subcircuit includes the impedance of the Ni/ns-C interface and the CPE2-R2 subcircuit represents the electrochemical double layer capacity and the leak resistance.

Table 2 Best fit equivalent circuit parameters for the complex impedance of ns-C electrodes.

Sample	Rs (Ω)	CPE1(Ss^α)	αCPE1	R1(Ω)	CPE2(Ss^α)	αCPE2	R2(Ω)
as dep	20	38e-6	0.909	186	487e-6	0.908	43280
300°C	34	105e-6	0.790	123	551e-6	0.912	9500
With SCBD ns-Ni layer	11	495e-6	0.660	112	834e-6	0.960	4500

responsible for double layer formation at nickel interface. This poor contact is probably related to the observed poor mechanical adhesion of the as deposited films. CPE_2-R_2 subcircuit is related to the double layer formation at the Ns-C/KOH interface, which takes place at lower frequencies. The Nyquist plot for the response of the ns-C electrode heated in air at 300° C for 15 minutes (Fig. 6) presents a similar capacitive character at low frequencies, but significantly differs from the Nyquist plot obtained from the as-deposited electrode at high frequencies. The high frequency semicircle exhibits a reduced radius compared to the as-deposited ns-C which suggests an improved contact at the interface between the sputtered nickel and the ns-C which blue shifts from ca. 10 Hz to ca. 15 Hz the frequency at which the capacitive response starts. Spectra's modifications are also appreciable by the equivalent circuit fit. As reported in Table 2, the value of R_s increases after thermal treatment, probably due to oxidation of the nickel surface during the heat treatment in air, CPE_1's alpha exponent moves from 0.9 to ca. 0.6 and R_1 value significantly decreases indicating a beneficial effect of the thermal treatment on the current injection from the sputtered Ni to the ns-C. Besides the changes in the complex impedance spectrum at high frequencies, after the thermal treatment we observed an improved mechanical adhesion between ns-C and Ni as evidence of a structural evolution at the interface between the carbon granular film and the smooth nickel substrate. We hypothesize that the thermal treatment leads to significant interfacial modifications which can be beneficial to electrode

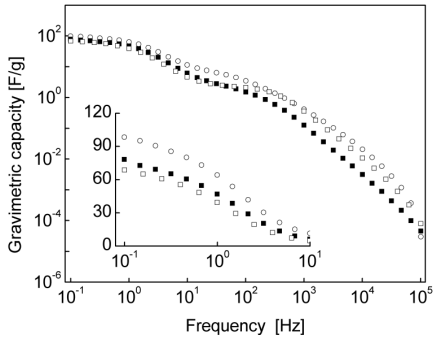

Fig.8 Frequency dependent gravimetric capacity (Equation 2) of ns-C electrodes as deposited (open squares), heated at 300°C for 15 minutes (solid squares) and with nanostructured rough Ni current collector (open circles).

performances without affecting the overall ns-C structural properties. These can proceed via different routes: (i) a thermally induced structural relaxation of the ns-C, (ii) the germination of ordered sp2 structures catalyzed by Ni (De Jong and Geus 2000; Esconjauregui et al. 2009) and (iii) the formation of carburized nickel due to the high solubility of carbon in the metal Ni (it is known that carbon, in presence of oxygen on the surface in the form of CO, could react with nickel, yet at as low temperature as 250°C, forming nickel carbide (Coad and Rivière 1971; Snyder et al. 1980). These heat induced processes may be responsible for structural relaxation at the interface between the two materials resulting in an improved film adhesion and electrical charge injection from the Ni metal current collector to the ns-C film. Similar evolution of the electrode complex impedance is observed when a thin film, ca. 30 nm thick, of cluster assembled Ni is deposited by SCBD between the sputtered nickel and the ns-C. The Nyquist plot of the complex impedance of the electrode with nanostructured Ni (ns-Ni) current collector, reported in Fig. 6, shows an high frequency arc with even further reduced radius in comparison to the as-deposited and heated electrodes with flat current collector. The reduced radius, which shifts at ca. 21 Hz the frequency at which the imaginary impedance part start increasing linearly, is interpreted as the sign of an interface contact enhancement obtained by the improved matching between the current collector and the active material surface texture achieved without post deposition treatments. The equivalent

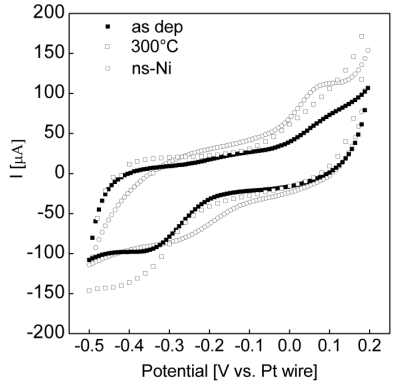

Fig.9 Cyclic voltammetry of ns-C electrodes as deposited (solid squares), heated at 300°C for 15 minutes (open squares) and with ns-Ni current collector (open circles) immersed in KOH 1M solution as aqueous electrolyte performed at 40 mV/s in the potential range between -0.5 and 0.2 V.

circuit parameter R_1 determined by data fitting and reported in Table 2 highlights this evolution moving from ca. 190 Ω for the as deposited ns-C electrode to ca. 110 Ω in case of ns-C electrode with nanostructured current collector deposited by SCBD. The frequency dependence of gravimetric capacity is reported in Fig. 8 for as deposited and heated electrodes, and is described by equation 2

$$C(f) = -\frac{Z'(f)}{2\pi f\,|Z(f)|^2}\frac{1}{m}, \quad (2)$$

where f is the frequency, Z' is the impedance imaginary part and m is the weight of the ns-C. Post deposition thermal treatment does not strongly affect the capacitance of the electrodes in the low frequency domain even if a slight increase is observed after the thermal treatment. The major consequence of the thermal treatment is a decrease of ns-C electrode capacity in the high- and mid-frequencies regime where, as previously mentioned, the adhesion between active material and current collector is crucial for charge injection in the electrode material. The improvement of such contact is crucial for an efficient double layer formation and an enhancement of the specific gravimetric capacitance value extrapolated at 0.1 Hz from ca. 70

F/g to ca. 100 F/g is observed when a nanostructured current collector is employed. These values are in agreement with the gravimetric capacity values calculated from the CV curves acquired at 40 mV/s on the three different electrodes and reported in Fig.9. The cyclic voltammetries confirm the capacitive behavior in the potential region where the EIS is performed (for all the electrodes the OCP is about -90 mV) and by Equation 1 a gravimetric capacity of 70, 80 and 124 F/g is calculated respectively for the as-deposited electrode, the thermal threated electrode and the electrode with nanostructured current collector.

4 Conclusions

Electrochemical impedance spectroscopy and cyclic voltammetry have been performed on nanostructured carbon electrodes grown by the assembling of carbon clusters generated in a pulsed microplasma cluster source. The double layer capacity of the interface ns-C/KOH 1M, calculated from EIS and CV measurements, shows specific gravimetric capacity in agreement with other forms of porous carbon materials, even if a poor electric contact at the interface between ns-C and nickel current collector is observed. To improve electrode performance, two different strategies have been employed without affecting ns-C porosity: a short thermal treatment at 300°C, and the deposition of a thin inter layer of nanostructured ns-Ni between the current collector and the active material. Both approaches lead to a substantial modification of impedance spectra in the high frequency range and a blue shift of the frequency at which the impedance imaginary part starts increasing due to double layer formation, suggesting an enhanced contact at Ni/C interface to be responsible for improved electrode performance. We demonstrate that the preparation of a nanostructured current collector via deposition of nickel nanoparticles, thus obtaining a surface morphology of the substrate similar to the ns-C texture, can significantly improve the active material capacitive behavior without the need for thermal treatment. These results overcome some limitation typical of nanostructured material in terms of metal/nanostructure contact geometries (Adams et al. 2003; Léonard and Talin 2011) and in terms of post deposition treatments such as sintering and annealing. Deposition of nanostructured current collector provides new perspectives for the use of cluster assembled nanostructured electrodes in electrochemistry applications.

Acknowledgements

We thank M. Galluzzi for AFM characterization and M. Marino for discussions. This work has been supported by the VII FP EU project NANOTOTOUCH.

References

Adams D.M. et al., J. Phys. Chem. B (2003) doi: 10.1021/jp0268462

Aricò A.S., Bruce P, Scrosati B., Tarascon JM., van Schalkwijk W., Nat. Mat.(2005) doi:10.1038/nmat1368

Barborini E., Piseri P., Milani P., *J.* Phys. D: Appl. Phys. (1999) doi:10.1088/0022-3727/32/21/102

Bongiorno G., Podestà A., Ravagnan L., Piseri P., Milani P., Lenardi C., Miglio S., Bruzzi M., Ducati C., J. Mater. Sci.: Mater. Electron. (2006) doi:10.1007/s10854-006-8089-4

Bottani C.E., Ferrari A.C., Li Bassi A., Milani P., Piseri P., Europhys. Lett. (1998) doi:10.1209/epl/i1998-00267-5

Chmiola J., Largeot C. , Taberna P.L., Simon P., Gogotsi Y., Science (2010) doi: 10.1126/science.1184126

Coad J.P., Rivière J.C., Surface Sci.(1971) doi: 10.1016/0039-6028(71)90148-8

Conway B.E., Electrochemical Supercapacitors (Kluwer Academic/Plenum, New York, 1999)

De Jong K.P., Geus J.W., Catalysis Review (2000) doi: 10.1081/CR-100101954

Diederich L., Barborini E., Piseri P., Podestà A., Milani P., Schneuwly A., Gallay R., Appl. Phys. Lett. (1999) doi:10.1063/1.125111

Esconjauregui S.,. Whelan C.M, Maex K., Carbon (2009) doi:10.1016/j.carbon.2008.10.047

Frackowiak E., Phys. Chem. Chem. Phys. (2007) doi: 10.1039/B618139M

Frackowiak E., Béguin F., Carbon (2001) doi:10.1016/S0008-6223(00)00183-4

Grahame D.C., Chem. Rev. (1947) doi: 10.1021/cr60130a002

Guo Y.G., Hu I.S., Wan L.J., Adv. Mat. (2008) doi:10.1002/adma.200800627

Kötza R., Carlenb M., Electrochimica Acta (2000) doi:10.1016/S0013-4686(00)00354-6

Lenardi C., Barborini E., Briois V., Lucarelli L., Piseri P., Milani P., Diam. Relat. Mater. (2001) doi: 10.1016/S0925-9635(00)00426-X

Léonard F., Talin A.A., Nat. Nanotechnol. (2011) doi:10.1038/nnano.2011.196

Milani P., Piseri P., Barborini E., Podesta A., Lenardi C., J. Vac. Sci. Technol. A (2001) doi:10.1116/1.1331289

Nian Y.R., Teng H., J. Electroanal.Chem. (2003) doi:10.1016/S0022-0728(02)01299-8

Pandolfo A.G., Hollenkamp A.F., J. of Power Sources (2006) doi:10.1016/j.jpowsour.2006.02.065

Piseri P., Podestà A., Barborini E., Milani P., Rev. Sci. Instrum. (2001) doi:10.1063/1.1361082

Piseri P., Vahedi Tafreshi H., Milani P., Curr. Opin. in Solid State and Mater. Sci. (2004) doi:10.1016/j.cossms.2004.08.002

Portet C., Taberna P.L., Simon P., Laberty-Robert C., Electrochimica Acta (2004) doi:10.1016/j.electacta.2003.09.043

Ravagnan L., Piseri P., Bruzzi M., Miglio S., Bongiorno G., Baserga A., Casari C.S., Li Bassi A., Lenardi C., Yamaguchi Y., Wakabayashi T., Bottani C.E., Milani P., Phy. Rev. Lett. (2007) doi:10.1103/PhysRevLett.98.216103

Robertson J., Prog. in Solid State Chem. (1991) doi:10.1016/0079-6786(91)90002-H

Simon P., Gogotsi Y., Nat. Mat. (2008) doi:10.1038/nmat2297

Simon P., Gogotsi Y., Phil. Trans. R. Soc. A (2010) doi: 10.1098/rsta.2010.0109

Snyder J.R., Smith M.A., Levenson L.L., J. Vac. Sci. Technol. (1980) doi:10.1116/1.570472

Wegner K., Piseri P., Vahedi Tafreshi H., Milani P., Phys. D: Appl. Phys. (2006) doi:10.1088/0022-3727/39/22/R02

Zhai Y., Dou Y., Zhao D., Fulvio P.F., Mayes R.T., Dai S., Adv. Mat (2011) doi: 10.1002/adma.201100984

Zhang L.L., Zhao X.S., Chem. Soc. Rev. (2009) doi: 10.1039/B813846J

Thermal treatment in inert atmosphere

The strategies proposed in the previous section enhance the mechanical and electrical properties of the ns-C based electrodes but some questions still remain. Unexpectedly, the gravimetric capacitance of both as deposited and heated-in-air ns-C thin films was found to decrease with increasing ns-C thickness (see figure 3.5A). However, SCBD, as ballistic deposition of clusters with low kinetic energy, is expected to originate materials with volumetric structural properties, such as density, pore fraction and size distribution, that do not evolve upon increasing thickness. We thus assume that the gravimetric surface area of ns-C available for the formation of the EDL should be constant and independent of the amount of deposited clusters (i.e. the film thickness).
In order to assess if the electrode soaking in the KOH causes any structural modifications of the active material which can be responsible for the drop of the gravimetric capacity, the time evolution of the complex impedance spectrum of the as deposited ns-C electrodes has been monitored. As shown in figure 3.6A, complex impedance spectra acquired every 30 minutes up to 3 hours exhibit a gradual rise in intensity of the impedance phase peak at high frequencies (> 1Hz, before the EDL formation) which indicates that the electrode is not stable. A similar evolution has been observed in the case of ns-C electrodes heated in air at 300°C for 15 minutes. As the complex impedance in this range of frequencies is ascribable to the behavior of the Ni/C interface, this finding suggests a deterioration in the current collector/active material interface probably due to the release, upon ions adsorption, of the residual stress of the cluster assembled film that may cause cracking and/or delamination of the ns-C layer. This points out a non optimized electrode fabrication protocol. Encouraged by the results, discussed in the previous section, obtained by the short post deposition annealing in air of the 200 nm thick ns-C electrode, we decided to perform a longer heat treatment.

However, as the ns-C heated in air at 300°C for more than 15 minutes burns due to the presence of oxygen, we performed a longer thermal treatment at same temperature but in an oxygen free atmosphere, i.e under argon fluxing. The thermal treatment protocol consisted in 15 minutes at the constant temperature of 300°C, reached by an heating ramp of 5°C/min up to 300°C and followed by a slow temperature cooling (ca. 2°C/min). No significant change in the ns-C thickness is measured by AFM as consequence of thermal treatment proving that at this temperature neither material losses or structural rearrangements occur. Thermally induced modifications of the ns-C structure and surface chemistry have

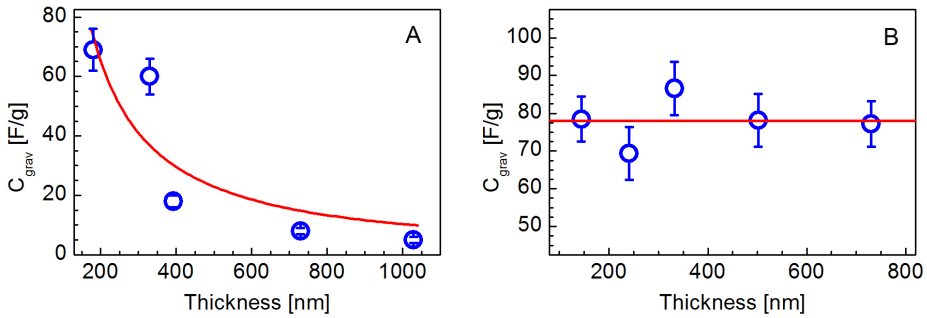

Figure 3.5: EDL gravimetric capacitance versus thickness of ns-C based electrode soaked in KOH 1M as deposited (A) and heated at 300°C in Ar atmosphere (B).

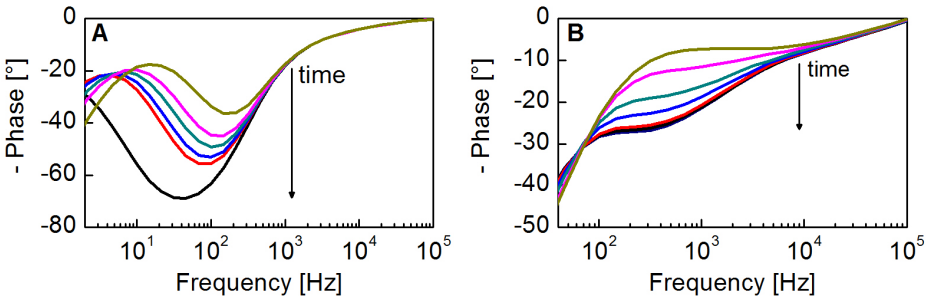

Figure 3.6: Time evolution of the complex impedance phase spectrum of an ns-C based electrode soaked in KOH 1M in the case of no thermal treatment (A) and thermal treatment at 300°C in Ar atmosphere (B). Impedance spectra are acquired every 30 minutes up to 3 hours.

been investigated by means of Raman spectroscopy and XPS, respectively. The Raman spectrum of the thermal treated ns-C is consistent with the one of the as deposited sample and no signatures of thermally induced structural changes in the ns-C thin film are present (see figure 3.7A). After the thermal treatment, a slightly increase of the C-C signal is observable in the XPS spectrum, as reported in figures 3.7B. The surface groups due to carbon atoms bonded to oxygen are still present. The lack of significant differences between the thickness and the structure of the heated and the as deposited films suggests that also the ns-C porosity is preserved.

Although the ns-C structure is invariant upon the performed thermal treatment,

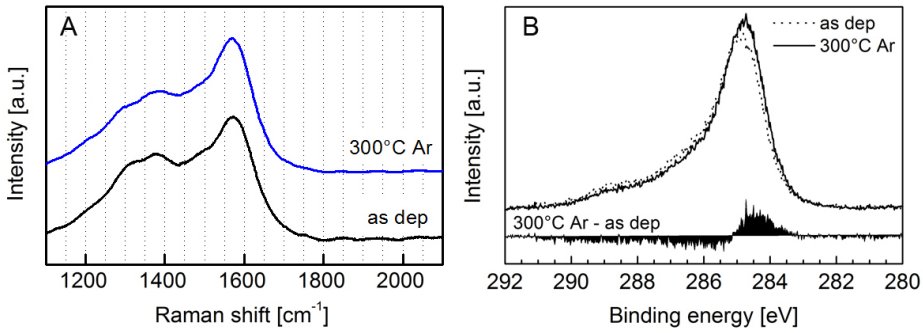

Figure 3.7: (A) Raman spectrum and (B) C1s x-ray photoemission line (after Shirley background removal) of ns-C as deposited and heated at 300°C in Ar atmosphere.

we expect the heating to lead to significant modifications at the current collector/active material interface (e.g. carburization and carbon graphitization) that, as previously discussed, can be beneficial to electrode performances. Moreover, we hypothesize that a thermally induced structural relaxation of the ns-C that improve its mechanical properties can proceed. As a matter of fact the time evolution of the complex impedance spectra of the heated electrode shows an increased stability in the high frequency range where the impedance phase tends to stabilize after an initial relaxation (see figure 3.6B). Furthermore, the phase peak of the electrode heated in inert atmosphere is significantly blue shifted and less pronounced compared to the one of the as deposited sample suggesting an enhanced and optimized contact between the nickel and the carbon (the decrease of the complex impedance phase peak from ca. 70° to ca. 30° indicates an improved injection of charge from the current collector to the active material). Besides this evidence, the specific double layer gravimetric capacity of a ns-C thin film 200 nm thick heated at 300°C in argon atmosphere was found to be ca. 78 F/g. This value is in agreement with the gravimetric capacitance of a ns-C electrode with the same thickness heated in air at 300°C for 15 minutes, confirming that the porosity of the carbon is not appreciably altered by the thermal treatment and suggesting that, as discussed in the previous section, only structural rearrangements at the Ni/C interface of the electrode proceed at this temperature. Moreover, in the case of the ns-C electrodes heated in argon atmosphere we measured a linearly increase of the EDL capacity upon increasing of the ns-C thickness, as expected by the SCBD growth regime. This result demonstrates that the specific gravimetric capacity of cluster assembled carbon does not de-

pend on the amount of deposited ns-C (see figure 3.5B) and leads, therefore, to the possibility of tailoring the amount of energy stored by the electrode in the EDL by the accurate control of the carbon thickness.

In conclusion, three different approaches have been shown as successful electrode fabrication strategies to characterize the EDL energy storage properties of ns-C thin films: (i) a short thermal treatment in air and (ii) the employment of a nanostructured current collector are viable routes in the case of ns-C films with thickness up to 200 nm, while (iii) a longer post deposition thermal treatment in inert atmosphere is needed for ns-C films with higher thickness. These approaches do not affect the ns-C nanostructure but are devoted to the enhancement of the carbon adhesion to the metallic substrate as well as to the improvement of the contact interface between the current collector and the active material which governs the injection of charge in the ns-C. The employment of a nanostructured current collector deposited by SCBD demonstrates the possibility of optimize the electric contact between two materials by the tailoring of their interface morphology and is, thus, particularly promising toward the use of cluster assembled thin films as active materials in electrode supported on temperature sensitive substrates. The linear relationship between the thickness of ns-C and its EDL capacitance proves that the ns-C porosity is preserved over a wide range of thicknesses and confirms the ballistic nature of the SCBD growth regime. Furthermore, it is relevant toward the ability to tune the amount of energy stored in the EDL by the accurate control of the amount of deposited material.

3.2.2 Ns-C/RTIL electrolyte

Aqueous electrolytes, such as acids (e.g., H_2SO_4) and alkalis (e.g., KOH), are widely employed as standard electrolytes in supercapacitors mainly thanks to their high ionic conductivity (up to ~ 1 Scm^{-1}) and low cost. However, they have the inherent disadvantage of a relatively low electrochemical stability window of ca. 1 V that harshly limits the amount of energy storable in the EDL to few watt hours per kilogram. Enhancing the voltage of the device is viable route to overcome this problem. Non-aqueous electrolyte mixtures such as propylene carbonate or acetonitrile, containing dissolved quaternary alkyl ammonium salts, are employed in many commercial supercapacitors, particularly those targeting higher energy applications [8]. Commercially available supercapacitors based on organic electrolytes easily reach operating voltages up to 2.5 V but suffer of limitations associated with the operating temperature making these devices unsafe

at 50-60°C. In this context the employment of room temperature ionic liquids (RTILs) as electrolytes may significantly increase the specific energy of the device, owing to the significant increase in their electrochemical stability window that can exceeds 5V. Moreover, RTILs are excellent ionic conductors, virtually non volatile and thermally stable up to 300° C, and are therefore considered the key toward the development of green, safe and high specific energy supercapacitors [60, 137]. However, the development of RTIL based supercapacitors is still in its infancy and further advance is needed to ensure their full exploitation. The challenge is in the choice of ionic liquids that feature wide electrochemical stability windows combined with high ionic conductivity, as well as in the design of electrode nanostructures capable of assuring proper wettability by the ionic liquid [138].
Besides the technological potential, RTILs have been recently demonstrated to be unique and innovative probes for the structural characterization of porous electrode material [102, 139–141]. Indeed, as room temperature molten salts, they are entirely composed by anions and cations that can directly interact with the electrode surface without the mediation of the solvent. This offers the advantage of a well identified ion size, which can be crucial not only in providing information about the electrode porosity but also in understanding the EDL charge storage mechanism in nanoporous materials.

In this section we present and discuss the characterization of the electrochemical capacitive behavior of cluster assembled carbon thin films soaked in room-temperature ionic liquids. We investigated the EDL capacitance of the interface between ns-C electrodes and four different RTILs ([Bmim][NTf2], [Emim][NTf2], [C12mim][NTf2] and [BPyr][NTf2]) featuring the same anion, which provides hydrophobic character, and different cations, so to disentangle the role of electrode material and the influence of ionic liquid nature from the interface properties. We found evidence of good impregnation of the ns-C nanoporous matrix by the different RTILs, suggesting that the ns-C has an open porosity easily accessible by the tested ionic liquids, and we measured an electrochemical stability window higher than 3V for all the RTILs employed. Furthermore, we observed an increase in the interfacial EDL capacity moving from a RTIL featuring larger cation as the [C12mim] to RTILs featuring smaller cation as the [Emim] and the [Bmim], suggesting that in the latter case the porosity of the ns-C is better exploited due to an optimized match between the size of the ns-C pores and the dimension of the electrolyte ions. [Bmim][NTf2] provided the highest EDL capacity: ca. 75 F/g. These features, together with the intrinsic versatility of SCBD in producing

patterned depositions on virtually any kind of substrate by using a stencil mask approach and its compatibility with standard planar microtechnology processes, inspired the fabrication of a thin film planar ns-C based supercapacitor.

The results of this study are reported in the following manuscript submitted to Carbon (Elsevier).

Planar thin film supercapacitor based on cluster-assembled nanostructured carbon and ionic liquid electrolyte

Luca Giacomo Bettini, Massimiliano Galluzzi, Alessandro Podestà, Paolo Milani and Paolo Piseri

Dipartimento di Fisica and CIMaINa, Università degli Studi di Milano, via Celoria 16, 20133 - Milano, Italy

Abstract. The fabrication of a planar supercapacitor based on cluster-assembled nanostructured carbon (ns-C) thin films deposited by supersonic cluster beam deposition and ionic liquid as electrolyte has been demonstrated. Cluster-assembled carbon has a density of about 0.5 g/cm^3 and a highly disordered structure with predominant sp^2 hybridization, high surface roughness and granular nanoscale morphology. The electric double layer (EDL) capacity of ns-C films (thickness variable in the range of 140÷500 nm) was investigated by electrochemical impedance spectroscopy and cyclic voltammetry employing four different hydrophobic room-temperature ionic liquids featuring the same anion and with different cations as electrolyte. Evidence of good impregnation of the ns-C nanoporous matrix by the different ionic liquids was found. The highest EDL capacity, 75 F/g, was obtained by using [Bmim][NTf2], the ionic liquid with the shortest alkyl chain. Using [Bmim][NTf2] a supercapacitor with single electrode area of 0.2 cm^2 and specific capacity of ~80μF/cm^2 was obtained.

1. Introduction

Supercapacitors are electrochemical double-layer (ECDL) capacitors composed by two polarizable electrodes and an ion-conducting electrolyte [1, 2]. They utilize double layer capacitance where the ions of the electrolyte are adsorbed on the charged electrode resulting in a Helmholtz layer with a thickness of half the diameter of the adsorbed solvated ions [3]. Supercapacitors are attractive for their high energy and power densities and their long cycle life (> 100 000), in addition to the high specific power, the energy storage process is simpler and more reversible than in conventional batteries [1, 2, 4, 5].

Electrochemical inert materials with extremely high specific surface area are utilized for supercapacitor electrodes in order to form a double layer with a maximum number of electrolyte ions [6-8]. Carbonaceous materials, in their various forms, have been studied as electrodes for the fabrication of supercapacitors. Nanostructured carbons (ns-C) with large interfacial area (>1000 m^2/g) are subject of increasing interest for the exploitation of their porous structure in view of reaching very high value of gravimetric and/or volumetric capacity [6-10]. Activated carbon composites and fibers [11, 12] with surface areas up to 2000 m^2/g (measured by gas adsorption) as well as carbon nanotubes [13, 14] and graphene [15] have been used for the fabrication of ECDL.

The storable and releasable energy strongly depends not only on the carbon interfacial area but also on the electrochemical stability of the interface, i.e. the maximum applicable voltage before the activation of redox processes (the exchange of charges between the carbon and the electrolyte). Organic electrolytes are commonly employed instead of aqueous electrolytes due to their larger electrochemical stability windows (ca. 2-3 V for organic electrolyte versus 1 V for aqueous electrolyte); the use of room temperature ionic liquids (RTILs) instead of conventional aqueous and organic electrolytes is considered potentially advantageous [16]. RTILs are good ionic conductors characterized by a high thermal stability (up to 300°C) and by an electrochemical stability window that can exceeds 5V, moreover RTILs as virtually non-volatile liquids are environmental friendly electrolytes [17].

Power generation and storage for microelectromechanical systems (MEMS), miniaturized biomedical devices, sensors and integrated on-chip components, can significantly benefit from the fabrication and integration of planar thin film supercapacitors. Despite the growing demand for powering MEMS [18], few works in literature report on the fabrication of planar

thin film carbon-based supercapacitors: planar interdigitated microcapacitors using carbon nanotubes and nanostructured carbon onions have been proposed by Jiang et al. [19] and Pech et al. [20], respectively. Yoo et al. [21] demonstrated the fabrication of an all solid state ultrathin supercapacitor based on multilayer reduced graphene oxide with capacities up to 394 μF/cm^2. Recently, the integration of carbon based micro-supercapacitors onto silicon substrate has been reported by Durou et. al [22] and Huang et al. [23] using as active material activated carbon blended with binders and carbide derived carbon, respectively. All these methods require photolithographic techniques and high-temperature processing.

Supersonic cluster beam deposition (SCBD) of nanostructured carbon (ns-C) has been demonstrated as an alternative and easy technique for the fabrication of supercapacitors [24]. SCBD consists in a random stacking of low kinetic energy nanoparticles producing films with very low-density and high porosity [25, 26]. The use of supersonic expansions for carbon cluster deposition allows to obtain very high deposition rates and highly collimated beams [27, 28]; the highly collimated (divergence <20 mrad) and intense cluster beam typical of SBCD has been demonstrated suitable for the deposition of patterned nanostructured films by using stencil masks [28-32] on substrates kept at room temperature. Compared to standard porous carbons (e.g. activated carbons) and supercapacitor electrodes fabrication methods (e.g. lamination of the active material onto the current collector), which can be barely integrated with microfabrication and/or thin film deposition techniques, the synthesis of porous carbon via SCBD presents several advantages, such as the compatibility with temperature sensitive substrates and with standard planar microtechnology processes, that may be pivotal toward the development of miniaturized, planar and flexible supercapacitors [26]. The avoidance of binders to hold the ns-C to the current collector is another advantage of technological relevance.

Here we report the room temperature fabrication by SCBD of a planar thin film supercapacitor based on cluster-assembled carbon electrodes and ionic liquid electrolyte. We used electrochemical impedance spectroscopy (EIS) to characterize the nanostructured electrodes and the double layer capacity at the interface between ns-C electrodes and four different RTILs ([Bmim][NTf2], [Emim][NTf2], [C12mim][NTf2] and [BPyr][NTf2]) featuring the same anion and different cations, so to disentangle the role of electrode material and the influence of ionic liquid nature from the interface properties. The EIS measurements

are discussed with the support of atomic force microscopy (AFM) to better understand the role of surface morphology and ns-C film nanostructure. Cyclic voltammetry (CV) has been also applied, in order to measure the electrochemical stability window of the employed RTILs in contact with ns-C.

2. Experimental section

2.1 *Nanostructured carbon film deposition and characterization*

Cluster-assembled carbon films to test the electric double layer (EDL) energy storage properties have been deposited on 15 x 15 mm^2, 1 mm thick glass substrates that were previously coated with a thin metallic film (nickel with ca. 200 nm thickness) as current collector. Nickel deposition is carried out by Ar ion sputtering of a nickel target under vacuum (with an RF magnetron ion beam source; working pressure ~10^{-4} mbar). Ns-C is deposited on the top of the nickel coated substrate by SCBD with a Pulsed Microplasma Cluster Source (PMCS), described in detail elsewhere [27]. In brief, a graphite target, inserted in the PMCS, is sputtered by a plasma which is confined by exploiting the pressure gradient produced by a jet of inert gas (He) impinging on a surface. Sputtered C atoms thermalize within the inert gas and condense to form clusters. The mixture of clusters and inert gas leaves then the PMCS internal cavity by expanding through a nozzle, thus forming a seeded supersonic beam of aerodynamically accelerated nanoparticles. These are finally collected on a substrate located on the beam trajectory to form a cluster-assembled nanostructured film. The cluster kinetic energy is low enough to avoid fragmentation upon landing, and hence a nanostructured film of relatively soft-landing particles retaining the structural properties of the gas-phase aggregates is grown. The typical density of such films from carbon clusters is approximately 0.5 g/cm^3. In the present work ns-C films with thickness in range between 140 and 500 nm have been deposited. The amount of deposited material was controlled during the deposition by a quartz microbalance placed closed to the sample. A post-deposition thermal treatment in air atmosphere was performed in a joule furnace for 15 minutes at constant temperature (300°C, measured with a K-type thermocouple) before the electrochemical characterization.

Cluster-assembled films were characterized by AFM using a Multimode Nanoscope IV microscope (Bruker) operated in tapping mode in air (standard single-crystal silicon tip with

curvature radius 5-10 nm and resonance frequency 250-350 kHz have been used). From AFM topographies, root mean square roughness (i.e. the standard deviation of surface heights) has been calculated. Film thickness has been measured from AFM topographical images captured in correspondence of film steps, as the average distance of film surface from the substrate (statistically evaluated from the histograms of height values in the AFM maps, where values pertaining to the substrate and to the film cluster in two well separated peaks). Raman spectra of ns-C films deposited on a silicon substrate were recorded by an optical-bench setup consisting in an Ar ion laser emitting at 514 nm (Spectra Physics, beamlok series 2065-7) as excitation source, a single monochromator (ActonSP-2558-9N) equipped with a 1200 blaze mm^{-1} grating, a notch filter (RazorEdge® long wave pass filter LP02-514RE-25), and a liquid nitrogen-cooled CCD camera.

2.2 *Electrochemical characterization*

Electrochemical measurements were carried out in a three electrodes home-built electrochemical cell equipped with a platinum coil as a counter electrode and a platinum wire as a pseudo reference electrode. The choice of a Pt wire or the pseudo-reference electrode is motivated by an attempt to keep contaminations of the RTIL test solution to a minimum. The cell was filled with a room temperature ionic liquid serving as the electrolyte and the area of the working electrode in contact with electrolyte inside the cell was ca. 0.8 cm^2.

Four different RTILS have been employed: 1-butyl-3-methylimidazolium bis(trifluoromethylsulfonyl)imide ([Bmim][NTf2]), 1-Ethyl-3-methylimidazolium bis(trifluoromethanesulfonyl)imide ([Emim][NTf2]), 1-dodecyl-3-methylimidazolium bis(trifluoromethylsulfonyl)imide ([C12mim][NTf2]) and 1-butyl-1-methylpyrrolidinium bis(trifluoromethylsulfonyl)imide ([BPyr][NTf2]). Impedance spectra were acquired with a potentiostat/galvanostat (Gamry Ref 600), in the frequency range from 10^{-2} to 10^5 Hz, under open circuit potential condition at AC perturbation amplitude of 5mV rms. The equivalent circuit fitting was performed using Gamry Echem Analyst software. Cyclic voltammetry (CV) curves are acquired at 80 mV/s in the potential range from -2 V to 2 V versus the Pt wire reference electrode.

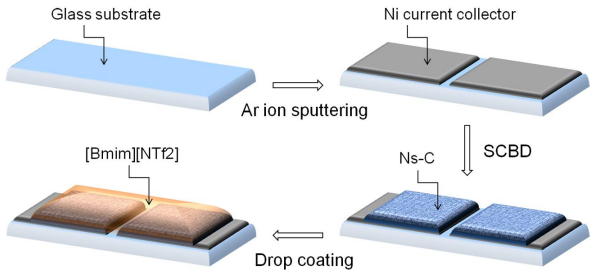

Figure 1. Sketch of the fabrication process of the planar ns-C based supercapacitor. Electrodes have a thickness of 200 nm, an area of 0.2 cm2 and are separated by a non conductive gap of 0.6 mm. [BMIM][NTf2] is employed as electrolyte.

2.3 *Supercapacitor fabrication*

The structure of a planar supercapacitor device fabricated by SCBD is reported in figure 1. Two ns-C electrodes of area ca. 20 mm^2 each and ca. 200 nm thickness, separated by a 0.6 mm gap, were deposited by use of a stencil mask over a glass substrate previously coated by Ar ion sputtering with ca. 200 nm of Ni. Electrodes were then covered with a thin layer of [Bmim][NTf2] by drop coating technique in order to form a RTIL layer allowing ionic contact between the two electrodes. Thanks to the high wettability of [Bmim][NTf2] over ns-C and to the negligible evaporation rate of RTILs, there was no need for device encapsulation: [Bmim][NTf2] was self confined inside the porous carbon matrix and did not spread over the current collector area left uncovered for electrical contacts.

3. Results and discussion

3.1 *Morphology and structure of the electrodes*

Figure 2 shows AFM topographies acquired on ns-C films with different thickness (see table 1 for the ns-C thickness corresponding to each panel in the figure). The vertical and horizontal scales in panels a, b, c, d and e are the same in order to allow direct comparison: scan size for all images is 2.5µm x 2.5µm (sampling is 1024x1024 pixels), and the vertical range in the colour map is 200 nm. The AFM data show a surface topography characterized

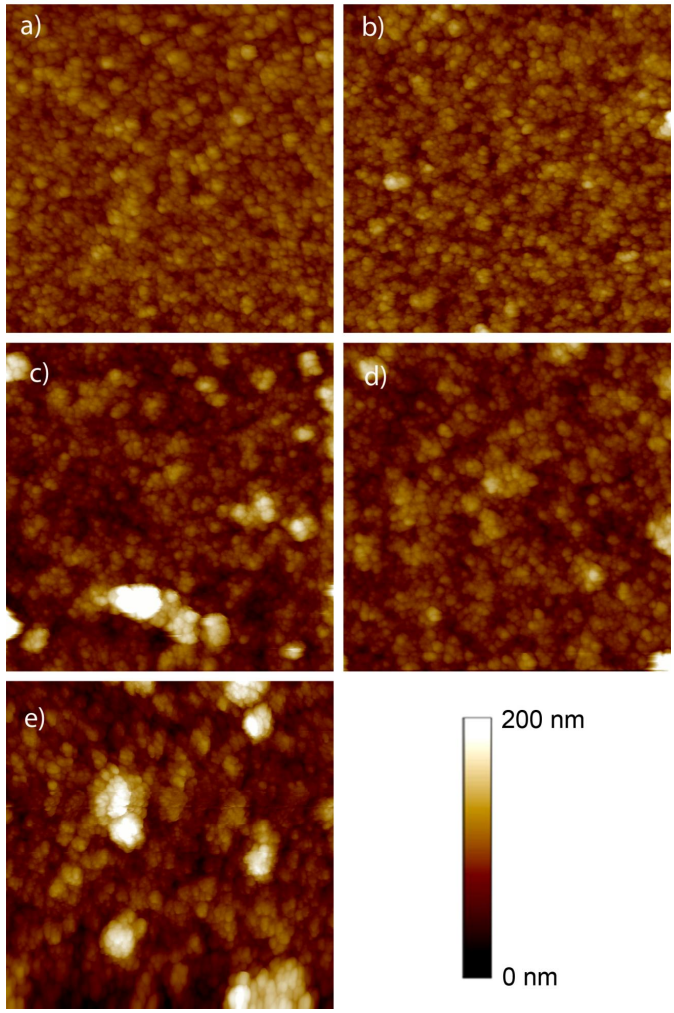

Figure 2. AFM images of ns-C film with different thickness: 144 nm (a), 201 nm (b), 270 nm (c), 332 nm (d) and 502 nm (e). All image sizes are 2.5 μm x 2.5 μm and the height scale is 200 nm. Thickness and roughness data of the films obtained by AFM analysis are reported in table 1.

Table 1. Structure parameters of films shown in figure 2 as determined by analysis of AFM topographic data.

Sample	Thickness (nm)	Roughness (nm)
A	144±11	16.8 ± 0.2
B	201±15	24 ± 4
C	270±20	45 ± 10
D	332±24	54 ± 17
E	502±39	65 ± 8

by the presence of a nanoscale granular structure as typically observed on cluster-assembled films [29, 33].

The granular nature of the film is the consequence of the ballistic deposition regime, where clusters impact at low kinetic energy on the surface thus avoiding substantial fragmentation and with only marginal diffusion and relaxation processes occurring after landing [29-31]. This results in a self-affine morphology [33] with a porosity that extends over different scales: from the pristine clusters morphology as determined by gas-phase aggregation, to the grains distribution throughout the surface as determined by the deposition process. The results of surface morphology AFM characterization are reported in table 1. Ns-C grown by SCBD, as previously reported in several papers [24, 26, 33], presents porous and low-density structure characterized by a BET area of ca. 700 m^2/g [34].

Typical Raman spectra of ns-C film deposited by SCBD are characterized by a broad peak at approximately 1350 cm^{-1} and a second one at about 1550 cm^{-1}, respectively related to the D band and the G band of graphite (not shown). Raman features are consistent with a highly disordered structure characterized by substantial dominance of sp_2 hybridization [35, 36]. Raman spectra and the morphological features of the films do not undergo significant modification after a mild thermal treatment in air at 300°C for 15 minutes [25].

3.2 *Cyclic voltammetry*

In figure 3 we report the cyclic voltammetry (CV) curves, acquired at 80 mV/s, for the interface between a 200 nm thick nanostructured carbon electrode and the four different RTILs. In all cases the curves have a nearly rectangular shape over the entire potential range,

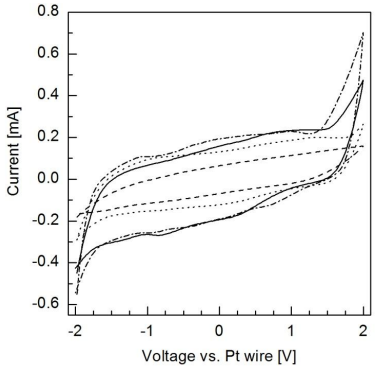

Figure 3. Cyclic voltammetry of ns-C electrode immersed four different RTILs acquired at the scan rate of 80 mV/s in the potential range between -2 and 0.2 V vs. Pt wire (continuous line, [Bmim][NTf2]; dashed line [C12mim][NTf2]; dotted line, [BPyr][NTf2]; dash-dotted lined, [Emim][NTf2]).

which indicates a capacitive response of the electrode and the absence of faradic reactions. An increase of both the anodic and cathodic currents is observed at the extremes of the scanned potential window, suggesting that the interface starts to be redox active. The electrochemical stability window reaches 4V for [C12mim][NTf2] and [BPyr][NTf2] and it is reduced to 3V for [Bmim][NTf2] and [Emim][NTf2]. ECDL capacity, calculated by equation 1

$$C = \frac{I}{s} \qquad (1)$$

where I is the average anodic current in the potential range between -1.6 and 1.4 V, where no faradic current is present, and s is the potential scan rate (V/s), strongly depends on the employed RTIL and is 0.6, 1.6, 1.8 and 2 mF for [C12mim][NTf2], [BPyr][NTf2], [Bmim][NTf2] and [Emim][NTf2], respectively. Since the ns-C films were simultaneously grown on four different nickel current collectors during the SCBD process, we assume that no differences in the cyclic voltammetry data acquired on the four different ns-C/RTIL interfaces are due to differences in the active material, i.e. ns-C. Thus, the changes in the

Table 2. Physical parameters found in literature for ionic liquids used in this work. All the experimental measures are carried in standard condition with T=298K and P=1atm.

RTIL	density (g/cm^3)	molar mass (g/mol)	viscosity (cP)	conductivity (mS/cm)	Cation effective size ($cm^3 mol^{-1}$)	Anion effective size ($cm^3 mol^{-1}$)
[Emim][NTf2]	1,52 [a]	391 [a]	34 [a]	9,2 [a]	99,2 [f]	158,7 [f]
[Bmim][NTf2]	1,43 [b]	419,37 [b]	52 [b]	4,0 [b]	133,6 [f]	158,7 [f]
[BPyr][NTf2]	1,41 [c]	422,41 [c]	85 [c]	2,2 [c]	144,3 [f]	158,7 [f]
[C12mim][NTf2]	1,26 [d]	531,58 [d]	154 [d]	0,6 [e]	271,1 [f]	158,7 [f]

[a] [37]
[b] [38]
[c] [39]
[d] [40]
[e] [41]
[f] [42]

electrochemical stability windows and in the EDL capacity should be totally ascribable to the differences between RTILs properties, which, as shown in table 2 [37-42], considerably change depending on the nature of the cation, and to their different interaction with ns-C porous structure. It is known that the relation between the ions size and the porous structure of electrode material plays a very important role, with a boost of capacity when the ionic radius matches the pores size [43-45]. Despite a substantial uncertainty in defining a representative value for ionic radius when the ion has a shape which is far from spherical, all the cations and anions that we have used possess a slender and asymmetrical shape, so the effective volume in table 2 can be considered a good indicator for ion size. We observe an increase in the interfacial double layer capacity moving from a RTIL featuring larger cation as the [C12mim] to RTIL featuring smaller cation as the [Emim] suggesting that in the latter case the porosity of the ns-C, which is known to be characterized by relatively small pore size [34], is better exploited.

3.3 *Electrochemical impedance spectroscopy*

EIS characterization of the ns-C/RTILs electrodes is presented in figure 4, which reports the Nyquist plots of the complex impedance data acquired in the frequency range between 0.1 MHz and 0.01 Hz on ns-C electrodes (thickness 200 nm) soaked with four different RTILs.

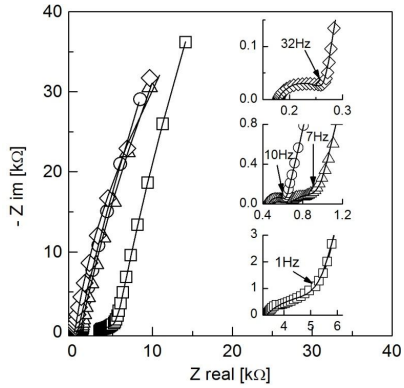

Figure 4 Nyquist plot of the complex impedance of a ns-C electrode 200 nm in thickness immersed in four different RTILs (symbols: open squares, [C12mim][NTf2]; open circles, [Bmim][NTf2]; open triangles, [BMPYR] [NTf2]; open rhombi, [Emim][NTf2]). The spectra are fitted (solid lines) with the equivalent circuit of figure 5. Fit parameters are reported in table 3.

All complex impedance spectra show common trends and two different features can be observed: (i) a high frequency arc and (ii) a low frequency straight line. The frequency at which this latter feature shows up, i.e. the knee frequency, depends on the employed electrolyte and is 1, 7, 10 and 32 Hz for [C12mim][NTf2], [BPyr][NTf2], [Bmim][NTf2] and [Emim][NTf2], respectively. The high frequency semi-circle is related to the RTIL ionic conductivity and to the interface contact resistance between the Ni current collector and the ns-C [46]. This contact interface plays a fundamental role for carrier injection from the Ni layer to the ns-C film and has to be finely optimized during the electrode preparation procedure in order to be able to properly characterize the ns-C/electrolyte interface. As a matter of fact, from previous investigations, we observed that a mild thermal treatment in air at 300°C for 15 minutes significantly improves the ns-C biasing [25]. The impedance properties of this interface can be modeled by an equivalent circuit composed by a parallel combination of a resistance, R1, which accounts for the charge transfer through the interface, and a constant phase element, CPE1, which represents the capacitive behaviour of the interface. The high frequency feature of the complex impedance plot can be fitted by the response of a resistor (Rs) in series with the parallel combination of a resistor (R1) and a

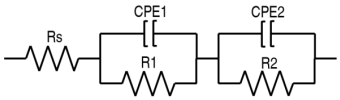

Figure 5. Equivalent circuit used to fit impedance data of figure.4. Rs includes the resistance of the electrolyte and the bulk resistance of the electrode, the CPE1-R1 subcircuit includes the impedance of the Ni/ns-C interface and the CPE2-R2 subcircuit represents the electrochemical double layer capacity and the leak resistance.

Table 3. Best fit equivalent circuit parameters for the complex impedance of ns-C electrodes reported in figure 4.

RTIL	Rs (Ω)	CPE1(Ss^α)	αCPE1	R1(Ω)	CPE2(Ss^α)	αCPE2	R2(Ω)
[Emim][NTf2]	179	27e-6	0.749	86	346e-6	0.903	199800
[Bmim][NTf2]	458	22e-6	0.765	174	360e-6	0.860	666400
[BPyr][NTf2]	667	13oe-6	0.531	324	338e-6	0.872	401200
[C12mim][NTf2]	3344	71e-6	0.528	2296	310e-6	0.888	661800

constant phase element (CPE1). Rs accounts for the cell overall response at 0.1 MHz (where impedance imaginary part is zero) and is dominated by the ionic conductivity of the RTIL employed [45]. A low ionic conductivity leads to high Rs values. Ionic liquid conductivity changes by varying the cation. For the RTILs employed in our study, the trend [Emim][NTf2] < [Bmim][NTf2] < [BPyr][NTf2] < [C12mim][NTf2] is known from literature data as reported in table 2. The same is reflected in the complex impedance as shown in the inset of figure 4 and in table 3 where the values of fitting parameters are reported. The low frequency linear part of the plot (below the knee frequency) is ascribable to the capacitive response of the ns-C/RTIL interface. Differences in the knee frequency between the different RTILs that we employed are related to the overall series resistance of the double layer capacity which is represented by the sum of Rs and R1 (the higher the series resistance, the lower the knee frequency). From an electric circuit point of view, the capacitive response of the ns-C/RTIL interface can be modeled as a capacity even if, according to the EIS reported data, the low frequency complex impedance deviates from the capacitor ideal behaviour (a straight line with infinite slope) basically due to the nano-porous nature of the electrode and to restricted mobility of ions in the ns-C complex topology [44, 47].

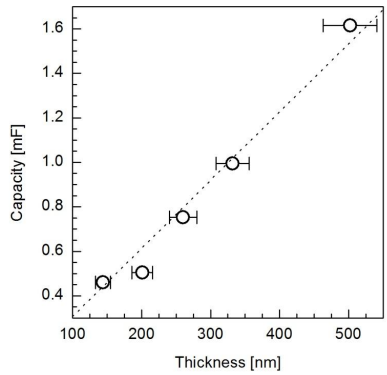

Figure 6. Double layer capacity calculated at 0.01 Hz by equation 2 of five electrodes with varying ns-C thickness immersed in [BMIM][NTf2]. A dotted line has been drawn to highlight the linear trend.

The complex impedance in this range of frequencies can be better fitted by the response of a constant phase element, CPE2, rather than a simple capacitance, leading thus to the equivalent circuit shown in figure 5 which describes the overall complex impedance of the electrodes. The α exponent of CPE2 obtained by the equivalent circuit fit is still always about 0.9 (see table 3), which confirms the essentially capacitive behaviour of the interface in agreement with CV curves. The interface double layer capacities were calculated from Equation 2 [47],

$$C(f) = -\frac{Z'(f)}{2\pi f |Z(f)|^2} \qquad (2)$$

(where f is the frequency and Z' is the impedance imaginary part) at 0.01 Hz, and resulted to be 0.38, 0.46, 0.47 and 0.50 mF for ionic liquid featuring [C12mim], [Emim], [BPyr] and [Bmim], respectively. This trend reflects the trend already observed in the CV curves reported in figure 3: the use of [C12mim][NTf2] as electrolyte leads to a reduced double layer capacity in comparison to the other three RTILs considered. This is ascribable to the increased size of the cation for two reasons: firstly, longer alkyl tails hamper penetration and diffusion of ions into the nano-porous ns-C matrix [43], and secondly because the larger

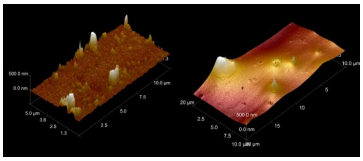

Figure 7. AFM 3D image of a ns-C electrode before (left) and after (right) the immersion in ionic liquid [BMIM][NTf2] showing a complete coverage of nanostructured surface.

cation size determines, upon surface adsorption, a lesser amount of charge per unit of surface. On top of that there is no significant difference in the double layer capacity values as determined by EIS for [Emim][NTf2], [Bmim][NTf2] and [BPyr][NTf2] which feature only slight differences in cation size (see table 2) even if a difference in double layer capacity was appreciable from CV curves.

To further characterize the properties of the ns-C/RTIL system, we investigated the evolution of the double layer capacity of the ns-C/RTIL interface varying the ns-C film thickness from ca. 140 nm to ca. 500 nm and employing [Bmim][NTf2] as the electrolyte. Figure 6 reports the double layer capacity calculated at 0.01 Hz from EIS spectra using equation 2 versus the ns-C film thickness. A clear linear relationship relates the double layer capacity to the amount of electrode material indicating that the ratio between the accessible surface in the porous ns-C film volume and the amount of deposited clusters remains constant during the SCBD growth process (the ns-C density is also essentially constant during film growth, as confirmed by comparison between film thickness as obtained by quartz microbalance thickness monitor and post deposition measurements by AFM). The results shown in figure 6, besides supporting that the pores accessibility is not affected by the increased carbon thickness, also indicate a good carbon wettability by hydrophobic [Bmim][NTf2]. The linear trend suggests that the [Bmim][NTf2] fully impregnates the nanostructured carbon matrix and highlights the surface chemistry affinity between ns-C and [Bmim][NTf2] over a wide range of thickness values. This is also confirmed by AFM tapping mode image (figure 7) of the ns-C electrode after immersion in [Bmim][NTf2]. The sample surface, spincoated (7000 rpm for 20min) in order to remove the excess of liquid, is completely and homogeneously covered by liquid showing that RTIL is thoroughly permeating the nano-pores and strongly bound to the interface. The measured capacities

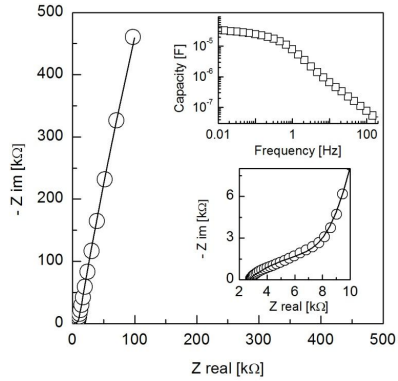

Figure 8. Nyquist plot of the complex impedance of the planar ns-C based supercapacitor. In the sketch is reported the plot of the EDL capacity (calculated by equation2) vs. frequency.

normalized by the ns-C weight leads to a mean gravimetric capacity of 75±3 F/g which is in agreement with other forms of activated carbon [48].

3.4 *Supercapacitor characterization and performances*

The energy storage properties of the planar supercapacitor (figure 1) were measured by fitting EIS data (Nyquist plot of the experimental data are reported in figure 8 and best fit parameters are listed in table 4) with the calculated response of the equivalent circuit from figure 5. Considering a maximum operating voltage of 3V, as estimated by the CV curves of figure 3, and a series resistance of ca. 10kΩ, resulting from the sum of Rs and R1, we calculate a volumetric specific power and a volumetric specific energy of 14W/cm^3 and 2.6e-3 Wh/cm^3, respectively (volumes including both the ns-C and the current collector). The obtained performances overcome standard energy storage devices (e.g. dielectric capacitors and thin film batteries) designed for power microelectronics applications, and they are comparable with the highest volumetric specific power and volumetric specific energy values obtained with other forms of carbon [20]. Compared to CNTs and graphene based supercapacitors [19, 21], the use of ns-C offers the advantage of allowing room temperature deposition process and requiring only a mild post-deposition thermal treatment. The control over the carbon thickness on the nanometer scale, the uniformity of the deposits and the

Table 3. Best fit equivalent circuit parameters for the complex impedance of the ns-C based planar supercapacitor.

Rs (Ω)	CPE1(Ss^α)	αCPE1	R1(Ω)	CPE2(Ss^α)	αCPE2	R2(Ω)
2660	15e-6	0.449	7572	25.5e-6	0.898	14.2e6

avoidance of binders are other features of technological relevance. Further improvements of the overall performance for supercapacitor applications are expected as a consequence of an optimized design of the device, such as the employment of interdigitated electrodes and the available room for decreasing the width of the non conductive gap between the electrodes.

4. Conclusions

We demonstrated the fabrication of a thin film planar supercapacitor by supersonic cluster beam deposition. Electrochemical impedance spectroscopy and cyclic voltammetry highlighted a quasi-ideal capacity response revealing that the surface chemistry and morphology of the nanostructured carbon allows the penetration and the reversible ion adsorption in the ns-C porous matrix of RTILs ions over a wide range of ns-C thickness. These evidences clearly show that the nanometric structure of the ns-C, which is fundamental for the double layer formation mechanism, is characterized by an open porosity, easily wettable and accessible by RTILs. We measured an electrochemical stability window higher than 3V for all the RTILs tested.

The device is easily implementable on a wide range of different substrates (e.g. glass, SiO2, polymers) and compatible with planar technology. The measured performances in terms of energy and power density, together with the intrinsic versatility of SCBD in producing patterned depositions on virtually any kind of substrate by using a stencil mask approach, are appealing for the fabrication of thin electrodes for microscale energy storage devices to be integrated with MEMS.

References

[1] Conway B.E., Electrochemical Supercapacitors: Scientific fundamentals and technological applications
(Kluwer Academic/Plenum, New York, 1999)
[2] Kötz R and Carlen M 2000 *Electrochim. Acta* **45** 2483-98
[3] Grahame DC 1947 *Chem. Rev* **41** 441-501
[4] Simon P and Gogotsi Y 2008 *Nat. Mat.* **7** 845-54
[5] Burke A 2007 *Electrochim. Acta* **53** 1083-91
[6] Zhang LL and Zhao XS 2009 *Chem. Soc. Rev.* **38** 2520-31
[7] Pandolofo AG and Hollenkamp AF 2006 *J. Power Sour.* **157** 11-27
[8] Frackowiak E and Béguin F 2001 *Carbon* **39** 937-50
[9] Gamby J, Taberna PL, Simon P, Fauvarque JF and Chesneau M 2008 *J. Power Sour.* **101** 109-16
[10] Fernandez JA, Morishita T, Toyoda M, Inagaki M, Stoeckli F and Centeno TA 2008 *J. Power Sour.* **175** 675-79
[11] Subramanian V, Luo C, Stephan AM, Nahm KS, Thomas S and Wei B 2007 *J. Phys. Chem. C* **111** 7527-31
[12] Kim C, Choi YO, Lee WJ and Yang KS 2004 *Electrochim. Acta* **50** 883-87
[13] Futaba DN, Hata K, Yamada T, Hiraoka T, Hayamizu Y, Kakudate Y, Tanaike O, Hatori H, Yumura M and Iijima S 2006 *Nat. Mat.* **5** 987-94
[14] Frackowiak E and Béguin F 2002 *Carbon* **40** 1775-87
[15] Zhang LL, Zhou R and Zhao XS 2010 *J. Mater. Chem.* **20** 5983-92
[16] Armand M, Endres F, MacFarlane DR, Ohno H and Scrosati B 2009 *Nat. Mater.* **8** 621-29
[17] Arbizzani C, Lazzari M, Soavi F, Mastragostino M and Conte M 2010 *ECS Trans.* **25** 25-30
[18] Cook-Chennault KA, Thambi N and Sastry AM 2008 *Smart Mater. Struct.* **17** 043001
[19] Jiang YQ, Zhou Q and Lin L 2009 *Micro Electro Mechanical Systems, 2009. MEMS 2009. IEEE 22nd International Conference on* 587-90
[20] Pech D, Brunet M, Durou H, Huang P, Mochalin V, Gogotsi Y, Taberna PL and Simon P 2010 *Nat. Nanotechnol.* **5** 651-654
[21] Yoo JJ *et al.* 2011 *Nano Lett.* **11** 1423-27

[22] Durou H, Pech D, Colin D, Simon P, Taberna PL and Brunet M 2012 *Microsyst. Technol.* **18** 467-73

[23] Huang P, Heon M, Pech D, Brunet M, Taberna PL, Gogotsi Y, Lofland S, Hettinger JD and Simon P 2013 *J. Power Sour.* **225** 240-4

[24] Diederich L, Barborini E, Piseri P, Podestà A, Milani P, Schneuwly A and Gallay R 1999 *Appl. Phys. Lett.* **75** 2662- 4

[25] Bettini LG, Bardizza G, Podestà A, Milani P and Piseri P 2012 Electrochemical Impedance Spectroscopy on nanostructured carbon electrodes grown by Supersonic Cluster Beam Deposition *submitted to J. Nanopart. Res.*

[26] Bongiorno G, Podestà A, Ravagnan L, Piseri P, Milani P, Lenardi C, Miglio S, Bruzzi M and Ducati C 2006 *J. Mater. Sci.: Mater. Electron.* **17** 427-41

[27] Barborini E, Piseri P and Milani P 1999 *J. Phys. D: Appl. Phys.* **32** L105

[28] Barborini E, Piseri P, Podestà A and Milani P 2000 *Appl. Phys. Lett.* **77** 1059-61

[29] Piseri P, Podestà A, Barborini E and Milani P 2001 *Rev. Sci. Instrum.* **72** 2261-67

[30] Piseri P, Tafreshi HV and Milani P 2004 *Curr. Opin. in Solid State and Mater. Sci.* **8** 195-202

[31] Wegner K, Piseri P, Tafreshi HV and Milani P 2006 *Phys. D: Appl. Phys.* **39** R439

[32] Barborini E *at al.* 2008 *J. Micromech. Microeng.* **18** 055015

[33] Milani P, Podestà A, Piseri P, Barborini E, Lenardi C and Castelnovo C 2001 *Diam. Relat. Mater.* **10** 240-7

[34] Lenardi C, Barborini E, Briois V, Lucarelli L, Piseri P and Milani P 2001 *Diam. Relat. Mater.* **10** 1195-200

[35] Robertson J 1991 *Prog. in Solid State Chem.* **21** 199-333

[36] Ravagnan L, Piseri P, Bruzzi M, Miglio S, Bongiorno G, Baserga A, Casari CS, Li Bassi A, Lenardi C, Yamaguchi Y, Wakabayashi T, Bottani CE and Milani P 2007 *Phy. Rev. Lett.* **98** 216103

[37] Matsumoto H, Yanagida M, Tanimoto K, Nomura M, Kitagawa Y and Miyazaki Y 2000 *Chem. Lett.* **29** 922–23

[38] Hapiot P and Lagrost C 2008 *Chem. Rev.* **108** 2238–64

[39] MacFerlane DR, Sun J, Golding J, Meakin P and Forsyth M 2000 *Electrochim. Acta* **45** 1271-78

[40] Tariq M, Carvalho PJ, Coutinho JAP, Marrucho IM, Lopes JNC and Rebelo LPN 2011 *Fluid Phase Equilibria* **301** 22–32

[41] Coleman S, Byrne R, Alhashimy N, Fraser KJ, MacFarlane DR and Diamond D 2010 *Phys. Chem. Chem. Phys.* **12** 7009–17

[42] Rebelo LPN, Lopes JNC, Esperanca JM, Guedes HJR, Lachwa J, Najdanovic-Visak V and Visak Z 2007 *Acc. Chem. Res***. 40** 1114–21

[43] Largeot C, Portet C, Chmiola J, Taberna PL, Gogotsi Y and Simon P 2008 *J. Am. Chem. Soc* **130** 2730–1

[44] Merlet C, Rotenberg B, Madden PA, Taberna PL, Simon P, Gogotsi Y and Salanne M 2012 *Nat. Mater*. **11** 306-10

[45] Largeot C, Taberna PL, Gogotsi Y and Simon P 2011 *Electrochem. Solid-State Lett.* **14** A174- 6

[46] Portet C, Taberna PL, Simon P and Laberty-Robert C 2004 *Electrochim. Acta* **49** 905-12

[47] Taberna PL, Simon P and Fauvarque JF 2003 *J. Electrochem. Soc.* **150** A292-A300

[48] Balducci A, Taberna PL, Simon P, Plée D, Mastragostino M and Passerini S 2007 *J. Power Sour.* **165** 922-7

3.3 Conclusions

Nanostructured carbon (ns-C) thin films with density of ca. 0.5 g/cm^3 have been deposited by SCBD in order to assess their electrochemical properties. Both aqueous and ionic liquid electrolyte have been employed. The electrode fabrication issue has been addressed by several strategies aiming to optimize the interfacial mechanical and electrical contact between the ns-C and the current collector. A thermal treatment in air and the deposition of a cluster assembled current collector have been successfully tested in the case of ns-C thin film 200 nm thick. However, a longer thermal treatment in inert atmosphere was required for thicker films soaked in aqueous electrolyte. This was not necessary when ionic liquids were employed.

Ns-C thin films showed a good wettability in electrolyte solution and a high and accessible surface area leading to a specific gravimetric capacity of 78 and 75 F/g in aqueous and ionic liquid electrolyte, respectively. Although these values are slightly lower than the typical gravimetric capacities of the porous forms of carbon commonly employed as active material in supercapacitor electrodes [9], we believe that ns-C may play an outstanding role as active material in the growing field of thin film electrodes for supercapacitor applications. A non-encapsulated planar ns-C based supercapacitor employing an ionic liquid as electrolyte has been fabricated as proof-of-principle. Compared to standard porous carbons (e.g. activated carbons) and supercapacitor electrodes fabrication methods (e.g. lamination of the active material onto the current collector), which can be barely integrated with microfabrication and/or thin film deposition techniques, the synthesis of porous carbon via SCBD presents several advantages, such as the control over the carbon thickness on the nanometer scale, the compatibility with temperature sensitive substrates and the integrability with standard planar microtechnology processes, that are pivotal toward the development of miniaturized, planar and flexible supercapacitors. The no need for binders to hold the ns-C to the current collector is another advantage of technological relevance.

Nevertheless, in order to meet the demand for high specific power density, which is one of the principal advantage of carbon based supercapacitors over batteries, it is crucial to increase the relatively low conductivity of ns-C by a synthetic strategy which preserves the intrinsic porosity of the cluster assembled carbon growth by SCBD and does not hamper its potential for electrochemical energy storage applications.

Chapter 4

Nickel:carbon nanocomposites grown by SCBD

The interfacial properties exhibited by ns-C and discussed in chapter 3 are encouraging toward the use of porous carbon grown by SCBD as electrode material for electrochemical energy storage. However, the intrinsic disordered sp2 structure of ns-C harshly hampers its electrical conductivity and restrains its viability as electrode capacitive material in practical applications where relative high power is needed. Thermal treatments both in air and in inert atmosphere were demonstrated to enhance the overall electrode performances with particular positive effects on the charge injection from the current collector to the porous carbon layer and vice versa. The inclusion of metal nanoparticles in the ns-C matrix at the deposition stage has been selected as route toward the synthesis of a carbon based porous material with optimized properties. By this chapter the growth of nickel:carbon (Ni:C) cluster assembled nanocomposites and the characterization of their electrochemical properties will be presented and discussed. Preliminary results on the structural modifications of ns-C catalyzed by the embedded Ni upon a mild thermal treatment and on their impact on the Ni:C electrochemical properties will be introduced in the last part of the chapter.

4.1 Ni:C nanocomposite: overview

Carbon materials containing metal nanoparticles represent complex systems, known as metal:carbon nanocomposites, with several original and adjustable properties that are not present in the individual constituents. Among various forms of carbon, amorphous carbon can particularly benefit from the inclusion of metallic nanoparticles and its physical properties can be significantly extended by the co-presence of the two phases. Moreover, embedded metal nanoparticles can chemically combine with carbon forming carbides. According to their tendency

to form hard and thermodynamically stable metal carbide compounds, one can distinguish metals with high chemical affinity (e.g. Ti and W), low chemical affinity (e.g. Co and Ni) and metals non miscible with carbon (e.g. Pt, Au and Cu).

Among different metal:carbon nanocomposites, Ni:C has been extensively studied for its promising tribological [142], mechanical [143], electric [144, 145] and magnetic [144] properties. Ni is also an efficient catalyst for the formation of ordered graphitic structures, such as carbon nanotubes, fibres and graphene [146–151] and thus, its inclusion in an amorphous carbon matrix is a feasible route to tailor the hosting carbon structure. Furthermore, its oxide, NiO, has attractive features, such as low cost and chemical stability, that are interesting toward its use in electrochemical energy storage applications [152, 153]. Recently, Ni:C prepared by loading activated carbons and carbon nanotubes with NiO by chemical precipitation methods [154–157] and nickel-embedded carbon nanofibers prepared by electrospinning [158] have been studied as electrode materials for energy storage showing that the nanocomposites have enhanced electrochemical performances, charge−discharge properties and specific capacity densities compared to the pure carbon electrodes.

The accurate control over the nanostructure synthesis process is pivotal toward the fabrication of nanocomposite materials with selected properties and significant efforts are devoted to the study of deposition procedures that assure a fine-tuning of the nickel:carbon mixing. Ion beam co-sputtering [159], pulsed laser ablation [32, 160] and plasma enhanced chemical vapor deposition [161] are among the different synthesis techniques that have been recently reported in the literature. Enhancements of both the electrical conductivity [32] and of the graphitic order [159] were observed and ascribed to the incorporation of Ni in the carbon matrix.

Here, I present the growth of porous Ni:C nanocomposite thin films by the supersonic cluster beam co-deposition of Ni and C clusters separately produced in two different PMCSs. Compared to other Ni:C synthetic techniques [32, 159, 161], where atoms of the different elements are simultaneously ablated from a composite target or chemically interact at high temperatures, the SCBD apparatus, employed in this work for the codeposition of nickel and carbon (see figure 1.3), avoids the interaction between C and Ni atoms during the formation process of the clusters. Preformed clusters of C and Ni are mixed only after the supersonic expansion, at the deposition stage, where their low kinetic energy, together with the cold temperature of the substrate, which is kept at RT, substantially prevents

Sample	Ni concentration (%)	Thickness (nm)
A	0	183±17
B	5	189±19
C	14	180±28
D	28	197±15
E	35	203±15

Table 4.1: Ni:C nanocomposite thin films grown by SCBD with different nominal Ni volumetric concentration.

their fragmentation and coalescence upon landing.

To highlight the role of the inclusion of Ni clusters in the ns-C matrix, four Ni:C nanocomposites featuring equal thickness ($\sim$ 200 nm) and different nominal Ni volumetric concentration ($5 \div 35$ %) were synthesized at room temperature by SCBD (see table 4.1). The control over the relative volumetric concentrations of the two phases in the nanocomposites is achieved by a robust pre-characterization of the growth rates of Ni and C thin films deposited operating the PMCSs with the same parameters employed during the codeposition process.

The STEM and HRTEM micrographs of the Ni:C nanocomposite (figure 4.1) show a uniform mixing of the two phases characterized by bigger carbon aggregates with quite broad size distribution and smaller Ni nanoparticles more homogeneous in size. Ns-C matrix exhibits a disordered structure characterized by a random assembly of highly curved graphene sheets that resemble the nanostructure of the pure ns-C system (see figure 3.1B for comparison), indicating that, under the standard conditions of the SCBD process, the inclusion of Ni clusters in the ns-C does not catalyze the formation of long-range ordered carbon structures. Fast Fourier transform (FFT) analysis of the selected area in figure 4.1C reveals three lattice spacings (1.5 Å, 2.1 Åand 2.4 Å) ascribable to the presence of oxidized nickel (NiO), probably formed after nanocomposite exposure to air. The analysis of lattice spacing indicates that no carburized nickel is present. Even if signatures of non-oxidized nickel have not been found by HRTEM, we cannot exclude the presence in the nanocomposites of metallic nickel and/or non-stoichiometric NiO. For this reason, hereafter we will refer to the nickel based clusters included in the ns-C matrix simply as Ni clusters. As expected by the low kinetic energy deposition regime, interaction between Ni and C clusters is negligible and the overall structure of the carbon matrix keeps its characteristic short range sp2 order. This is also confirmed by the Raman spectra

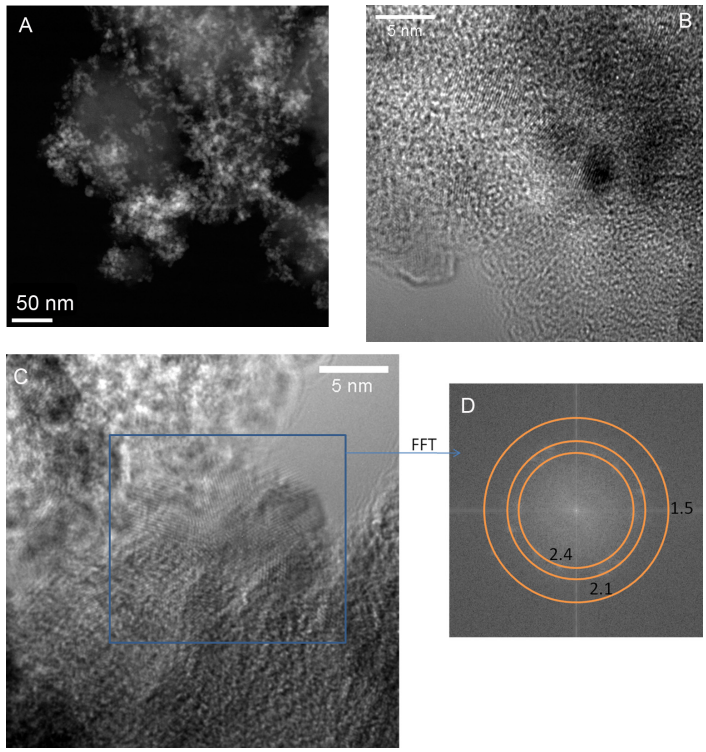

Figure 4.1: Dark field STEM (A), HRTEM micrographs (B and C) of Ni:C nanocomposite (sample B of table 4.1) grown by SCBD and fast Fourier transform (FFT) diffractogram (D) of the selected area in panel C. In dark field micrograph the brightest spots are the Ni clusters while the carbon clusters are darker (black is the vacuum), in the HRTEM micrographs the contrast is inverted.

shown in figure 4.2A. No significant differences are observable between the typical Raman spectra of the Ni:C and ns-C thin films, proving that the amorphous structure of the cluster assembled carbon is not altered by the codeposition of Ni nanoparticles. Furthermore, the nanocomposite retains a surface morphology characterized by nanograins as typically observed on cluster assembled films (see figures 4.2B and 3.1A for comparison).

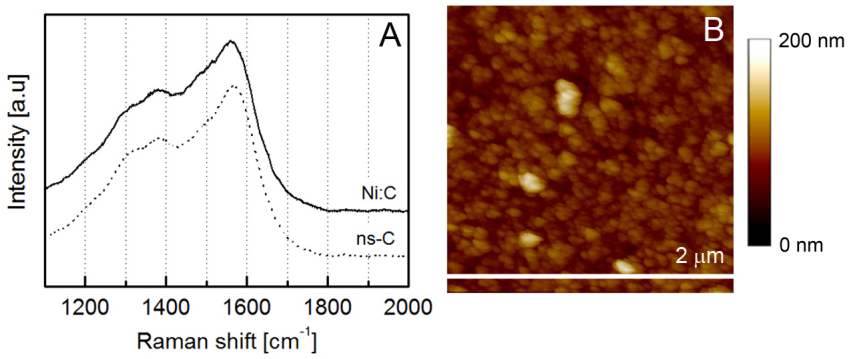

Figure 4.2: Typical Raman spectrum (A) and AFM topographic map (B) of a Ni:C nanocomposite deposited by SCBD.

4.2 Ni:C nanocomposite: electrochemical energy storage

Despite the uniform inclusion of Ni nanoparticles in the carbon film does not significantly affect its structure and morphology, differences in the physico-chemical properties between the nanocomposites and the ns-C are expected as consequence of the Ni presence in the carbon matrix. In order to assess these differences as well as the viability of Ni:C as active material in EDL energy storage applications, electrochemical characterization of the deposited nanocomposites soaked in KOH 1M solution as aqueous electrolyte has been performed.
Figure 4.3A shows the cyclic voltammetry (CV) curve, acquired at a scan rate of 40 mV/s, of the interface between a Ni:C nanocomposite electrode deposited by SCBD (sample D of table 4.1) and the KOH. CV curve basically has a quasi-rectangular shape in the potential region between -0.4 and 0.1 V, indicating that the main contribution to the capacity is the charge and discharge of the double layer, and presents a slightly distorted shape over the entire potential window with an increase of both the anodic and cathodic currents at the extremes of the scanned potential window, which can be associated to the presence of slow electron transfer processes probably due to oxygen-containing functional groups on the carbon surface (see the ns-C XPS spectrum of figure 3.2B). The current peaks at about 0.05 V, in the anodic direction, and -0.25 V, in the cathodic direction are also ascribable to chemical reactions due to both the carbon surface oxides and to oxygen dissolved in the electrolyte solution that promote a Faradaic pseudocapacitive mechanism [59, 162, 163]. The typical CV curve of a ns-C electrode

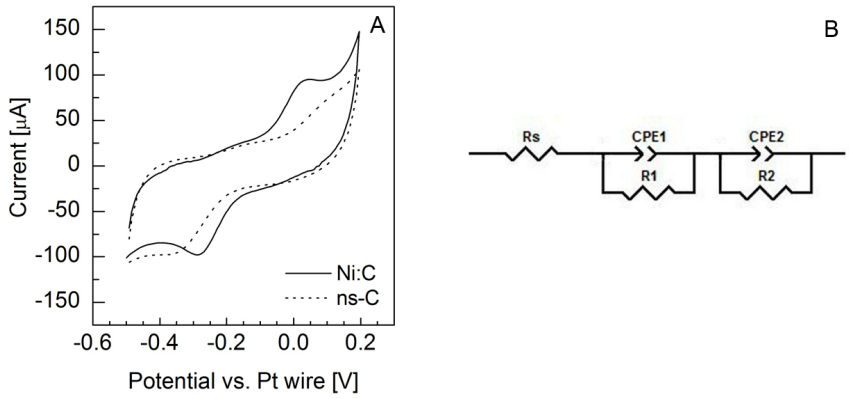

Figure 4.3: (A) Cyclic voltammetry of a Ni:C (continuous line) and a pure ns-C (dotted line) electrode immersed in KOH 1M solution as aqueous electrolyte performed at 40 mV/s in the potential range between -0.5 and 0.2 V. (B) Equivalent circuit used to fit impedance data of figure 4.4. Rs includes the resistance of the electrolyte, the CPE1-R1 subcircuit includes the impedance of the current collector/active material interface as well as the conductivity of the active material and the CPE2-R2 subcircuit represents the electrochemical double layer capacity and the leak resistance.

immersed in KOH (dotted line in figure 4.3A) shows that the electrochemical stability window of the electrode is not reduced as consequence of the inclusion of the Ni nanoparticles.

The electric double layer (EDL) formed at the interface of the Ni:C nanocomposites soaked in KOH 1M solution has been characterized by means of electrochemical impedance spectroscopy (EIS) in the frequency range between 10^5 and 10^{-1} Hz. The as deposited Ni:C electrodes do not show the temporal evolution of the complex impedance spectrum observed on the as deposited pure ns-C electrodes (see section 3.2.1) but exhibit a rapid spectral stabilization indicating that the inclusion of Ni clusters in the ns-C prevents the deterioration of the electrodes. It is likely that the nickel embedding reduces the mechanical stress of the porous matrix improving its adhesion to the current collector. Figure 4.4A reports the Nyquist plots of the complex impedance, acquired after spectral stabilization, of Ni:C electrodes featuring constant thickness (200 nm) and different Ni volumetric concentration. All complex impedance spectra show common trends and two different features can be observed: (i) a high frequency arc and (ii) a low frequency straight line. The frequency at which this latter feature starts, i.e. the knee frequency, is 2, 3, 7, 10 and 15 Hz respectively for 0,

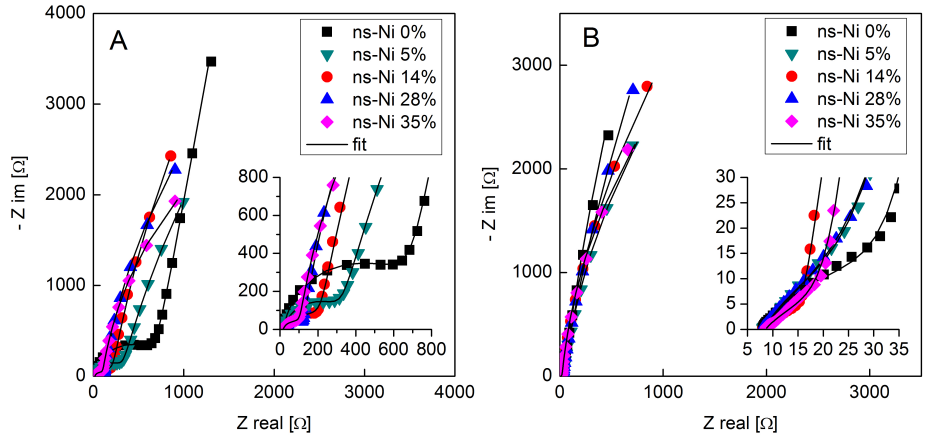

Figure 4.4: Nyquist plot of the complex impedance of the Ni:C nanocomposite electrodes immersed in KOH 1M, as deposited (A) and heated at 300°C in Ar atmosphere (B).

5, 14, 28 and 35 % Ni concentration, showing that the composition of the active material strongly affects the electrode properties. As highlighted in the section dedicated to the characterization of the pure ns-C system (see section 3.2), the high frequency semicircle is related to the electrolyte ionic conductivity and to the interface contact resistance between the Ni current collector and the active material. It is reasonable, as the knee frequency changes with varying Ni concentration, that the high frequency arc can provide also information about *bulk* properties of the active material, such as the electric conductivity. This part of the complex impedance spectrum can be modeled by an over-simplified equivalent circuit composed by a parallel combination of a resistance, R1, which accounts both for the charge transfer from the current collector to the active material and for the charge transport inside the active material, and a constant phase element, CPE1, which represents the capacitive behavior of the interface between the current collector and the active material. Therefore, the high frequency arc can be fitted by the equivalent complex impedance of a resistance, Rs, in series with a parallel combination of a resistance, R1, and a constant phase element, CPE1. The low frequency linear part of the plot (below the knee frequency) is ascribable to the capacitive response of the active material/electrolyte interface. From an electric circuit point of view, the capacitive response of this interface can be

Ni:C	Rs (Ω)	CPE1 (Ss^{α})	α CPE1	R1 (Ω)	CPE2 (Ss^{α})	α CPE2	R2 (Ω)
A	20	34e-06	0.930	632	435e-06	0.884	140e03
B	33	59e-06	0.863	301	707e-06	0.875	14e03
C	84	132e-06	0.695	198	604e-06	0.900	25e03
D	52	82e-06	0.749	105	613e-06	0.914	13e03
E	17	146e-06	0.787	86	680e-06	0.915	8e03

Table 4.2: Best fit equivalent circuit parameters for the complex impedance (figure 4.4A) of the as deposited Ni:C nanocomposites listed in table 4.1. The fit parameters refer to the electric circuit reported in figure 4.3.

modeled as a capacitance. However, as the low frequency part of the complex impedance spectrum deviates from the capacitor ideal behavior (a straight line with infinite slope in the Nyquist plot) due to the relative complicate ions motion in the porosity of the active material, EIS data in this range of frequencies must be fitted by a constant phase element, CPE2, instead of a simply capacitor leading to the overall equivalent circuit shown in figure 4.3B. Best fit equivalent circuit parameters for the complex impedance of the different Ni:C electrodes are reported in table 4.2.

In order to allow a direct comparison between the complex impedance spectra of the different samples, the EIS spectra reported in figure 4.4A are rigidly shifted to the same Rs value by the subtraction of a constant real impedance (typically few Ohms which arise from slight differences in the conductivity of the Ni current collector of the different electrodes). As observable in the figure, the radius of the high frequency arc decreases with increasing Ni loading. This part of the complex impedance spectrum is strictly related to the equivalent series resistance (ESR) that governs the rate at which the energy stored in the EDL can be used, i.e. the power P ($P \propto 1/ESR$, see equation 1.2). Considering the equivalent circuit of figure 4.3B, ESR is equivalent to the sum of Rs and R1. However, as consequence of the shift of the spectra, Rs value of different samples is constant and, as changes in ESR coincide with changes in the R1 parameter, from this point forward we will refer to R1 and/or ESR without distinction. As reported in the left panel of figure 4.5, R1 diminishes with increasing Ni loading moving from ca. 630Ω in the case of the pure ns-C electrode to ca. 86Ω for the Ni:C electrode with highest Ni concentration, with a trend roughly proportional to the inverse of the Ni volumetric concentration in the nanocomposite (R1$\propto$ 1/Ni[%]), suggesting an enhancement of the Ni:C electrical conductivity due to the Ni inclusion. The electric resistance R of a nanocomposite thin film across two nickel electrodes (ca. 0.5 cm^2) separated by a non conductive gap of 0.5 mm has been

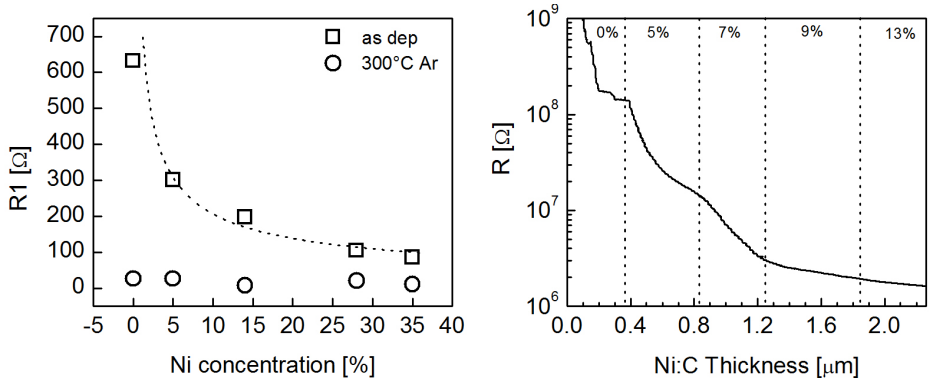

Figure 4.5: (left) Plot of the R1 parameter versus the Ni concentration in the different Ni:C nanocomposites as deposited (open squares) and heated (open circles) at 300°C in Ar atmosphere. (right) Electric resistance of the Ni:C nanocomposite measured in situ during the deposition process as function of the Ni concentration (volumetric percentage).

measured during the deposition process in order to assess any links between R1 and the *bulk* electric conductivity of the Ni:C thin films. Preliminary measurements of the electric resistance of the Ni:C nanocomposite are reported in the right panel of figure 4.5 as function of the amount of material deposited and of the volumetric concentration of nickel clusters controlled by the change of the operating parameters of the two PMCSs during the deposition. Despite the restricted concentration range which has been explored, the evolution of R at varying Ni volumetric percentages is consistent with the trend highlighted by R1, proving that the high frequency impedance arc provides information not only about the current collector/active material interface but also inherent to the electrical properties of the active material. As shown in figure 4.5, both R1 (measured by EIS) and R (measured in situ by a digital multimeter) indicate a drastic increase in the conductivity of the nanocomposite in comparison to the pure carbon system, even at very low nickel concentration. Three different mechanisms arising from the inclusion of Ni nanoparticles in the carbon matrix can be proposed in order to explain the enhanced conductivity of the nanocomposite: (i) the formation of Ni conductive paths in the amorphous carbon matrix, (ii) the nucleation of ordered sp2 structures catalyzed by the Ni and (iii) the n-type doping of the ns-C. However, the first two hypothesis do not seem to be fair explanations of the observed behavior. As matter of fact, the critical volume fraction, i.e. the percolation

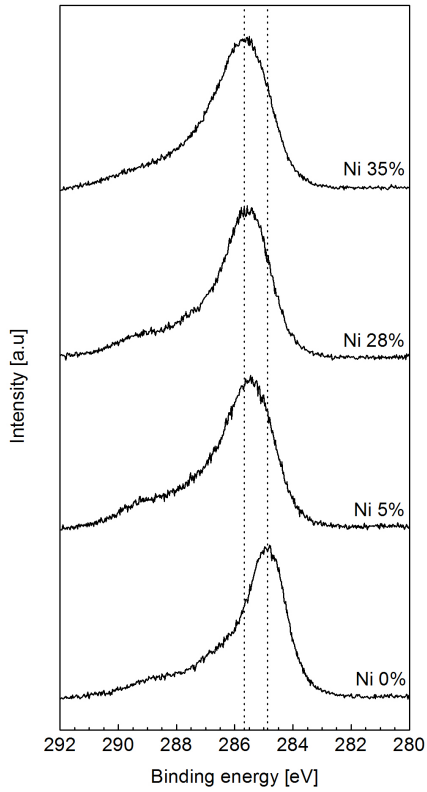

Figure 4.6: C1s x-ray photoemission lines (after Shirley background removal and normalization) of Ni:C nanocomposite thin films with different Ni volumetric concentration (from 0% to 35%).

threshold, at which a conductive 3D network can form in a dielectric medium is expected to be ca. 0.3 [164], well above the Ni concentration (5%) at which the drop in the nanocomposite resistivity is measured. Since one of the dominant transport mechanisms in ns-C thin films is the hopping conduction [72, 165], the nucleation of ordered sp2 sites may provide additional hopping centres that lead to the measured increase in the nanocomposite conductivity. However, despite nickel, in the presence of carbon, is known to catalyze the formation of graphitic structures at relatively low temperatures [146, 148, 150], no signatures of carbon structural evolution in the nanocomposite are observable both in the Raman spectrum of figure 4.2 and in the HRTEM micrographs of figure 4.1, suggesting

that the low kinetic energy of the clusters prevents any catalytic effect of the nickel at room temperature and that, consequently, the overall disordered sp2 structure is not affected by the Ni inclusion. Thus, the hypothesis of doping of the ns-C by the inclusion of Ni clusters appears as the most feasible explanation for the enhancement of the nanocomposite conductivity. This is supported by the C1s x-ray photoemission lines reported in figure 4.6, where the binding energy of the main C1s peak (related to sp2 carbon-carbon bonds) gradually moves from ca. 284.8 eV (ns-C without Ni) to ca. 285.7 eV (Ni:C, Ni 35%) as the amount of Ni clusters incorporated in the ns-C is increased. The observed shift toward higher binding energy is ascribable to an upshift of the Fermi level of the ns-C and, thus, is consistent with an n-type doping effect which can lead to the measured increase in the macroscopic conductivity [166–169].

$$C_{EDL}(f) = -\frac{Z^{'}(f)}{2\pi f \left|Z(f)\right|^2} \tag{4.1}$$

$$U_{vol} = \frac{1}{2} C_{EDL} E^2 \frac{1}{V} \tag{4.2}$$

$$P_{vol} = \frac{1}{4} \frac{E^2}{R1} \frac{1}{V} \tag{4.3}$$

The impact of Ni clusters inclusion, in terms of modification of the electrode interface area available for EDL formation, is evaluated by the analysis of the part of the complex impedance spectra below the knee frequency. EDL capacity (C_{EDL}) calculated at 0.1 Hz by equation 4.1 (where f is the frequency and $Z^{'}$ is the impedance imaginary part, see reference [170] for derivation) has been used to estimate the specific volumetric density of energy U_{vol} and power P_{vol} (equations 4.2 and 4.3, respectively) stored at the interface between the Ni:C thin films and the KOH. We considered a maximum operating voltage (E) of 1V, in agreement with the electrochemical stability window of the electrolyte employed. U_{vol} and P_{vol} values obtained for the different electrodes are reported in figure 4.7A as function of the Ni loading. However, as these data are acquired after the stabilization of the impedance spectrum, the EDL capacity of the pure ns-C electrode yields an understimate of the volumetric energy density of the cluster assembled carbon due to the deterioration of the contact interface between the current collector and the active material which occurs upon ions adsorption in non-heated ns-C electrodes (see section 3.2.1). Therefore, in figure 4.7A is reported the volumetric energy density of the pure ns-C electrode calculated using

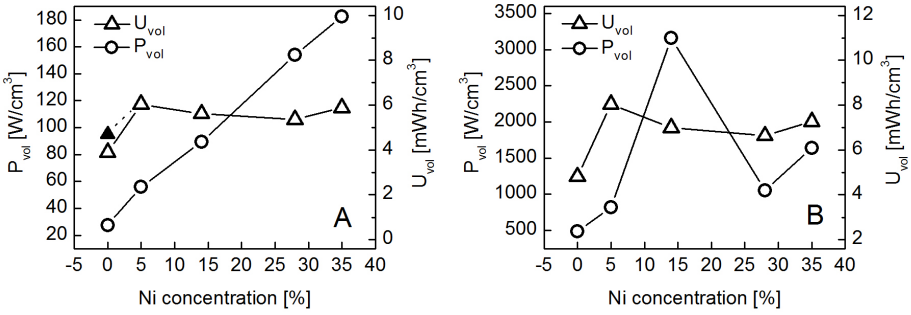

Figure 4.7: Specific volumetric power, P_{vol}, and specific volumetric energy, U_{vol}, of the Ni:C nanocomposite electrodes as deposited (A) and heated at 300°C in Ar atmosphere (B).

the C_{EDL} value as obtained by the complex impedance data acquired both after the spectral stabilization (3.9 ± 0.4 mWh/cm^3, open triangle symbol) and before electrode deterioration (4.7 ± 0.4 mWh/cm^3, closed triangle symbol). We believe this latter value to be more representative in order to compare the amount of energy stored in the ns-C electrode with the energy density of the Ni:C electrodes.

The volumetric energy, U_{vol}, of the different ns-C based electrodes is almost independent upon Ni concentration, with a mean value of about 5.5 ± 0.5 mWh/cm^3, meaning that the Ni clusters embedding does not cause significant changes in the EDL capacity (C_{EDL}). This evidence is also supported by the almost similar CPE2 value obtained by the equivalent circuit fit of the complex impedance of the different Ni:C electrodes (see table 4.2) and proves that the inclusion of Ni nanoparticles in the carbon matrix preserves the porosity of the nanocomposite and does not alter the electrode interfacial area available for EDL formation over a wide range of volumetric concentrations. However, as the weight of the nanocomposite increases with increasing Ni concentration, the specific gravimetric capacitance drops from ca. 78 to 22 F/g moving from pure ns-C electrode to the Ni:C electrode with the highest Ni loading. Incorporation of Ni clusters in the ns-C has been shown to affect the porous matrix electric conductivity and is, therefore, crucial in determining the rate at which the energy stored in the EDL can be released, i.e. the power (see equation 4.3). As shown in figure 4.7A, the specific volumetric power, P_{vol}, of the Ni:C electrodes linearly increases upon the increase of the Ni loading, as can be expected combining equation 4.3 with the trend of ESR observed in electrodes with increasing Ni concentration.

In conclusion, SCBD was established as viable route for the synthesis of Ni:C nanocomposite thin films with tunable Ni concentration and with interesting properties in view of electrochemical energy storage applications. The electrochemical properties of the Ni:C thin films soaked in KOH aqueous solution were studied in terms of electrolyte accessibility, AC impedance response and electrochemical stability window by means of cyclic voltammetry and electrochemical impedance spectroscopy. The presence of embedded Ni nanoparticles in the ns-C film significantly improves the electrical conductivity of the cluster assembled carbon without affecting its specific surface area. The maximum energy storable in the EDL by the five different Ni:C electrodes is almost constant, meaning that the Ni loading does not critically alter the electrode porosity accessible by the electrolyte. The improved electrical conductivity reduces the overall electrode series resistance leading to a linear increase of the maximum volumetric power delivered by the EDL capacitor upon increasing volumetric concentration of Ni clusters in the active material. Therefore, by the fine control of both the amount of deposited nanocomposite material and of the Ni volumetric percentage in the carbon matrix is possible to synthesize electrodes with tunable specific power and energy densities. Furthermore, the inclusion of Ni nanoparticles in the ns-C favors the relaxation of the residual stress typical of thin films grown by room temperature deposition processes, such as SCBD, avoiding the cracking and the delamination of the film upon soaking in the electrolyte.

4.2.1 Thermal treatment in inert atmosphere

Nickel is widely employed as catalyst for the formation of ordered graphitic structures, such as carbon nanotubes, fibres and graphene [146–151]. Furthermore, Ni has low but nevertheless sufficient affinity to carbon to result in the formation of metastable nickel carbide, yet at as low temperature as 250°C [171, 172]. Although no ordered sp2 structures have been observed in the Ni:C nanocomposites grown at room temperature, their formation in the ns-C matrix can be promoted by post deposition thermal treatments, as demonstrated by Agostino et al. in the case of Ni:C films deposited by SCBD employing a single PMCS operating with a composite nickel-carbon cathode [85]. Provided that a thermal induced graphitization of the ns-C does not significantly reduce the high surface area and the porosity of the nanocomposite, it can further enhance the charge transport through the carbon matrix resulting potentially promising toward the synthesis of high-power supercapacitor electrodes.

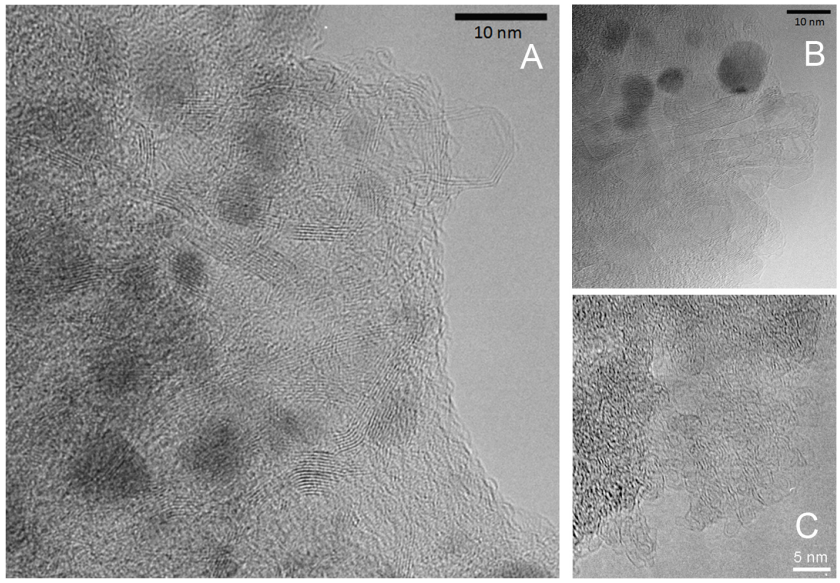

Figure 4.8: HRTEM micrographs of Ni:C nanocomposite, sample B of table 4.1 (A and B), and of pure ns-C (C) heated at 300°C in Ar atmosphere.

Ns-C structural modifications catalyzed by the embedded Ni nanoparticles have been explored by a mild thermal treatment under fluxed argon atmosphere at 300°C. The thermal treatment protocol of the samples consisted in 15 minutes at the constant temperature of 300°C, reached by an heating ramp of 5°C/min up to 300°C and followed by a slow temperature cooling (ca. 2°C/min).
HRTEM micrographs of heated Ni:C films (figure 4.8A and B) show an enhanced graphitic order. Heated nanocomposites are rich in ordered tubular onion-like structures, consisting of concentric curved graphitic sheets, uniformly distributed across the samples. These structures are not observed in a pure ns-C film which underwent the same thermal treatment (figure 4.8C), indicating that the presence of Ni (even in its oxidized phase) favors the graphitisation of amorphous carbon at temperature as low as 300°C. The transformation of part of the ns-C induces a mean thickness reduction of the 25±4% (see figure 4.9) due to the difference in the densities between ns-C (0.5 g/cm^3) and graphite (2.2 g/cm^3). If we assume that the volume fraction of Ni in the nanocomposite is not altered upon heating, this reduction is ascribable to the graphitization of ca. the 40% of ns-C. Carbon structural modifications upon thermal treatments were investi-

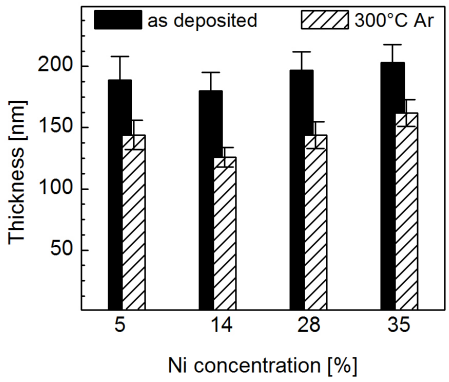

Figure 4.9: Thickness of the Ni:C nanocomposites before and after the thermal treatment at 300°C in Ar atmosphere.

gated also by means of Raman spectroscopy and reported in figure 4.10A. Despite the Raman response of the carbon in the heated nanocomposite is still consistent with an overall amorphous structure, it significantly differs from the one of the as deposited Ni:C film. After the thermal treatment the G peak becomes sharper and slightly upshifts from ca. 1560 cm^{-1}, in the case of the as deposited nanocomposite, to ca. 1570 cm^{-1}. Moreover, D and G peaks are better resolved. This evolution is coherent with the presence of ordered graphitic structures in the ns-C matrix, as observed after the thermal treatment by means of HRTEM (figure 4.8). The Raman contribution of the graphitic carbon has been isolated by the subtraction of the Raman spectrum of the as deposited Ni:C from the spectrum of the heated sample (in order to obtain a difference spectrum ascribable to the concentric curved graphitic sheets formed in the nanocomposite as consequence of the thermal treatment the spectra have been arbitrarily rescaled and offset). The difference spectrum, reported in figure 4.10B, exhibits a broad Raman peak around 1360 cm^{-1} (the defect band, D) and a sharper peak 1580 cm^{-1} (the graphitic band, G) with greater insisty. This spectrum resembles the Raman response of closed graphitic nano-shells (carbon onions) [173–175]. By using the empirical Tuinstra-Koenig relation [176, 177] (equation 4.4, where $I(D)/I(G)$ is ratio between the intensity of the D and G peaks of the spectrum and $C(\lambda)$ is 4.4 nm when $\lambda = 514$ nm as in our case [177, 178]), a graphitic crystallite size L_a of ca. 8 nm is estimated. This size is consistent with the dimensions of the spherical and tubular graphitic structures observed in the heated Ni:C by HRTEM

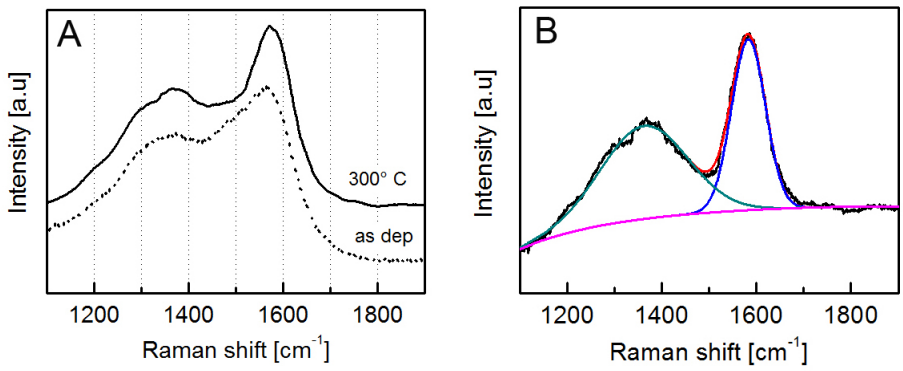

Figure 4.10: (A) Raman spectra of Ni:C nanocomposite (sample B of table 4.1) as deposited (dotted line) and thermal treated at 300°C in Ar atmosphere (continuous line). (B) Difference between the Raman spectra of the heated and the as deposited nanocomposite. The Gaussian fit of the D and G peaks is reported.

microscopy.

$$\frac{I(D)}{I(G)} = \frac{C(\lambda)}{L_a} \tag{4.4}$$

In order to evaluate the evolution of the interfacial properties of Ni:C nanocomposites as consequence of the formation of the onion-like carbon nanostructures catalyzed by the nickel, EIS characterization has been performed. Nyquist plots of the complex impedance of heated Ni:C nanocomposite electrodes synthesized in the same batch of the electrode studied in section 4.2 and soaked in KOH 1M solution as aqueous electrolyte are reported in figure 4.4B. The response curve of the circuit of figure 4.3, obtained by the equivalent circuit fit (best fit parameters are reported in table 4.3), is shown. Impedance spectra have been rigidly shifted at the same real axis intercept at 0.1 MHz to accommodate the differences in the conductivity of the nickel current collector of the electrodes due to slight inhomogeneities in the sputter deposition (see the Rs value in table 4.3) and to allow a direct comparison between the different samples. As consequence of the heating, the high frequency arc observed in the as deposited Ni:C electrodes (figure 4.4A) disappears and is replaced by a diagonal line with a slope of about 45°. Considering the best fit parameters, this is reflected in the decreasing of the αCPE1 exponent from ca. 0.8 to ca. 0.6 for as deposited and heated electrodes, respectively. Such value of the α exponent of the CPE1 element indicates a shift from

Ni:C	Rs (Ω)	CPE1 (Ss^{α})	α CPE1	R1 (Ω)	CPE2 (Ss^{α})	α CPE2	R2 (Ω)
A	20	496e-06	0.651	27	642e-06	0.916	61e03
B	8	1.68e-03	0.582	27	620e-06	0.915	14e03
C	18	462e-06	0.651	8	503e-06	0.913	20e03
D	17	927e-06	0.641	21	537e-06	0.893	42e03
E	17	1.40e-03	0.578	12	670e-06	0.918	17e03

Table 4.3: Best fit equivalent circuit parameters for the complex impedance (figure 4.4B) of the Ni:C nanocomposites listed in table 4.1 and heated at 300°C in Ar atmosphere.

a capacitor-like to a warburg-like behavior (see section 2.2.3) in the frequency range related both to the current collector/active material interface and to the charge transport in the porous matrix, suggesting an enhanced charge injection from the collector to the active layer as well as an improved charge transport in the Ni:C. As a matter of fact, R1 values are significantly reduced compared to the ones obtained by the fit of the complex impedance spectra of the as deposited nanocomposite electrodes. However, a clear trend of R1 as function of the Ni loading is not observable (see table 4.3 and the left panel of figure 4.5). As R1 is related to the electric transport properties of the porous matrix of the electrode, its drop after the thermal treatment is consistent with the presence of the ordered sp2 structures catalyzed by the nickel. It is likely that similar graphitic structures lead to additional hopping centers that enhance the nanocomposite conductivity. Furthermore, after the heating, the sum of the volumetric fraction of the highly ordered graphitic carbon (roughly estimated by the decrease of the nanocomposite thickness) and of the Ni is ca. 0.16, 0.33, 0.49 and 0.51 for the samples grown with a nominal Ni concentration of 5, 14, 28 and 35%, respectively. These concentrations are well above (0.49 and 0.51) or near (0.16 and 0.33) the percolation threshold and suggest that, besides providing additional hopping centres, graphitic sites may form, together with Ni nanoparticles, a percolative network for the charge transport inside the porous matrix. The decrease of R1 in the case of the ns-C electrode with no embedded Ni nanoparticles does not arise from a thermally induced enhancement of the electric conductivity of the carbon. As exhibited by both the Raman spectrum of figure 3.7 and the HRTEM micrograph of figure 4.8, no graphitization is expected in the ns-C after the thermal treatment and the drop of R1 is thus reasonably ascribable to an enhanced electric contact at the interface between the ns-C and the Ni current collector (for a thorougher discussion of the consequences of thermal treatments on the electrode biasing see section 3.2). However, as the equivalent circuit employed to

explain the experimental data suffers from oversimplification, it does not allow to separate the contributions of the current collector/active material interfacial contact and of the active material conductivity to the R1 parameter. Improvements of the equivalent circuit to better model the electrochemical impedance spectra and disentangle the electric resistance of the nanocomposite form the one of the current collector/active material interface are currently underway.
The impact of the nucleation of the graphitic structures in the ns-C matrix on the overall porosity of the nanocomposites has been studied by the analysis of the low frequency part of the electrochemical impedance spectra reported in figure 4.4. As this range of frequency concerns with the EDL formed at the interface between the pores of the Ni:C and the KOH, it is sensitive to any changes in the nanocomposite electrode porosity that might be induced by the heating. The values of CPE2 obtained by the equivalent circuit fit of the impedance spectra of the heated nanocomposite electrodes are slightly lower of the one obtained for the as deposited Ni:C electrodes (see tables 4.2 and 4.3 for comparison), revealing a decrease in the EDL capacity after the thermal treatment, as could be expected by the decrease in the thickness of the heated Ni:C thin films. However, this difference is too slight to be ascribable to the significant thermally induced reduction of the thickness. Indeed, as reported in figure 4.7B, if the EDL capacity is normalized by the Ni:C volume to calculate the specific energy densities, U_{vol} (see equations 4.1 and 4.2), stored in the EDL, these are about 20% higher than the one measured in the case of the non-heated samples. U_{vol} of the pure ns-C electrode does not change as consequence of the heating as discussed in section 3.2.1. As the energy density is directly related to the volumetric EDL capacity, which ultimately depends on the porous interfacial structure of the Ni:C electrodes, this enhancement indicates a modification of the overall porosity of the nanocomposites, which seems to increase and/or become more accessible for the ions of the electrolyte as consequence of the heating. Besides improving the Ni:C conductivity, the germination of the graphitic nanostructures in the ns-C matrix may modify the porous structure of the nanocomposites in terms of both void fraction and pores shape, leading thus to the enhancement of U_{vol}. Figure 4.7B shows that the specific volumetric power densities, P_{vol}, of the heated Ni:C are about one order of magnitude higher that the one of the as deposited nanocomposite, as expected by the decrease of the overall series resistance of the electrodes (see the evolution of R1 in figure 4.5). As discussed in the case of R1, the mechanism leading to the enhancement of P_{vol} cannot be univocally identified. It is reasonable to assume that it owes to the presence of ordered graphitic structures

catalyzed in the ns-C not only by the embedded Ni clusters but also by the nickel current collector. While the formation of the graphitic nanoparticles in the ns-C is due to the embedded Ni clusters and proceeds only in the nanocomposites, the thermally induced graphitization of the carbon at the active material/current collector interface is common to all the electrodes and contributes to the drop of the ESR (even in the pure ns-C electrode). Heated nanocomposites show higher volumetric power densities in comparison with the thermal treated ns-C electrode and, even if a clear trend relating P_{vol} to the Ni loading is not present, it is reasonable that the differences in the values of P_{vol} can be explained by differences in the electrode conductivity. We can further speculate, but cannot prove, that the disproportionately high volumetric power density exhibited by the nanocomposite with a nominal 14% Ni concentration owes to an optimal Ni:C volume ratio that maximize the thermally induced graphitization of the ns-C.

The synthesis of cluster assembled Ni:C nanocomposites is an interesting route not only toward the room temperature growth of porous materials with optimized properties but also in view of post deposition treatments that modify the structure of the nanocomposites preserving their porous nature. The high surface to volume ratio typical of clusters ensures a huge interfacial area between the clusters of the different materials which constitute the nanocomposite, facilitating their interaction. In the case of Ni:C nanocomposites, the inclusion of Ni nanoparticles in the ns-C matrix has been shown to enhance the carbon conductivity without affecting its high specific surface area. Furthermore, it has been demonstrated that embedded Ni nanoparticles catalyze the formation of ordered graphitic structures at relative low temperatures. We expect that other effects (e.g. carburization) can be induced in ns-C porous thin films that host metal nanoparticles different from Ni. Besides being an issue of fundamental interest, the interaction between carbon and metal clusters within the nanocomposite, as demonstrated in the case of Ni, can positively impact on the electrochemical properties of ns-C.

4.3 Conclusions

The codeposition of nickel and carbon clusters separately produced in different PMCSs has been demonstrated as a feasible route to synthesize porous nanocomposites. Four Ni:C thin films featuring the same thickness and different nickel volumetric concentration have been deposited. The nanocomposites showed a

uniform distribution of Ni nanoparticles in the ns-C matrix. As the low kinetic energy deposition regime typical of SCBD prevents the interaction between carbon and nickel clusters, the ns-C retains its characteristic amorphous structure and no graphitization is catalyzed by the nickel in the as deposited samples. Evidences of the presence of oxidized nickel have been found.
The electrochemical characterization of Ni:C based electrodes soaked in alkaline electrolyte showed a volumetric energy density independent on the amount of embedded Ni, indicating that the active material porosity is not affected by the inclusion of Ni. Conversely, as the Ni:C electrical conductivity is enhanced by the presence of nickel, a linearly increasing specific volumetric power density has been measured with increasing Ni loading. Moreover, nanocomposites showed a higher mechanical adhesion to the current collector which avoids cracking and delamination upon soaking in the electrolyte. Finally, a thermal treatment at 300°C of the Ni:C has been shown to promote the formation of ordered graphitic nanostructures in the nanocomposites which further increase the rate capability of the electrodes without reducing their volumetric energy density.
The inclusion of Ni in the ns-C overcomes the main shortcomings of ns-C based electrodes, such as the need for thermal treatment and the low electric conductivity, and is thus promising toward the use of ns-C based thin films as active material in supercapacitors. Compared to the synthesis techniques commonly employed to fabricate metal:carbon nanocomposite electrodes for electrochemical energy storage [154–158] which can be barely integrated with microfabrication and/or thin film deposition techniques, SCBD presents several advantages, such as the compatibility with standard planar microtechnology processes, that may be of particular interest toward the fabrication of thin film nanocomposite electrodes for miniaturized supercapacitors.

General conclusions

The PhD research activity reported in this thesis dealt with the synthesis and characterization of porous cluster assembled carbon thin films. Porous forms of carbon with high specific surface area are widely used in supercapacitors as electrode material for electrochemical energy storage. However, the growing demand for higher energy and power densities pushes the interest toward the development of porous carbon with tailored properties. Fabricating thin film based supercapacitors suitable for portable devices or integrable in micro electromechanical systems is another challenge that drives the development of new routes for the synthesis of nanostructured carbon. In this context, the intrinsic porosity of carbon grown by supersonic cluster beam deposition (SCBD) as well as the compatibility of the SCBD technique with planar technology and temperature sensitive substrates are appealing features that inspired this work.

The electrochemical energy storage properties of porous carbon (ns-C) thin films grown by the supersonic cluster beam deposition (SCBD) of carbon clusters produced in a pulsed vaporization source (PMCS) have been presented in this thesis through the study of the electric double layer (EDL) formed at the interface of ns-C based electrodes soaked in a liquid electrolyte. Ns-C behavior as electrode material has been characterized as function of deposition time (i.e. ns-C thickness), post deposition thermal treatment, metal nanoparticles embedding and electrolyte type. Our results demonstrate the strong potential of SCBD deposited ns-C as porous material in capacitive electrodes to be integrated in thin film electrochemical energy storage devices.

First of all, the EDL properties of ns-C were investigated employing a KOH 1 M aqueous solution as electrolyte. Electrochemical characterization showed

high gravimetric capacity values and a poor electric and mechanical contact at the interface between the ns-C and the nickel current collector. A short thermal treatment in air and the deposition of a thin inter layer of SCBD deposited ns-Ni between the current collector and the ns-C have been employed as strategies to improve electrode performances. Both these approaches led to an enhanced contact at Ni/C interface and to an increase of the EDL capacity. Specific gravimetric capacitance values up to 120 F/g have been measured. We demonstrated that the preparation of a nanostructured current collector via deposition of nickel nanoparticles, thus obtaining a surface morphology of the substrate similar to the ns-C texture, can significantly improve the active material capacitive behavior without the need for thermal treatment. These results overcome some limitations typical of nanostructured materials in terms of metal/nanostructure contact geometries and in terms of post deposition treatments such as sintering and annealing. The deposition of a nanostructured current collector provides new perspectives for the use of cluster assembled nanostructured electrodes in electrochemical applications. Moreover, a linear increase of the electrode EDL capacitance with the ns-C thickness has been measured, suggesting that the surface area to volume ratio of the cluster assembled carbon is constant. This finding agrees with the ballistic film growth typical of SCBD and is relevant toward the ability to tune the amount of energy stored in the EDL by the accurate control of the amount of deposited material.

From a more applicative point of view, the use of electrochemical capacitive devices based on thin film electrodes is hampered by the limited extension of thin film interfacial area which leads to low values of specific storable energy. For this reason the use of room temperature ionic liquids (RTILs) instead of conventional aqueous electrolytes is to be considered a potentially advantageous scenario. Thus, we moved to the characterization of the EDL formed at the interface between ns-C thin films and four different hydrophobic RTILs. This analysis showed that the nanostructure of the ns-C, which is fundamental for the double layer formation mechanism, is characterized by an open porosity, easily wettable and accessible by RTILs. A specific capacity up to 75 F/g was measured over a wide range of ns-C thicknesses. We demonstrated also the viability of SCBD for the fabrication of an ns-C based supercapacitor easily implementable on a wide range of different substrates (e.g. glass, SiO_2, polymers) and with a geometry compatible with planar technology. The measured performances, together with the intrinsic versatility of SCBD in producing patterned deposition, are appealing for the fabrication of thin electrodes for microscale energy storage

devices to be integrated in planar microsystems.

The fine control over the porous carbon structure at the synthesis stage is both a fundamental issue and a key for the breakthrough of nanomaterials in practical applications. In the last part of this thesis the codeposition of nickel and carbon clusters separately produced in different PMCSs has been demonstrated as a feasible route to synthesize nanocomposites with optimized properties. Ni:C nanocomposite electrodes featuring the same thickness and different volumetric nickel concentration (from 5% to 35%) exhibited an almost constant volumetric energy density, meaning that the porous nanostructure is not affected by the Ni inclusion, and a volumetric power density linearly related to the Ni loading, proving the enhancement in the nanocomposite electric conductivity due to the inclusion of Ni clusters. Embedded nickel nanoparticles were shown to catalyze the formation of tubular onion-like carbon structures upon mild thermal treatment in inert atmosphere. Electrochemical characterization of the heated nanocomposite electrodes revealed that the germination of ordered sp2 structures preserves the high surface area available for EDL formation and further improves the energy storage properties in terms of deliverable power.

The findings of my PhD work establish the feasibility of the SCBD technique for the synthesis of highly porous carbon and metal:carbon nanocomposite thin films with promising potential in the electrochemical energy storage field. The results obtained by the codeposition of clusters of different materials disclose new stimulating perspectives toward the use of SCBD in the synthesis of nanocomposites with tailored properties. Furthermore, SCBD thanks to its compatibility with temperature sensitive substrates and its highly collimated and intense cluster beam has been shown to be a suitable technique for the deposition of highly porous carbon easily integrable as electrode capacitive material in thin film based supercapacitors. From a more fundamental point, the work presented in this thesis assesses the viability of the electrochemical technique as tool to disclose the interfacial properties of cluster assembled materials which arise from their intrinsic porous nature. These preliminary results provide the basis for further developments of this research activity. The integration of electrochemical quartz crystal microbalance (EQCM) analysis, as gravimetric probe to measure mass changes at electrodes due to the ionic fluxes in the ns-C pore volume during electrochemical processes, as well as the development of improved equivalent electric circuits, as models to argue the physical properties of the electrode material from the fit of its impedance spectra, are two forthcoming routes that I'm going to implement to further extend the spectrum of information about the physico-chemical properties

of cluster assembled materials provided by interfacial electrochemical methods.

Appendix: the NanoToTouch project

This appendix briefly refers about the outreach activity carried out by the Interdisciplinary Centre for Nanostructured Materials and Interfaces (CIMAINA) and the Museum of Science and Technology 'Leonardo da Vinci' (MUST) of Milan within the EU-funded FP7 NanoToTouch project. I have been involved in this project since the beginning of my PhD research activity at CIMAINA in January 2010, and, as part of the core team, I contributed to the set-up and implementation of the OpenNanoLab opened at MUST by the CIMAINA in March 2010. The electrochemical characterization of the cluster assembled electrodes, which constitutes a large part of the experimental work presented in this thesis, has been entirely conducted in this so-called OpenNanoLab. Moreover, as all the researchers working in the lab, I took part in the science communication activities organized by the CIMAINA and the MUST to engage and inform the public about nanotechnology and nanoscience. Thanks to the achieved results I received a special mention for the Outreach Prize 2012 awarded by the Italian Physics Society (SIF).

The project

NanoToTouch is a project supported by the EU Seventh Framework Programme (EU FP7) that aims to create innovative spaces where the broad public can learn about nanoscience and nanotechnology. It proposes a straightforward way to do this by taking the laboratory environment and the research work out of the university and relocating them in the public space of science museums. Most importantly, NanoToTouch sets out to encourage the visitors of the museums

to interact with researchers in a totally new way: either by just stopping by to ask a question or observing the scientist's work as it takes place in the Museum. Thanks to the NanoToTouch project, in 2010 a real research laboratory on nanotechnology (i.e. the OpenNanoLab), where researchers from CIMAINA work daily on scientific research projects, has been created at MUST. The aim is to make possible for visitors of the Museum, at any time of the day, to observe researchers at work and communicate directly with them by asking questions. Also one of the key aims of the project is to allow researchers to listen to the views and needs of society, getting contexts and tools for communicating with non-experts.

The OpenNanoLab

The OpenNanoLab is a research lab for nanostructured materials characterization created by MUST and CIMAINA inside the public space of the Museum, with a specifically designed layout to promote interaction between the CIMAINA researchers and the Museum visitors. The core of the facility is an apparatus for electrochemical impedance spectroscopy (EIS) and intensity modulated photocurrent spectroscopy (IMPS). The setup includes a potentiostat/galvanostat, a glove-box for electrochemical measurements in controlled atmosphere and an optical system for controlled illumination of the nanostructured electrodes. The light source is a 150W Xenon lamp coupled to a monochromator and eventually modulated by an electro optical modulator. The setup of the facility was inspired by the potential for applications in the field of energy conversion and storage of nanostructured materials grown by supersonic cluster beam deposition (SCBD). Photo-electrochemical solar cells for the production of electrical energy or hydrogen and supercapacitors realized by SCBD are examples of devices that are currently under test in the OpenNanoLab.
The laboratory is open to the public by two glass walls that allow the visitors to observe researchers at work. For safety reasons visitors cannot enter in to the OpenNanoLab and researchers are requested to exit the laboratory in order to engage in dialogue with the public. For this purpose, a so-called interaction area has been specifically designed outside the laboratory.

The outreach activity

In the OpenNanoLab area visitors of the Museum can observe daily work processes of the scientists, asking questions and entering into a dialogue, not only

on the specific research conducted in the lab, but also on ethical and social aspects of nanotechnolgy. The presence of a real research laboratory in a museum creates significant opportunities for the communication of current research and the establishment of direct relationships between citizens and the scientific community. Visitors of the OpenNanoLab area of MUST are able both to engage in dialogue with researchers and to visit a small exhibition on nanotechnologies, which includes an interactive exhibit on solar cells where the standard silicon based technology is compared to new emerging technologies based on nanostructured thin films. The topic of renewable energies resulted very effective to easily get in touch with the public of the Museum.

Besides observing the scientist's work, several science outreach activities that combine interactive activities conducted by the explainers of the MUST with dialogue with researchers on issues of nanotechnology, energy and materials have been developed by CIMAINA and MUST and are offered to groups of visitors during the weekend and to schools during the week.

Furthermore, the daily science communication activity allow researchers to listen to the views and needs of society, getting contexts and tools for communicating with non-experts. The daily dialogue challenges the researchers working in the OpenNanoLab to consider new and different aspects of their work, thus extending their horizons and, hopefully, enabling them to be not only better communicators, but more complete researchers.

List of publications

As of December 2012

Refereed publications

L.G. Bettini, G. Bardizza, A. Podestà, P. Milani and P. Piseri, *Electrochemical Impedance Spectroscopy on nanostructured carbon electrodes grown by Supersonic Cluster Beam Deposition.* (accepted by Journal of Nanoparticle Research).

Publications under review

L.G.Bettini, M. Galluzzi, A. Podestà, P. Milani and P. Piseri, *Planar thin film supercapacitor based on cluster assembled nanostructured carbon and ionic liquid electrolyte.* (submitted to Carbon).

F. Riboni, L.G. Bettini, D. W. Bahnemann and E. Selli, *WO3-TiO2 vs. TiO2 photocatalysts: effect of the W precursor and amount on the photocatalytic activity of mixed oxides.* (submitted to Catalysis Today).

M. Altomare, M. Allieta, M. Pozzi, L.G. Bettini, E. Selli *H2 and O2 photocatalytic production on TiO2 nanotube arrays: effect of the anodization time on*

structural features and photoactivity. (submitted to Applied Catalysis B: Environmental).

Contributions at international congresses

16th International symposium on small particles and inorganic clusters (ISSPIC), Leuven, Belgium 8-13 July 2012, *Electrochemical impedance spectroscopy on highly porous nanocomposite carbon/nickel thin films grown by supersonic cluster beam deposition* (poster presentation), L.G. Bettini, G. Divitini, C. Ducati, A. Podestà, P. Milani and P. Piseri.

16th International conference on solid films and surfaces (ICSFS), Genoa, Italy 1-6 July 2012, *Electrochemical impedance spectroscopy on nanostructured carbon electrodes grown by supersonic cluster beam deposition* (poster presentation), L.G. Bettini, A. Podestà, P. Milani and P. Piseri.

5th Gerischer symposium. Photoelectrochemistry: from fundamentals to solar applications, Berlin, Germany 22-24 June 2011, *Photoelectrochemistry of Nanostructured Cluster Assembled TiO2 Photoanodes Deposited by FlameBeam* (poster presentation), L.G. Bettini, G. Bardizza, A. Podestà, P. Piseri and P. Milani.

Nanostructured Hybrid Materials for Energy Conversion and Storage (International summer school), Ostuni, Italy 5-10 June 2011, *Electrochemical Impedance Spectroscopy of Nanostructured Cluster Assembled Carbon Electrodes* (poster presentation), L.G. Bettini, A. Podestà, P. Milani and P. Piseri.

Nanotechnology for sustainable energy, Obergurgl, Austria 4-9 July 2010, *A facility for photoelectrochemical and electrochemical spectroscopy of nanostructured interfaces open to the general public of a science museum* (poster presentation), L.G. Bettini, G. Bardizza, F. Della Foglia, A. Podestà, P. Piseri, S. Calcagnini, S. Buratti, M. Xanthoudaki and P. Milani.

Bibliography

[1] Michael Graetzel. Solar energy conversion by dye-sensitized photovoltaic cells. *Inorganic Chemistry*, 44(20):6841–6851, 2005.

[2] Y.G. Guo, J.S. Hu, and L.J. Wan. Nanostructured materials for electrochemical energy conversion and storage devices. *Advanced Materials*, 20(15):2878–2887, 2008.

[3] B. Scrosati J.M. Tarascon A.S. Arico, P. Bruce and W. van Schalkwijk. Nanostructured materials for advanced energy conversion and storage devices. *Nature Materials*, 4:366 – 377, 2005.

[4] P.G. Bruce, B. Scrosati, and J.M. Tarascon. Nanomaterials for rechargeable lithium batteries. *Angewandte Chemie International Edition*, 47(16):2930–2946, 2008.

[5] H.W. Kroto, J.R. Heath, S.C. O'Brien, R.F. Curl, and R.E. Smalley. C60: Buckminsterfullerene. *Nature*, 318, 1985.

[6] S. Iijima. Helical microtubules of graphitic carbon. *Nature*, 354, 1991.

[7] K. S. Novoselov, A. K. Geim, S. V. Morozov, D. Jiang, Y. Zhang, S. V. Dubonos, I. V. Grigorieva, and A. A. Firsov. Electric field effect in atomically thin carbon films. *Science*, 306(5696):666–669, 2004.

[8] A.G. Pandolfo and A.F. Hollenkamp. Carbon properties and their role in supercapacitors. *Journal of Power Sources*, 157(1):11 – 27, 2006.

[9] L.L. Zhang and X.S. Zhao. Carbon-based materials as supercapacitor electrodes. *Chem. Soc. Rev.*, 38:2520–2531, 2009.

[10] J. Chmiola, C. Largeot, P.L. Taberna, P. Simon, and Y. Gogotsi. Monolithic carbide-derived carbon films for micro-supercapacitors. *Science*, 328(5977):480–483, 2010.

[11] D. Pech, M. Brunet, H. Durou, P. Huang, V. Mochalin, Y. Gogotsi, P.L. Taberna, and P. Simon. Ultrahigh-power micrometre-sized supercapacitors based on onion-like carbon. *Nature Nanotechnology*, 5(9):651–654, 2010.

[12] W. Gao, N. Singh, L. Song, Z. Liu, A. Reddy, L. Ci, R. Vajatali, Q. Zhang, B. Wei, and P.M. Ajayan. Direct laser writing of micro-supercapacitors on hydrated graphite oxide films. *Nature Nanotechnology*, 6(8):496–500, 2011.

[13] J.J. Yoo, K. Balakrishnan, J. Huang, V. Meunier, B.G. Sumpter, A. Srivastava, M. Conway, R. Mohana, L. Arava, J. Yu, R. Vajtai, and P.M. Ajayan. Ultrathin planar graphene supercapacitors. *Nano Letters*, 11(4):1423–1427, 2011.

[14] M. Kaempgen, C.K. Chan, J. Ma, Y. Cui, and G. Gruner. Printable thin film supercapacitors using single-walled carbon nanotubes. *Nano Letters*, 9(5):1872–1876, 2009.

[15] D.S. Su and R. Schlogl. Nanostructured carbon and carbon nanocomposites for electrochemical energy storage applications. *ChemSusChem*, 3(2):136–168, 2010.

[16] I.V Barsukov, C.S Johnson, J.E. Doninger, and V.Z. Barsukov. *New Carbon Based Materials for Electrochemical Energy Storage Systems: Batteries, Supercapacitors and Fuel Cells*. Springer, 2006.

[17] Walt A. de Heer. The physics of simple metal clusters: experimental aspects and simple models. *Rev. Mod. Phys.*, 65:611–676, 1993.

[18] Special issue on clusters. *Science*, 271:892–950, 1996.

[19] Y. Wang and N. Herron. Nanometer-sized semiconductor clusters: materials synthesis, quantum size effects, and photophysical properties. *The Journal of Physical Chemistry*, 95(2):525–532, 1991.

[20] A. P. Alivisatos. Semiconductor clusters, nanocrystals, and quantum dots. *Science*, 271(5251):933–937, 1996.

[21] F. Baletto and R. Ferrando. Structural properties of nanoclusters: Energetic, thermodynamic, and kinetic effects. *Rev. Mod. Phys.*, 77:371–423, 2005.

[22] P. Jena and S.N. Khanna. Physics of cluster assembled materials. *Materials Science and Engineering: A*, 217 - 218(0):218 – 222, 1996.

[23] A. Perez, P. Melinon, V. Dupuis, P. Jensen, B. Prevel, J. Tuaillon, L. Bardotti, C. Martet, M. Treilleux, M. Broyer, M. Pellarin, J. L. Vaille, B. Palpant, and J. Lerme. Cluster assembled materials: a novel class of nanostructured solids with original structures and properties. *Journal of Physics D: Applied Physics*, 30(5):709, 1997.

[24] P. Jensen. Growth of nanostructures by cluster deposition: Experiments and simple models. *Rev. Mod. Phys.*, 71:1695–1735, 1999.

[25] K. Wegner, P. Piseri, H. Vahedi Tafreshi, and P. Milani. Cluster beam deposition: a tool for nanoscale science and technology. *Journal of Physics D: Applied Physics*, 39(22):439, 2006.

[26] V. N. Popok, I. Barke, E. E.B. Campbell, and K.H. Meiwes-Broer. Cluster - surface interaction: From soft landing to implantation. *Surface Science Reports*, 66(10):347 – 377, 2011.

[27] G. Fuchs, P. Melinon, F. Santos Aires, M. Treilleux, B. Cabaud, and A. Hoareau. Cluster-beam deposition of thin metallic antimony films: Cluster-size and deposition-rate effects. *Phys. Rev. B*, 44:3926–3933, 1991.

[28] G. Corbelli, C. Ghisleri, M. Marelli, P. Milani, and L. Ravagnan. Highly deformable nanostructured elastomeric electrodes with improving conductivity upon cyclical stretching. *Advanced Materials*, 23(39):4504–4508, 2011.

[29] S. H. Baker, A. M. Asaduzzaman, M. Roy, S. J. Gurman, C. Binns, J. A. Blackman, and Y. Xie. Atomic structure and magnetic moments in cluster-assembled nanocomposite fe/cu films. *Phys. Rev. B*, 78:014422, 2008.

[30] W. Bouwen, P. Thoen, F. Vanhoutte, S. Bouckaert, F. Despa, H. Weidele, R. E. Silverans, and P. Lievens. Production of bimetallic clusters by a dual-target dual-laser vaporization source. *Review of Scientific Instruments*, 71(1):54–58, 2000.

[31] G. Bongiorno, C. Lenardi, C. Ducati, R.G. Agostino, T. Caruso, M. Amati, M. Blomqvist, E. Barborini, P. Piseri, S. La Rosa, E. Colavita, and P. Milani. Nanocrystalline metal/carbon composites produced by supersonic cluster beam deposition. *Journal of Nanoscience and Nanotechnology*, 5(7):1072–1080, 2005.

[32] K.D.G.I. Jayawardena, Y.Y. Tan, J. Fryar, H. Shiozawa, S.R.P. Silva, S.J. Henley, G.M. Fuge, B.S. Truscott, and M.N.R. Ashfold. Highly conductive nanoclustered carbon:nickel films grown by pulsed laser deposition. *Carbon*, 49(12):3781 – 3788, 2011.

[33] Shinohara N., Katoh R., and Sumiyama K. Electrical percolation during codeposition of fe and si clusters by a dual source pgccd system. *Materials Transactions*, 49(4):693–697, 2008.

[34] Sawa S., Tanaka N., Katoh R., and Sumiyama K. Ti and ni cluster composites prepared by a dual source plasma gas condensation cluster deposition system. *Materials Transactions*, 49(6):1219–1222, 2008.

[35] E. Barborini, P. Piseri, and P. Milani. A pulsed microplasma source of high

intensity supersonic carbon cluster beams. *Journal of Physics D: Applied Physics*, 32(21):105, 1999.

[36] E. Barborini, P. Piseri, A. Podestà, and P. Milani. Cluster beam microfabrication of patterns of three-dimensional nanostructured objects. *Applied Physics Letters*, 77(7):1059–1061, 2000.

[37] P. Milani, E. Barborini, P. Piseri, C.E. Bottani, A.C. Ferrari, and A. Li Bassi. Nanostructured carbon films from supersonic cluster beam deposition: structure and morphology. *The European Physical Journal D - Atomic, Molecular, Optical and Plasma Physics*, 9:63–68, 1999.

[38] P. Milani, A. Podesta, P. Piseri, E. Barborini, C. Lenardi, and C. Castelnovo. Cluster assembling of nanostructured carbon films. *Diamond and Related Materials*, 10(2):240 – 247, 2001.

[39] P. Piseri, A. Podestà, E. Barborini, and P. Milani. Production and characterization of highly intense and collimated cluster beams by inertial focusing in supersonic expansions. *Review of Scientific Instruments*, 72(5):2261–2267, 2001.

[40] P. Piseri, H. Vahedi Tafreshi, and P. Milani. Manipulation of nanoparticles in supersonic beams for the production of nanostructured materials. *Current Opinion in Solid State and Materials Science*, 8(3 - 4):195 – 202, 2004.

[41] T. Mazza, M. Devetta, P. Milani, G. Bongiorno, M. Coreno, and P. Piseri. Accessing the fractal dimension of free clusters in supersonic beams. *New Journal of Physics*, 13(2):023009, 2011.

[42] R.B. Heimann, S.E. Evsvukov, and Y. Koga. Carbon allotropes: a suggested classification scheme based on valence orbital hybridization. *Carbon*, 35(10 - 11):1654 – 1658, 1997.

[43] R. F. Curl. Dawn of fullerenes: Conjecture and experiment (nobel lecture). *Angewandte Chemie International Edition in English*, 36(15):1566–1576, 1997.

[44] H. Kroto. Symmetry, space, stars, and c60 (nobel lecture). *Angewandte Chemie International Edition in English*, 36(15):1578–1593, 1997.

[45] R. E. Smalley. Discovering the fullerenes (nobel lecture). *Angewandte Chemie International Edition in English*, 36(15):1594–1601, 1997.

[46] A. K. Geim. Random walk to graphene (nobel lecture). *Angewandte Chemie International Edition*, 50(31):6966–6985, 2011.

[47] K. S. Novoselov. Graphene: Materials in the flatland (nobel lecture). *Angewandte Chemie International Edition*, 50(31):6986–7002, 2011.

[48] Special issue on carbon nanostructures for energy. *Energy Environ. Sci.*, 4:604–604, 2011.

[49] Special issue on carbon nanostructures for energy. *Energy Environ. Sci.*, 4:585–1044, 2011.

[50] C. Vix-Guterl, E. Frackowiak, K. Jurewicz, M. Friebe, J. Parmentier, and F. Béguin. Electrochemical energy storage in ordered porous carbon materials. *Carbon*, 43(6):1293 – 1302, 2005.

[51] A.B. Fuertes, G. Lota, T.A. Centeno, and E. Frackowiak. Templated mesoporous carbons for supercapacitor application. *Electrochimica Acta*, 50(14):2799 – 2805, 2005.

[52] R. Kötz and M. Carlen. Principles and applications of electrochemical capacitors. *Electrochimica Acta*, 45(15 - 16):2483 – 2498, 2000.

[53] B. E. Conway. *Electrochemical Supercapacitors: Scientific Fundamentals and Technological Applications*. Springer, 1999.

[54] Y. Zhai, Y. Dou, D. Zhao, P.F. Fulvio, R.T. Mayes, and S. Dai. Carbon materials for chemical capacitive energy storage. *Advanced Materials*, 23(42):4828–4850, 2011.

[55] E. Frackowiak and F. Béguin. Electrochemical storage of energy in carbon nanotubes and nanostructured carbons. *Carbon*, 40(10):1775 – 1787, 2002.

[56] P. Simon and Y. Gogotsi. Materials for electrochemical capacitors. *Nature Materials*, 7:845 – 854, 2008.

[57] E. Frackowiak. Carbon materials for supercapacitor application. *Phys. Chem. Chem. Phys.*, 9:1774–1785, 2007.

[58] Y. Zhang, H. Feng, X. Wu, L. Wang, A. Zhang, T. Xia, H. Dong, X. Li, and L. Zhang. Progress of electrochemical capacitor electrode materials: A review. *International Journal of Hydrogen Energy*, 34(11):4889 – 4899, 2009.

[59] E. Frackowiak and F. Béguin. Carbon materials for the electrochemical storage of energy in capacitors. *Carbon*, 39(6):937 – 950, 2001.

[60] A. Burke. R and d considerations for the performance and application of electrochemical capacitors. *Electrochimica Acta*, 53(3):1083 – 1091, 2007.

[61] C. Masarapu, H. F. Zeng, K. H. Hung, and B. Wei. Effect of temperature on the capacitance of carbon nanotube supercapacitors. *ACS Nano*, 3(8):2199–2206, 2009.

[62] L. L. Zhang, R. Zhou, and X. S. Zhao. Graphene-based materials as supercapacitor electrodes. *J. Mater. Chem.*, 20:5983–5992, 2010.

[63] C. Liu, Z. Yu, D. Neff, A. Zhamu, and B. Z. Jang. Graphene-based supercapacitor with an ultrahigh energy density. *Nano Letters*, 10(12):4863–4868, 2010.

[64] S. W. Lee, B. M. Gallant, H. R. Byon, P. T. Hammond, and Y. Shao-Horn. Nanostructured carbon-based electrodes: bridging the gap between thin-film lithium-ion batteries and electrochemical capacitors. *Energy Environ. Sci.*, 4:1972–1985, 2011.

[65] H. Durou, D. Pech, D. Colin, P. Simon, P.L. Taberna, and M. Brunet. Wafer-level fabrication process for fully encapsulated micro-supercapacitors with high specific energy. *Microsystem Technologies*, 18:467–473, 2012.

[66] P. Huang, M. Heon, D. Pech, M. Brunet, P.L. Taberna, Y. Gogotsi, S. Lofland, J.D. Hettinger, and P. Simon. Micro-supercapacitors from carbide derived carbon (cdc) films on silicon chips. *Journal of Power Sources*, 225(0):240 – 244, 2013.

[67] D. Pech, M. Brunet, P.L. Taberna, P. Simon, N. Fabre, F. Mesnilgrente, V. Conédéra, and H. Durou. Elaboration of a microstructured inkjet-printed carbon electrochemical capacitor. *Journal of Power Sources*, 195(4):1266 – 1269, 2010.

[68] J. Lee, J. Kim, and T. Hyeon. Recent progress in the synthesis of porous carbon materials. *Advanced Materials*, 18(16):2073–2094, 2006.

[69] Z. Hu and M.P. Srinivasan. Mesoporous high-surface-area activated carbon. *Microporous and Mesoporous Materials*, 43(3):267 – 275, 2001.

[70] Y Gogotsi, A. Nikitin, H. Ye, W. Zhou, J.E. Fischer, B. Yi, H.C. Foley, and M.W. Barsoum. Nanoporous carbide-derived carbon with tunable pore size. *Nat. Mater.*, 2:591–594, 2003.

[71] B. Sakintuna and Y. Yurum. Templated porous carbons:âĂL' a review article. *Industrial and Engineering Chemistry Research*, 44(9):2893–2902, 2005.

[72] G. Bongiorno, A. Podestàă, L. Ravagnan, P. Piseri, P. Milani, C. Lenardi, S. Miglio, M. Bruzzi, and C. Ducati. Electronic properties and applications of cluster-assembled carbon films. *Journal of Materials Science: Materials in Electronics*, 17:427–441, 2006.

[73] C. S. Casari, A. Li Bassi, L. Ravagnan, F. Siviero, C. Lenardi, P. Piseri, G. Bongiorno, C. E. Bottani, and P. Milani. Chemical and thermal stability of carbyne-like structures in cluster-assembled carbon films. *Phys. Rev. B*, 69:075422, 2004.

[74] M. Bogana, L. Ravagnan, C. S. Casari, A. Zivelonghi, A. Baserga, A. Li

Bassi, C. E. Bottani, S. Vinati, E. Salis, P. Piseri, E. Barborini, L. Colombo, and P. Milani. Leaving the fullerene road: presence and stability of sp chains in sp 2 carbon clusters and cluster-assembled solids. *New Journal of Physics*, 7(1):81, 2005.

[75] L. Ravagnan, G. Bongiorno, D. Bandiera, E. Salis, P. Piseri, P. Milani, C. Lenardi, M. Coreno, M. de Simone, and K.C. Prince. Quantitative evaluation of sp/sp2 hybridization ratio in cluster-assembled carbon films by in situ near edge x-ray absorption fine structure spectroscopy. *Carbon*, 44(8):1518 – 1524, 2006.

[76] L. Ravagnan, T. Mazza, G. Bongiorno, M. Devetta, M. Amati, P. Milani, P. Piseri, M. Coreno, C. Lenardi, F. Evangelista, and P. Rudolf. sp hybridization in free carbon nanoparticles-presence and stability observed by near edge x-ray absorption fine structure spectroscopy. *Chem. Commun.*, 47:2952–2954, 2011.

[77] D. Donadio, L. Colombo, P. Milani, and G. Benedek. Growth of nanostructured carbon films by cluster assembly. *Phys. Rev. Lett.*, 83:776–779, 1999.

[78] C. Lenardi, E. Barborini, V. Briois, L. Lucarelli, P. Piseri, and P. Milani. Nexafs characterization of nanostructured carbon thin-films exposed to hydrogen. *Diamond and Related Materials*, 10(3 - 7):1195 – 1200, 2001.

[79] A. C. Ferrari, B. S. Satyanarayana, J. Robertson, W. I. Milne, E. Barborini, P. Piseri, and P. Milani. Electron field emission from cluster-assembled carbon thin films. *EPL (Europhysics Letters)*, 46(2):245, 1999.

[80] C. Ducati, E. Barborini, P. Piseri, P. Milani, and J. Robertson. Influence of cluster-assembly parameters on the field emission properties of nanostructured carbon films. *Journal of Applied Physics*, 92(9):5482–5489, 2002.

[81] M. Bruzzi, S. Miglio, M. Scaringella, G. Bongiorno, P. Piseri, A. Podestà, and P. Milani. First study of humidity sensors based on nanostructured carbon films produced by supersonic cluster beam deposition. *Sensors and Actuators B: Chemical*, 100(1 - 2):173 – 176, 2004.

[82] S. Miglio, M. Bruzzi, M. Scaringella, D. Menichelli, E. Leandri, A. Baldi, G. Bongiorno, P. Piseri, and P. Milani. Development of humidity sensors based on nanostructured carbon films. *Sensors and Actuators B: Chemical*, 111 - 112(0):140 – 144, 2005.

[83] L. Diederich, E. Barborini, P. Piseri, A. Podestà, P. Milani, A. Schneuwly, and R. Gallay. Supercapacitors based on nanostructured carbon electrodes grown by cluster-beam deposition. *Applied Physics Letters*, 75(17):2662–

2664, 1999.

[84] T. Caruso, R. G. Agostino, G. Bongiorno, E. Barborini, P. Piseri, P. Milani, C. Lenardi, S. La Rosa, and M. Bertolo. Writing submicrometric metallic patterns by ultraviolet synchrotron irradiation of nanostructured carbon and tio$_x$–carbon films. *Applied Physics Letters*, 84(17):3412–3414, 2004.

[85] R. G. Agostino, T. Caruso, G. Chiarello, A. Cupolillo, D. Pacilè, R. Filosa, V. Formoso, E. Colavita, L. Papagno, C. Ducati, E. Barborini, C. Lenardi, G. Bongiorno, P. Piseri, and P. Milani. Thermal annealing and hydrogen exposure effects on cluster-assembled nanostructured carbon films embedded with transition metal nanoparticles. *Phys. Rev. B*, 68:035413, 2003.

[86] G. A. Bongiorno. *Synthesis and characterization of metal-carbon nanocomposites.* Phd thesis, Università degli Studi di Milano, 2004/2005.

[87] G. Benedek, H. Vahedi-Tafreshi, E. Barborini, P. Piseri, P. Milani, C. Ducati, and J. Robertson. The structure of negatively curved spongy carbon. *Diamond and Related Materials*, 12(3 - 7):768 – 773, 2003.

[88] E. Barborini, P. Piseri, P. Milani, G. Benedek, C. Ducati, and J. Robertson. Negatively curved spongy carbon. *Applied Physics Letters*, 81(18):3359–3361, 2002.

[89] A. Volta. On the Electricity Excited by the Mere Contact of Conducting Substances of Different Kinds. *Royal Society of London Philosophical Transactions Series I*, 90:403–431, 1800.

[90] M. G. Walter, E. L. Warren, J. R. McKone, S. W. Boettcher, Q. Mi, E. A. Santori, and N. S. Lewis. Solar water splitting cells. *Chemical Reviews*, 110(11):6446–6473, 2010.

[91] M. Graetzel. Dye-sensitized solar cells. *Journal of Photochemistry and Photobiology C: Photochemistry Reviews*, 4(2):145 – 153, 2003.

[92] C. Zoski. *Handbook of electrochemistry.* Elsevier, 2006.

[93] V. S. Bagotsky. *Fundamentals of Electrochemistry, 2nd Edition.* Wiley, 2005.

[94] H. Helmholtz. Studien uber electrische grenzschichten. *Annalen der Physik*, 243(7):337–382, 1879.

[95] M. Gouy. Sur la constitution de la charge électrique à la surface d'un électrolyte. *J. Phys. Theor. Appl.*, 9(1):457–468, 1910.

[96] D. L. Chapman. A contribution to the theory of electrocapillarity. *Philosophical Magazine Series 6*, 25(148):475–481, 1913.

[97] O. Stern. The theory of the electrolytic double-layer. *Zeit. Elektrochem.*,

30:508 – 516, 1924.

[98] D. C. Grahame. The electrical double layer and the theory of electrocapillarity. *Chemical Reviews*, 41(3):441–501, 1947.

[99] J. H. Bae, J. Han, and T. D. Chung. Electrochemistry at nanoporous interfaces: new opportunity for electrocatalysis. *Phys. Chem. Chem. Phys.*, 14:448–463, 2012.

[100] S. Park, H. C. Kim, and T. D. Chung. Electrochemical analysis based on nanoporous structures. *Analyst*, 137:3891–3903, 2012.

[101] J. Chmiola, G. Yushin, Y. Gogotsi, C. Portet, P. Simon, and P. L. Taberna. Anomalous increase in carbon capacitance at pore sizes less than 1 nanometer. *Science*, 313(5794):1760–1763, 2006.

[102] C. Largeot, C. Portet, J. Chmiola, P. Taberna, Y. Gogotsi, and P. Simon. Relation between the ion size and pore size for an electric double-layer capacitor. *Journal of the American Chemical Society*, 130(9):2730–2731, 2008.

[103] H. Boo, S. Park, B. Ku, Y. Kim, J. H. Park, H. C. Kim, and T. D. Chung. Ionic strength-controlled virtual area of mesoporous platinum electrode. *Journal of the American Chemical Society*, 126(14):4524–4525, 2004.

[104] J. Bisquert. Physical electrochemistry of nanostructured devices. *Phys. Chem. Chem. Phys.*, 10:49–72, 2008.

[105] F. Fabregat-Santiago, G. Garcia-Belmonte, I. Mora-Sero, and J. Bisquert. Characterization of nanostructured hybrid and organic solar cells by impedance spectroscopy. *Phys. Chem. Chem. Phys.*, 13:9083–9118, 2011.

[106] W.G Pell and B.E Conway. Voltammetry at a de levie brush electrode as a model for electrochemical supercapacitor behaviour. *Journal of Electroanalytical Chemistry*, 500(1 - 2):121 – 133, 2001.

[107] B. Tribollet M. E. Orazem. *Electrochemical Impedance Spectroscopy.* Wiley, 2008.

[108] D. D. Macdonald, E. Sikora, and G. Engelhardt. Characterizing electrochemical systems in the frequency domain. *Electrochimica Acta*, 43(1 - 2):87 – 107, 1998.

[109] D. D. Macdonald. Reflections on the history of electrochemical impedance spectroscopy. *Electrochimica Acta*, 51(8 - 9):1376 – 1388, 2006.

[110] B. Chang and S. Park. Electrochemical impedance spectroscopy. *Annual Review of Analytical Chemistry*, 3(1):207–229, 2010.

[111] M.R. Shoar Abouzari, F. Berkemeier, G. Schmitz, and D. Wilmer. On

the physical interpretation of constant phase elements. *Solid State Ionics*, 180(14 - 16):922 – 927, 2009.

[112] B. Tribollet V. Vivier I. Frateur B. Hirschorn, M. E. Orazem and M. Musiani. Constant-phase-element behavior caused by resistivity distributions in films. *Journal of The Electrochemical Society*, 157(12):452 – 457, 2010.

[113] U. Rammelt and G. Reinhard. On the applicability of a constant phase element (cpe) to the estimation of roughness of solid metal electrodes. *Electrochimica Acta*, 35(6):1045 – 1049, 1990.

[114] J. B. Jorcin, M. E. Orazem, N. Pébère, and B. Tribollet. Cpe analysis by local electrochemical impedance spectroscopy. *Electrochimica Acta*, 51(8 - 9):1473 – 1479, 2006.

[115] S. H. Liu. Fractal model for the ac response of a rough interface. *Phys. Rev. Lett.*, 55:529–532, 1985.

[116] T. Pajkossy. Electrochemistry at fractal surfaces. *Journal of Electroanalytical Chemistry and Interfacial Electrochemistry*, 300(1 - 2):1 – 11, 1991.

[117] G.J. Brug, A.L.G. van den Eeden, M. Sluyters-Rehbach, and J.H. Sluyters. The analysis of electrode impedances complicated by the presence of a constant phase element. *Journal of Electroanalytical Chemistry and Interfacial Electrochemistry*, 176(1 - 2):275 – 295, 1984.

[118] C.H. Hsu and F. Mansfeld. Technical note: concerning the conversion of the constant phase element parameter y0 into a capacitance. *Corrosion*, 57(9):747 – 748, 2001.

[119] B. Hirschorn, M. E. Orazem, B. Tribollet, V. Vivier, I. Frateur, and M. Musiani. Determination of effective capacitance and film thickness from constant-phase-element parameters. *Electrochimica Acta*, 55(21):6218 – 6227, 2010.

[120] B. Ulgut. Demystifying transmission lines: What are they, why are they useful? *Gamry: Application Note*, 2009.

[121] R. de Levie. On porous electrodes in electrolyte solutions: I. capacitance effects. *Electrochimica Acta*, 8(10):751 – 780, 1963.

[122] R. de Levie. On porous electrodes in electrolyte solutions iv. *Electrochimica Acta*, 9(9):1231 – 1245, 1964.

[123] A. Lasia. Impedance of porous electrodes. *Journal of Electroanalytical Chemistry*, 397(1 - 2):27 – 33, 1995.

[124] A. Lasia. Porous electrodes in the presence of a concentration gradient. *Journal of Electroanalytical Chemistry*, 428(1 - 2):155 – 164, 1997.

[125] H. Keiser, K.D. Beccu, and M.A. Gutjahr. Abschatzung der porenstruktur poroser elektroden aus impedanzmessungen. *Electrochimica Acta*, 21(8):539 – 543, 1976.

[126] C. Hitz and A. Lasia. Experimental study and modeling of impedance of the her on porous ni electrodes. *Journal of Electroanalytical Chemistry*, 500(1 - 2):213 – 222, 2001.

[127] H. K. Song, Y. H. Jung, K. H. Lee, and L. H. Dao. Electrochemical impedance spectroscopy of porous electrodes: the effect of pore size distribution. *Electrochimica Acta*, 44(20):3513 – 3519, 1999.

[128] A. Hasbach, U. Retter, K. Siegler, and W. Kautek. On the impedance of porous electrodes - double-layer charging and charge transfer on an inhomogeneous inside electrode surface. *Journal of Electroanalytical Chemistry*, 561(0):29 – 35, 2004.

[129] G. Bongiorno, M. Blomqvist, P. Piseri, P. Milani, C. Lenardi, C. Ducati, T. Caruso, P. Rudolf, S. Wachtmeister, S. Csillag, and E. Coronel. Nanostructured cnx films grown by supersonic cluster beam deposition. *Carbon*, 43(7):1460 – 1469, 2005.

[130] P. Milani, P. Piseri, E. Barborini, A. Podestà, and C. Lenardi. Cluster beam synthesis of nanostructured thin films. *The 47th international symposium: Vacuum, thin films, surfaces/interfaces, and processing NAN06*, 19(4):2025–2033, 2001.

[131] L. Ravagnan, F. Siviero, C. Lenardi, P. Piseri, E. Barborini, P. Milani, C. S. Casari, A. Li Bassi, and C. E. Bottani. Cluster-beam deposition and *in situ* characterization of carbyne-rich carbon films. *Phys. Rev. Lett.*, 89:285506, 2002.

[132] L. Ravagnan, P. Piseri, M. Bruzzi, S. Miglio, G. Bongiorno, A. Baserga, C. S. Casari, A. Li Bassi, C. Lenardi, Y. Yamaguchi, T. Wakabayashi, C. E. Bottani, and P. Milani. Influence of cumulenic chains on the vibrational and electronic properties of *sp*-sp^2 amorphous carbon. *Phys. Rev. Lett.*, 98:216103, 2007.

[133] J. Robertson. Hard amorphous (diamond-like) carbons. *Progress in Solid State Chemistry*, 21(4):199 – 333, 1991.

[134] F. Sette, G. K. Wertheim, Y. Ma, G. Meigs, S. Modesti, and C. T. Chen. Lifetime and screening of the c1s photoemission in graphite. *Phys. Rev. B*, 41:9766–9770, 1990.

[135] L. Ostrovskaya, A. Podestà, P. Milani, and V. Ralchenko. Influence of surface morphology on the wettability of cluster-assembled carbon films.

EPL (Europhysics Letters), 63(3):401, 2003.

[136] A. Podestà, G. Bongiorno, P. E. Scopelliti, S. Bovio, P. Milani, C. Semprebon, and G. Mistura. Cluster-assembled nanostructured titanium oxide films with tailored wettability. *The Journal of Physical Chemistry C*, 113(42):18264–18269, 2009.

[137] C. Arbizzani, M. Lazzari, F. Soavi, M. Mastragostino, and M. Conte. Ilhypos ionic liquid-based supercapacitors. *ECS Transactions*, 25(23):25–30, 2010.

[138] M. Armand, F. Endres, D.R. MacFarlane, H. Ohno, and B. Scrosati. Ionic-liquid materials for the electrochemical challenges of the future. *Nature Materials*, 8(8):621 – 629, 2009.

[139] E. Frackowiak. Supercapacitors based on carbon materials and ionic liquids. *Journal of the Brazilian Chemical Society*, 17:1074 – 1082, 10 2006.

[140] C. Largeot, P. L. Taberna, Y. Gogotsi, and P. Simon. Microporous carbon-based electrical double layer capacitor operating at high temperature in ionic liquid electrolyte. *Electrochemical and Solid-State Letters*, 14(12):A174–A176, 2011.

[141] C. Merlet, B. Rotenberg, P. A. Madden, P.-L. Taberna, P. Simon, Y. Gogotsi, and M. Salanne. On the molecular origin of supercapacitance in nanoporous carbon electrodes. *Nature Materials*, 11:306–310, 2012.

[142] S. Kukielka, W. Gulbinski, Y. Pauleau, S.N. Dub, and J.J. Grob. Composition, mechanical properties and friction behavior of nickel/hydrogenated amorphous carbon composite films. *Surface and Coatings Technology*, 200(22 - 23):6258 – 6262, 2006.

[143] Y. Pauleau, F. Thiéry, L. Latrasse, and S.N. Dub. Characteristics of copper/carbon and nickel/carbon composite films produced by microwave plasma-assisted deposition techniques from argon - methane gas mixtures. *Surface and Coatings Technology*, 188 - 189(0):484 – 488, 2004.

[144] K. Sedlackovaą, P. Lobotka, I. Vavra, and G. Radnoczi. Structural, electrical and magnetic properties of carbon - nickel composite thin films. *Carbon*, 43(10):2192 – 2198, 2005.

[145] A. Sylvestre, S. Kukielka, D.M. Nguyen, W. Gulbinski, and Y. Pauleau. Dielectric properties of nickel containing amorphous hydrogenated carbon films prepared by microwave plasma-assisted deposition technique. *Reviews on advanced materials science*, 15(3):185 – 191, 2007.

[146] R. Lamber, N. Jaeger, and G. Schulz-Ekloff. Electron microscopy study of the interaction of ni, pd and pt with carbon: I. nickel catalyzed graphiti-

zation of amorphous carbon. *Surface Science*, 197(3):402 – 414, 1988.

[147] M. L.Toebes, J. H. Bitter, A.J. van Dillen, and K. P. de Jong. Impact of the structure and reactivity of nickel particles on the catalytic growth of carbon nanofibers. *Catalysis Today*, 76(1):33 – 42, 2002.

[148] S. Esconjauregui, C. M. Whelan, and K. Maex. The reasons why metals catalyze the nucleation and growth of carbon nanotubes and other carbon nanomorphologies. *Carbon*, 47(3):659 – 669, 2009.

[149] J. A. RodriĄguez-Manzo, C. Pham-Huu, and F. Banhart. Graphene growth by a metal-catalyzed solid-state transformation of amorphous carbon. *ACS Nano*, 5(2):1529–1534, 2011.

[150] R. Anton. On the reaction kinetics of ni with amorphous carbon. *Carbon*, 46(4):656 – 662, 2008.

[151] K. P. De Jong and J. W. GEUS. Carbon nanofibers: Catalytic synthesis and applications. *Catalysis Reviews*, 42(4):481–510, 2000.

[152] M. Wu, J. Gao, S. Zhang, and A. Chen. Comparative studies of nickel oxide films on different substrates for electrochemical supercapacitors. *Journal of Power Sources*, 159(1):365 – 369, 2006.

[153] U.M. Patil, R.R. Salunkhe, K.V. Gurav, and C.D. Lokhande. Chemically deposited nanocrystalline nio thin films for supercapacitor application. *Applied Surface Science*, 255(5):2603 – 2607, 2008.

[154] Y.L. Tai and H. Teng. Modification of porous carbon with nickel oxide impregnation to enhance the electrochemical capacitance and conductivity. *Carbon*, 42(11):2335 – 2338, 2004.

[155] G. Yuan, Z. Jiang, A. Aramata, and Y. Gao. Electrochemical behavior of activated-carbon capacitor material loaded with nickel oxide. *Carbon*, 43(14):2913 – 2917, 2005.

[156] Q. Huang, X. Wang, J. Li, C. Dai, S. Gamboa, and P.J. Sebastian. Nickel hydroxide/activated carbon composite electrodes for electrochemical capacitors. *Journal of Power Sources*, 164(1):425 – 429, 2007.

[157] J. Y. Lee, K. L., K. H. An, and Y. H. Lee. Nickel oxide/carbon nanotubes nanocomposite for electrochemical capacitance. *Synthetic Metals*, 150(2):153 – 157, 2005.

[158] J. Li, E. Liu, W. Li, X. Meng, and S. Tan. Nickel/carbon nanofibers composite electrodes as supercapacitors prepared by electrospinning. *Journal of Alloys and Compounds*, 478(1 -2):371 – 374, 2009.

[159] G. Abrasonis, M. Krause, A. Mucklich, K. Sedlackovaą, G. Radnoczi,

U. Kreissig, A. Kolitsch, and W. Moller. Growth regimes and metal enhanced 6-fold ring clustering of carbon in carbon - nickel composite thin films. *Carbon*, 45(15):2995 – 3006, 2007.

[160] N. Benchikh, F. Garrelie, C. Donnet, B. Bouchet-Fabre, K. Wolski, F. Rogemond, A.S Loir, and J.L. Subtil. Nickel-incorporated amorphous carbon film deposited by femtosecond pulsed laser ablation. *Thin Solid Films*, 482(1 - 2):287 – 292, 2005.

[161] C.N. He, X.W. Du, J. Ding, C.S. Shi, J.J. Li, N.Q. Zhao, and L. Cui. Low-temperature cvd synthesis of carbon-encapsulated magnetic ni nanoparticles with a narrow distribution of diameters. *Carbon*, 44(11):2330 – 2333, 2006.

[162] J.J. Van Benschoten, J.Y. Lewis, W.R. Heineman, D.A. Roston, and P.T. Kissinger. Cyclic voltammetry experiment. *Journal of Chemical Education*, 60(9):772, 1983.

[163] B.E. Conway, V. Birss, and J. Wojtowicz. The role and utilization of pseudocapacitance for energy storage by supercapacitors. *Journal of Power Sources*, 66(1-2):1 – 14, 1997.

[164] S. Kirkpatrick. Percolation and conduction. *Rev. Mod. Phys.*, 45:574–588, 1973.

[165] M. Bruzzi, P. Piseri, S. Miglio, G. Bongiorno, E. Barborini, C. Ducati, J. Robertson, and P. Milani. Electrical conduction in nanostructured carbon and carbon-metal films grown by supersonic cluster beam deposition. *The European Physical Journal B - Condensed Matter and Complex Systems*, 36:3–13, 2003.

[166] H. Rauf, T. Pichler, M. Knupfer, J. Fink, and H. Kataura. Transition from a tomonaga-luttinger liquid to a fermi liquid in potassium-intercalated bundles of single-wall carbon nanotubes. *Phys. Rev. Lett.*, 93:096805, 2004.

[167] R. Larciprete, A. Goldoni, S. Lizzit, and L. Petaccia. The electronic properties of carbon nanotubes studied by high resolution photoemission spectroscopy. *Applied Surface Science*, 248(1-4):8 – 13, 2005.

[168] S. Bhattacharyya, S. J. Henley, D. Lock, N. P. Blanchard, and S. R. P. Silva. Semiconducting phase of amorphous carbon-nickel composite films. *Applied Physics Letters*, 89(2):022113, 2006.

[169] S. Huh, J. Park, K.S. Kim, B.H. Hong, and S.B. Kim. Selective n-type doping of graphene by photo-patterned gold nanoparticles. *ACS Nano*, 5(5):3639–3644, 2011.

[170] P. L. Taberna, P. Simon, and J. F. Fauvarque. Electrochemical characteris-

tics and impedance spectroscopy studies of carbon-carbon supercapacitors. *Journal of The Electrochemical Society*, 150(3):A292–A300, 2003.

[171] J.P. Coad and J.C. Riviere. Auger spectroscopy of carbon on nickel. *Surface Science*, 25(3):609 – 624, 1971.

[172] J. R. Snyder, M. A. Smith, and L. L. Levenson. Adhesion of nickel films on graphite. *Journal of Vacuum Science and Technology*, 17(1):421–424, 1980.

[173] S. Tomita, T. Sakurai, H. Ohta, M. Fujii, and S. Hayashi. Structure and electronic properties of carbon onions. *The Journal of Chemical Physics*, 114(17):7477–7482, 2001.

[174] D. Roy, M. Chhowalla, H. Wang, N. Sano, I. Alexandrou, T.W. Clyne, and G.A.J. Amaratunga. Characterisation of carbon nano-onions using raman spectroscopy. *Chemical Physics Letters*, 373(1-2):52 – 56, 2003.

[175] M. Choucair and J.A. Stride. The gram-scale synthesis of carbon onions. *Carbon*, 50(3):1109 – 1115, 2012.

[176] F. Tuinstra and J. L. Koenig. Raman spectrum of graphite. *The Journal of Chemical Physics*, 53(3):1126–1130, 1970.

[177] A. C. Ferrari and J. Robertson. Interpretation of raman spectra of disordered and amorphous carbon. *Phys. Rev. B*, 61:14095–14107, 2000.

[178] D.S. Knight and W.B. White. Characterization of diamond films by raman spectroscopy. *Journal of Materials Research*, 4:385–393, 1989.